Characterisation of Channelrhodopsin-2 in a neuronal culture model

A dissertation submitted to the University of Bristol in accordance with the requirements for award of the degree of PhD in the Faculty of Medical Sciences

Word count – 29,290

Abstract

Neurones are highly electrically active cells. A long sought-after goal of neuroscience has to be able to control neuronal activity in a precise fashion, both in space and time. Recently, the cloning of novel light-gated ion channels from algae has enabled this experimental possibility. In particular, Channelrhopdopsin-2 (ChR2), a non-specific cation channel that is opened upon illumination with blue light, has revolutionized the field. However not much is known about the specific kinetics, and voltage and temperature dependence of ChR2. This information is critical for understanding how the channel will function when used to probe neuronal connectivity and drive behaviour when used in vivo. In this thesis I have examined these questions, using ChR2 in primary neuronal cultures as a model system to carefully measure channel activity following light stimulation.

Author’s declaration

I declare that the work in this dissertation was carried out in accordance with the requirements of the University's Regulations and Code of Practice for Research Degree Programmes and that it has not been submitted for any other academic award. Except where indicated by specific reference in the text, the work is the candidate's own work. Work done in collaboration with, or with the assistance of, others, is indicated as such. Any views expressed in the dissertation are those of the author.

SIGNED: .....Thomas Chater..... DATE:.....2012/3/31....

Table of contents

8. General discussion and final conclusions
   8.1. Channelrhodopsin-2
   8.2. PKMzeta
   8.3. Neuronal cultures as an experimental paradigm

Chapter 1

Introduction

Neuroscience is a relatively new field, preceded by pharmacology. It was only until the turn of the Twentieth century that Cajal showed that the nervous system had incredible complexity and diversity of structure in its neuronal population (Cajal 1888). Since then neuroscience has exploded as a field, as the true depth and incredible complexity of the brain has become apparent, and the resultant difficulties in understanding this ultra-wired system of individual cells has driven the evolution of new techniques capable of probing neuronal tissue.

1.1 The complexity of the brain

A typical human brain contains several billion neurones (one more recent estimate is around 20 x 10^9, (Pelvig, Pakkenberg et al. 2008)) all acting in a connected and synergistic fashion. These cells form specialised interfaces with one another called synapses. Synapses are micro-regions of cells evolved for chemical communication between cells across a small gap called the synaptic cleft. Until the advent of electron microscopy, it was not possible to investigate the ultrastructure of synapses. However, since the 1960's scientist were able to probe these regions, starting at the neuromuscular junction, a tractable target due to its relatively large size, and afterwards proceeding into the cortex.

1.2 Neurones are highly specialised

Neurones are a diverse population of cells. Neurones have complex morphologies, with a cell body (soma) from which arises many neurites. These projecting fibres are either axonal (the apical surface of the cell) or dendritic (basal). One axonal projection from a single neurone may stretch metres, bifurcate many times, and what originates as a single neurite may eventually make up to 370,000

synapses (Arbuthnott and Wickens 2007). Dendritic arbours are no less complex, typically being more local to the cell (extending up to a few millimetres away) but being highly branched. Figure 1.1 shows some examples of the morphological variety exhibited by neurones.

Dendrites are also the site of the specialised structures known as dendritic spines (Ethell and Pasquale 2005) . Dendritic spines are femto-litre sized projections that act as one of the primary sites for both excitatory and inhibitory synapses. These small structures physically compartmentalise both electrical and biochemical signalling (Yuste and Bonhoeffer 2001; Cingolani and Goda 2008; Grunditz, Holbro et al. 2008).

Within the dendritic spine an electron dense structure can be detected using electron microscopy. This is termed the post-synaptic density (PSD), and contains many different types of protein, from receptors to scaffolding molecules. This densely packed region of the cell is capable of responding to signalling molecules entering the cell, such as calcium, and altering its structure, either by receptor trafficking, conformational changes within the PSD, or *de novo* protein synthesis and the creation of new synapses.

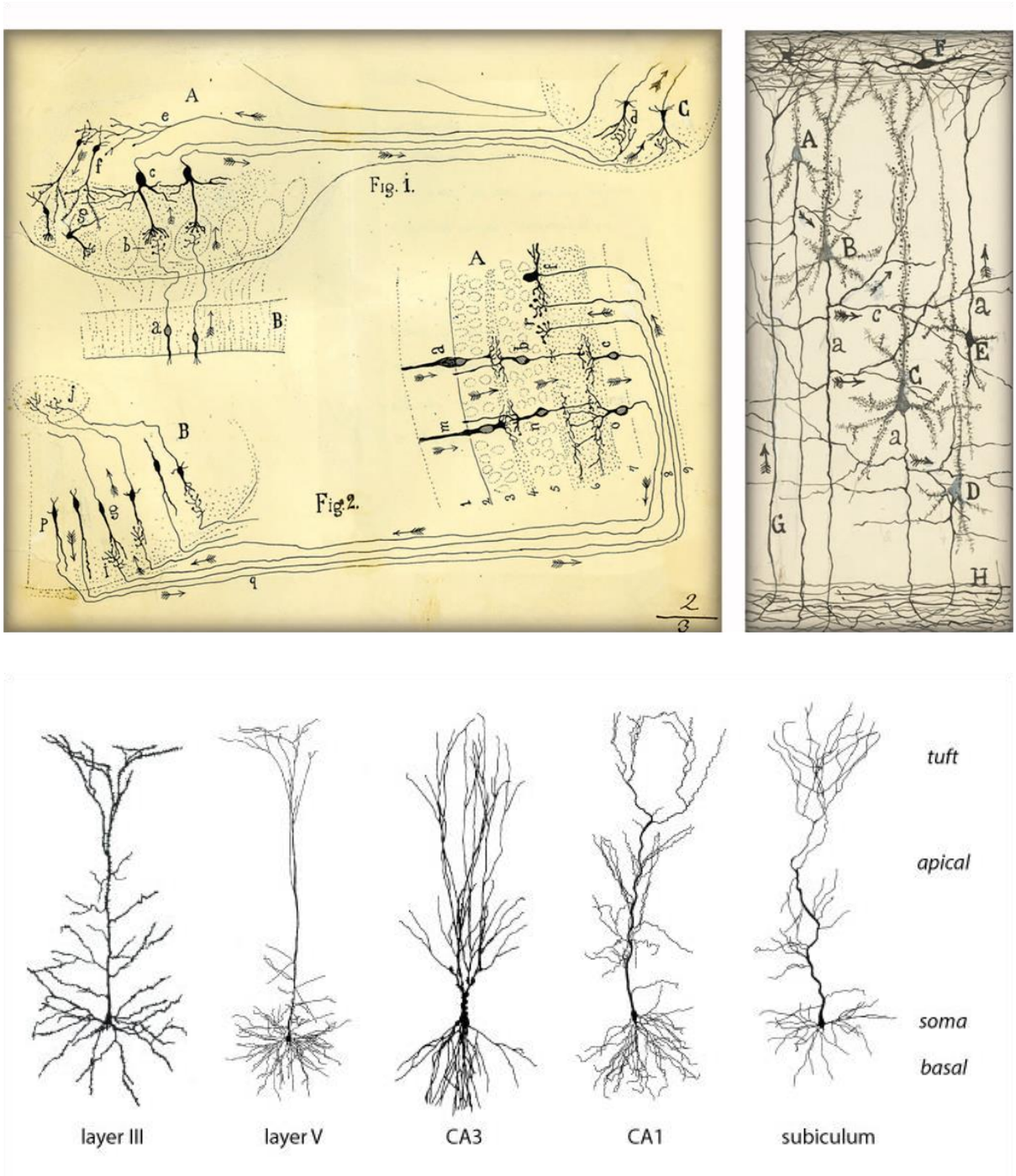

Figure 1.1 - an example of the diversity neurones

Top, left – Cajal, taken from (DeFelipe 2010) visual and olfactory neuronal pathways showing current, right, and in the cerebral cortex

Bottom – diversity of pyramidal neurones from different areas of the cortex

Taken from (Spruston 2008)

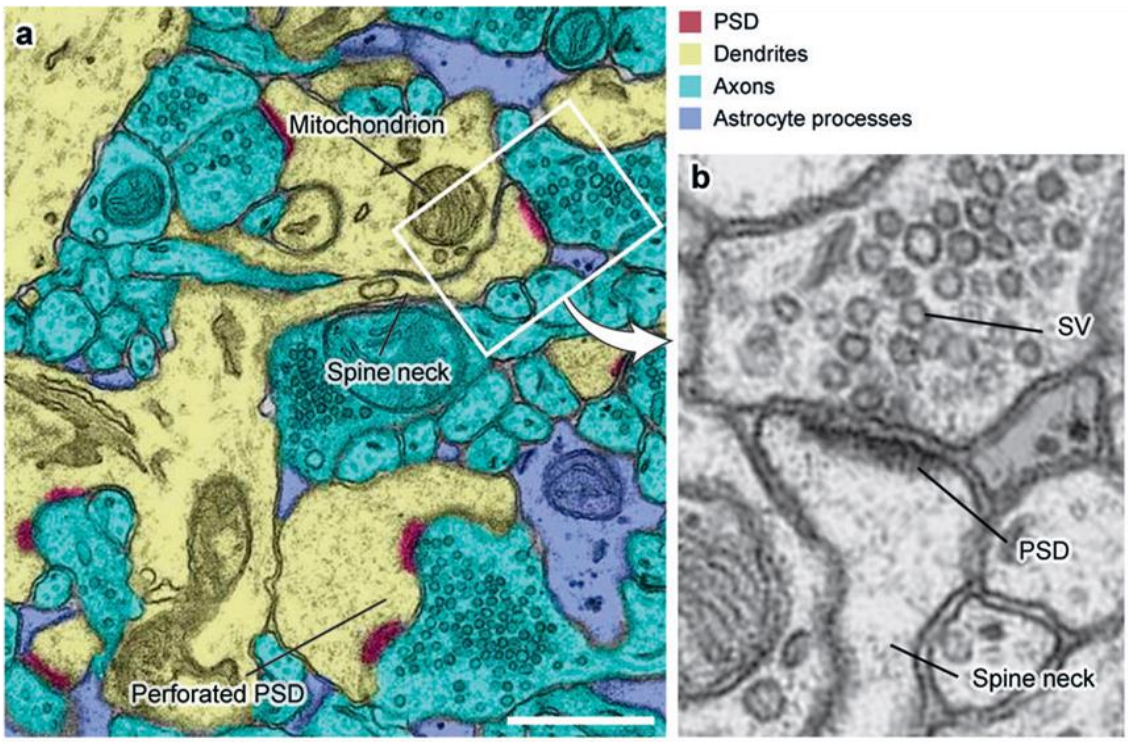

Figure 1.2 - the ultrastructure of synapses

Left, an EM slice taken from the CA1 region of the hippocampus. Several structures are visible, including mitochondria, post-synaptic densities, and synaptic vesicles

Right, a magnified view of the boxed area in the left image, showing synaptic vesicles (SV) and the electron-dense post-synaptic density (PSD)

Taken from (Sheng and Hoogenraad 2007)

1.3 Synaptic plasticity

Neurones are capable of changing their inputs and outputs in response to stimuli. The change in efficacy of neurones' synaptic sites is called synaptic plasticity. This was first identified in the rabbit hippocampus by Bliss and Lomo (Bliss and Lomo 1973). This study showed that a tetanic electrical stimulus was capable of driving plastic changes in neurones, with the stimulated neurones potentiating their output for hours after a stimulus. This phenomenon was termed long term

potentiation (LTP). The converse correlate to LTP, long term depression (LTD, (Lynch, Dunwiddie et al. 1977)), also involves neurones changing their output post-stimulation, but in LTD there is a long-lasting decrease in neuronal output. The introduction of LTP and LTD set in motion a way of understanding and probing neuronal plasticity that has persisted up to the current day.

Typically, the underlying mechanism of synaptic plasticity is due to the insertion or removal of 2-amino-3-(5-methyl-3-oxo-1,2- oxazol-4-yl)propanoic acid (AMPA) receptors. These changes in synaptic strength allow neurones, and the brain as a whole, to store information. The insertion of AMPA receptors to the surface of the synapse is depicted in figure 1.3, and the bidirectional nature of synaptic plasticity in figure 1.4.

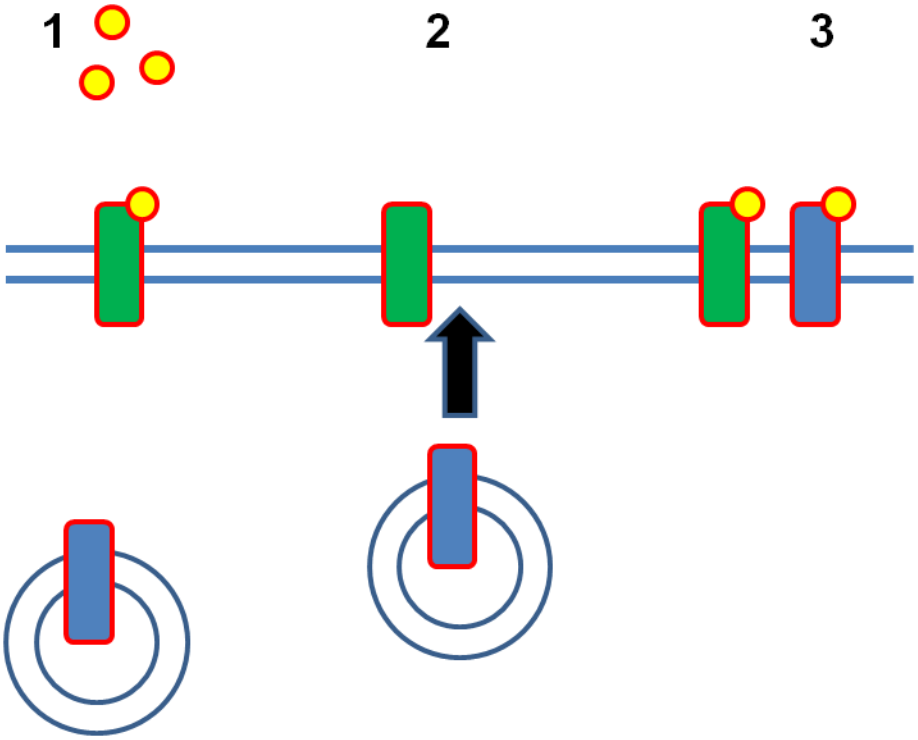

Figure 1.3 – simplified schematic of insertion of AMPA receptors in response to NMDA receptor activation

At 1, synapse only contains NMDA receptors (green). Upon agonist binding (yellow circles), NMDA receptors open and let calcium and sodium into the post-synaptic cell.

2 – AMPA receptors (blue) are now inserted into the post-synaptic membrane from fusion of intracellular vesicles with the post-synaptic membrane

3- Synapse now has both AMPA and NMDA receptors, both of which can respond to agonist binding

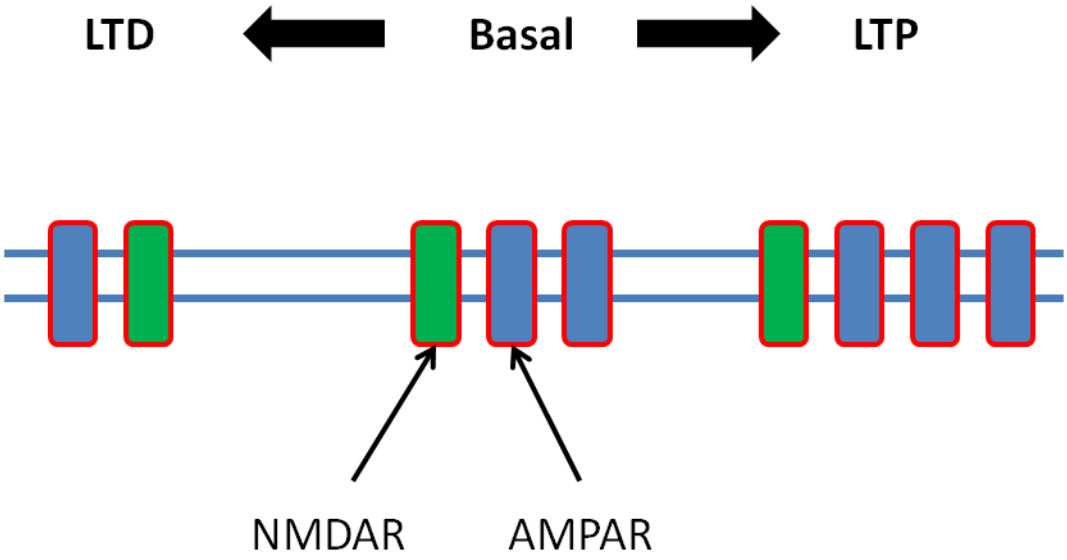

Figure 1.4 – the principle underlying bidirectional synaptic plasticity

Synapses in their basal state contain both NMDA receptors (green) and AMPA receptors (blue). After stimulation, levels of AMPA receptors either increase or decrease. A decrease in synaptic AMPA (left hand side) that persists is long term depression (LTD). An increase in AMPA receptor number at the synapse that persists is long term potentiation (LTP)

1.4 Excitatory glutamate receptors

AMPA receptors are responsible for the majority of the excitatory depolarisation seen at excitatory synapses. AMPARs are tetrameric ionotropic glutamate receptors, composed of 4 possible subunits GluA1-4 (Boulter, Bettler et al. 1992; Jonas 1993; Hollmann, Boulter et al. 1994) . These exist as hetrodimers, and the trafficking of these receptors underlies much of the changes observed in LTP and LTD (Siegelbaum and Kandel 1991; Nicoll and Malenka 1995; Malinow and Malenka 2002). AMPARs open, and allow an influx of cations, depolarising the post-

synaptic cell. This depolarisation, if large enough, can cause opening of voltage-gated post-synaptic Na^+ channels, and the propagation of the electrical signal throughout the post-synaptic neurone.

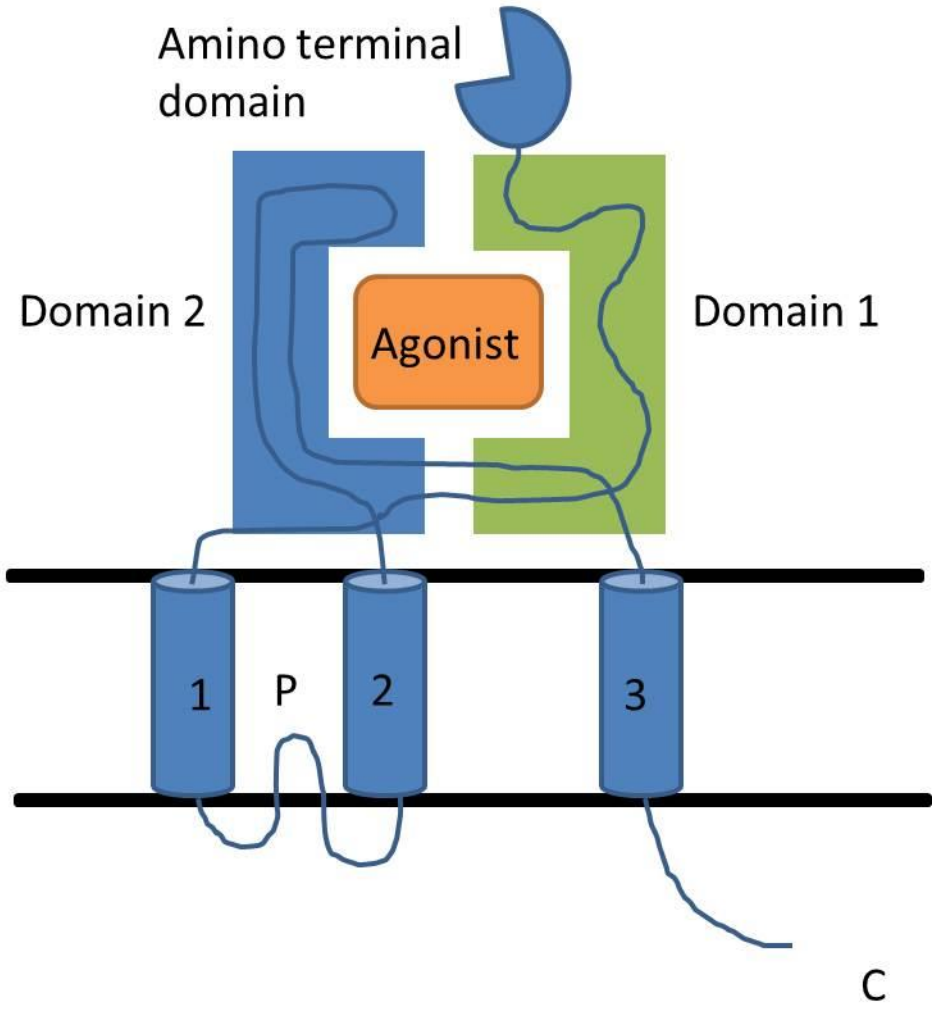

Figure 1.5 – the structure of an AMPA receptor subunit.

AMPA receptor subunit consists of an N-terminal extracellular region, three transmembrane regions (labelled 1,2 and 3), a re-entrant loop (P), and an intracellular region

Adapted from (Mayer and Armstrong 2004)

Glutamate receptors are not just restricted to AMPARs. NMDA (N-methyl-d-aspartic) and kainate receptors are also ionotropic receptors with glutamate as a ligand (see figure 1.6). Many forms of LTP are NMDA-receptor dependent (Malenka

and Bear 2004), with activation of NMDA receptors leading to an influx of calcium, and the entrainment of various intracellular calcium dependent processes.

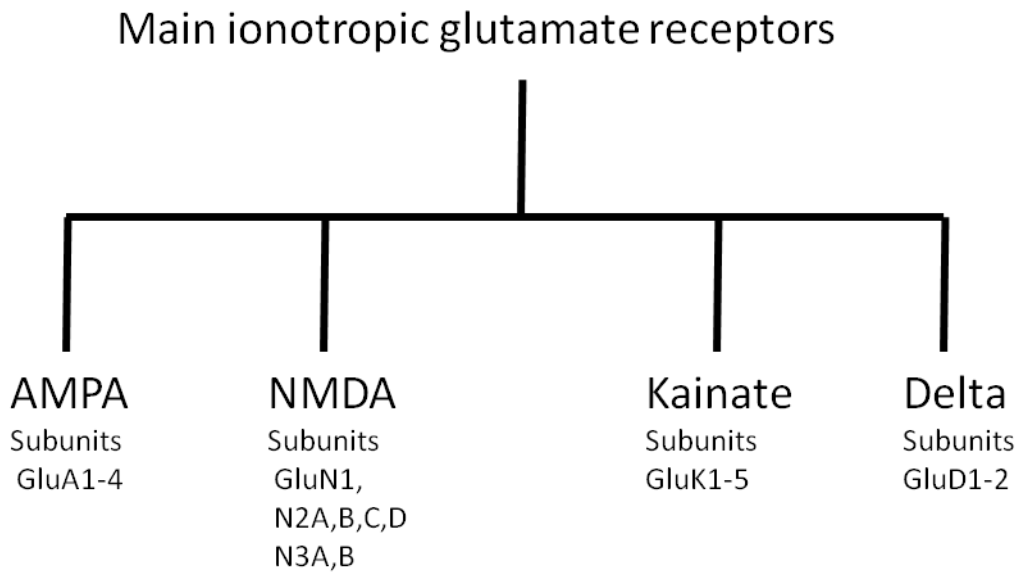

Figure 1.6 - The family of ionotropic glutamate receptors

1.5 Experimental approaches to neuroscience

There are significant challenges to experimental neuroscience, especially in the higher organisms such as mammals. As stated above, the brain is composed of many individual cells, which themselves are divided into many subtypes (neurones, astrocytes, microglia), and the neuronal population of the brain as a whole shows highly specific connectivity. The brain, in its native state, is a soft gel, extremely vulnerable to insults, whether they be metabolic (e.g. following an ischaemic incident such as a stroke) or physical (head impacts, cranial trauma, surgical intervention).

Due to the problems listed above, neuroscience has tended to be reductionist in much of its approach. Rather than trying to record and analyse from the entirety of the brain in concert, several sections of neuroscience employ smaller, less complex

systems. These may be simpler model organisms (with *Caenorhabditis elegans* and *Drosophila melanogaster* being popular choices), or simpler preparations dissected out from higher organisms, for example brain slices and dissociated cultures.

1.6 Dissociated neuronal cultures

All of the neuronal work in this thesis has been performed in the experimental context of dissociated embryonic cultures. In brief, the preparation of a culture involves the dissection out of brain regions from an animal (in this case embryonic (E) day 18 rat embryos), and the separation of this mass of tissue into individual neurones. These are then plated onto glass coverslips (with a suitable adhesive substrate) and then used 7-21 days later (for further details see Materials and Methods, Chapter 2). Dissociated cultures have been used for more than 30 years (Banker and Cowan 1977; Banker and Cowan 1979; Kaech and Banker 2006), and are a widely used experimental paradigm in neuroscience.

1.7 Advantages and disadvantages of dissociated neuronal culture

There are some disadvantages to dissociated cultures. The highly reductionist nature of cultures means the loss of specific patterns of brain connectivity. Intraneuronal wiring between cultured cells is effectively random, with a loss of the precisely defined connectome found in the intact brain. However, the simplified nature of dissociated cultures allows simpler questions regarding neuronal function to be addressed.

Neuronal cultures allow unprecedented access to neurones and their subcellular regions (soma, axon, dendrite and spines). The culture is effectively two dimensional, with neurones growing out across a flat substrate, and relinquishing the normal three dimensional environment found in the native brain. This 2-D arrangement allows ease of experimental access. In an imaging context cells are easily visible and there is no issue with imaging through layers of tissue. This is also true of light activation of proteins. In an electrophysiological context, access for

electrodes and manipulators is practical, and in both cases perfusing on different solutions and/or drugs is simple. In this thesis I have used the dissociated neuronal culture paradigm to explore several avenues of neuronal function, via several techniques, including electrophysiology (Chapters 3 and 4), imaging (all chapters), attempts to grow neurones in more complex extracellular environments (Chapter 7) and co-culture of other cell types (Chapter 8).

1.8 Optogenetics

The field of neuroscience is a relatively young area, pursuing a relatively difficult goal. The mammalian brain is in the head, encased in a hard bony skull, and has the consistency of a soft blancmange-like solid. It is composed of several billion individual neurones, which themselves come in a wide variety of different types. And this huge conglomeration of separate cells are wired and connected in precisely defined ways. This connectivity can be local (less than 1 mm) or not so local (axonal projections of 1 metre plus, e.g. cortico-spinal motor neurones).

Neurones are active on extremely fast time scales, in the order of milliseconds. To usefully monitor and perturb neuronal cells, circuits and systems, it is imperative that the experimenter has tools to be able to do this.

Historically electrophysiology has been one of the defining techniques to shape neuroscience. Neurones are highly electrically active cells, able to fire action potentials at a rate of several per second. Electrophysiology has made it possible to monitor these events, thanks to the advent of whole cell patch clamp electrophysiology.

While electrophysiology has undoubtedly revolutionized neuroscience, it is, by its very nature, intrusive. Both to stimulate or record from a cell or a region, the experimenter must physically perturb the local environment by the addition of an electrode. *In vivo* in mammals this is extremely challenging, as a window through the skull must be excised. Even in a dissociated culture paradigm, where access is relatively unfettered, the application of whole cell patch clamp techniques leads to dialysis of the neuronal intracellular solute, and washout of many of the cell's

signalling factors. Most forms of electrophysiology are also non-selective in a spatial sense. An electrode inserted into a brain slice or *in vivo* into an area of the brain will stimulate any neurones near it. This problem is avoided in whole cell patch clamp electrophysiology.

Electrophysiology has been combined with imaging for several years now. The advent of 2 photon microscopy, aligned and coupled to electrophysiological recording rigs has enabled neuroscientists to stimulate electrically, and then record calcium oscillations, or conversely, techniques such as glutamate uncaging allows the stimulation to be light based, and the recording electrical. For a broad review of the field of optogenetics see (Fenno L, Yizhar O et al. 2011).

1.9 Light sensitive proteins

Many organisms have endogenous proteins that are sensitive to light. Bacteria have light sensitive proteins (Oesterhelt and Stoeckenius 1971), plants are able to phototax and track the sun , *Drosophila melanogaster* larva have light sensitive neurones covering their larval body wall (Xiang, Yuan et al. 2010), as well as light sensitive proteins in their head. Mammals contain light-sensitive proteins in neurones in our retinas that allow us to sense the visible light spectrum (Hubbell and Bownds 1979).

1.10 Light sensitive proteins are typically highly conserved.

Proteins that cause currents across cell membranes in response to light were first discovered in 1971 (Oesterhelt and Stoeckenius 1971). This protein was a bacteriorhodopsin that acted as an ion pump, and was capable of being activated by light from the visible spectrum. Rhodopsins are typically highly conserved. They have 7-transmembrane regions, and use retinal as a co-factor to couple their activity (channel opening, pump activation) to photons of light (Henderson and Schertler 1990). Eight years later after Oesterhelt, another light sensitive protein from the

same family was discovered, the so called halorhodopsin (Matsuno-Yagi and Mukohata 1977). There was a significant gap before the discovery of channelrhodopsin-1(ChR1) in 2002 by Nagel (Nagel, Ollig et al. 2002). ChR1 is a light-activated proton pump, cloned from the free living algal species *Chlamydomonas reinhardtii,* which uses the channel for phototaxic behaviour. As ChR1 is a proton pump this meant that activation of this channel for sustained periods of time might result in significant changes in cellular pH. This is not particularly desirable as an experimental tool.

1.11 Channelrhodopsin-2

Channelrhodopsin-2 (ChR2) was discovered in 2003 by the same group that had cloned ChR1 (Nagel, Szellas et al. 2003). ChR2 is a nonselective cation channel; the main ion flow through the channel when open is sodium ions. This almost exactly mirrors the native neuronal ion flow responsible for the rising phase of an action potential. ChR2 only requires retinal as a cofactor, which is abundant in mammalian cells, and can be added to feeding media for invertebrates such as *C elegans* and *D melanogaster*. Figure 1.8 illustrates the activation of ChR2 and subsequent ion flow across the membrane. A recent study elucidated the crystal structure of a chimeric version of ChR1 and ChR2 down to a resolution of 2.3 angstroms (Kato HE, Zhang F et al., 2012) including the pore region.

It then took another two years before this new light-activated channel was first expressed in neurones. Expression of ChR2 in neuronal cells allowed the precise activation of the neurones, with pulses of blue light (Boyden, Zhang et al. 2005). Delivery of flashes of blue light (with a wavelength of approximately 470 nm) caused neurones expressing ChR2 to fire action potentials. This was true, non-invasive, optical activation of neurones.

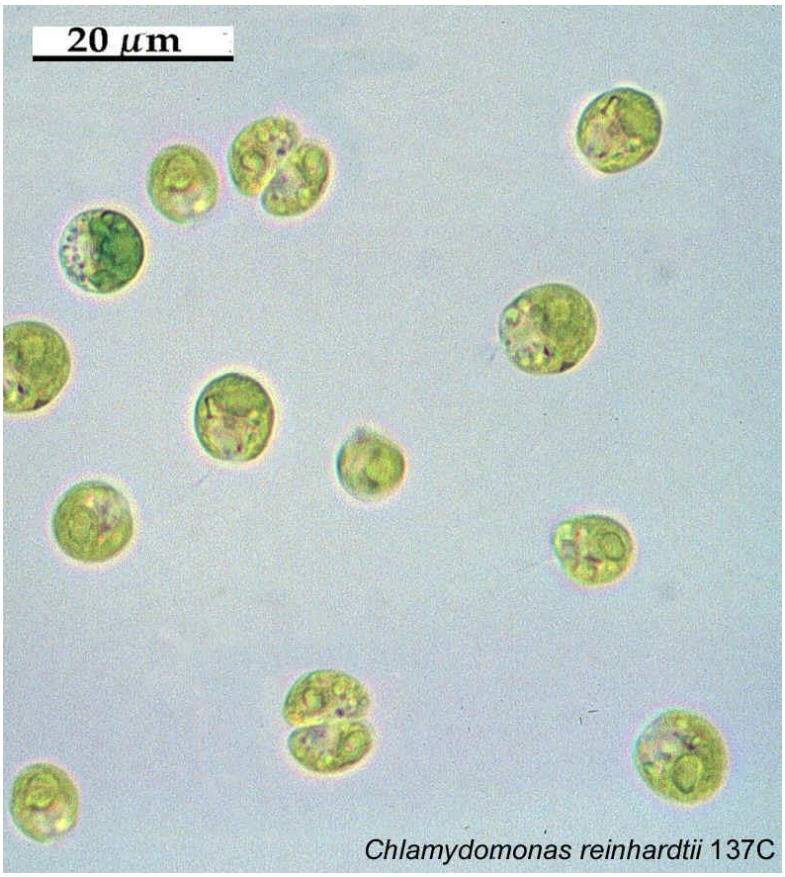

Figure 1.7 – example micrograph of *C reinhardtii*

Image showing the unicellular algal species *C reinhardtii*. Both ChR1 and ChR2 were isolated from this species

Scale bar 20 μm

Taken from (http://www.ibvf.cartuja.csic.es/Cultivos/micro-a-chlam.htm)

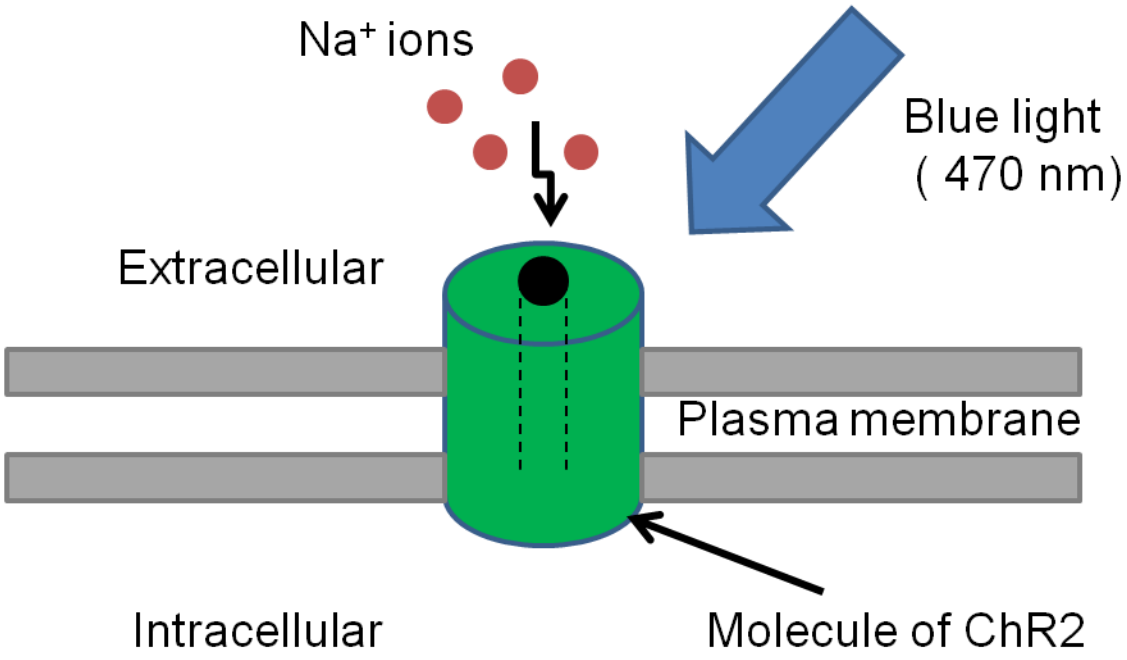

Figure 1.8 – Schematic of activation of ChR2

Activation scheme for ChR2. Upon illumination with blue light, ChR2 opens and lets cations pass across the membrane through the channel pore, resulting in a net depolarisation of the cell

1.12 Expressing an algal protein in mammalian cells

It is worth considering how unlikely this strategy was to begin with. Expressing a non-mammalian protein into neurones, which works without any need to add additional cofactors, and also is well expressed by neurones, which traditionally are considered some of the most fragile cells to work on. Not only that, but ChR2 is a 'single component' tool, encoded by one gene, expressed as one protein. ChR2 is in some ways the perfect experimental tool. Expression of ChR2 in neurones has very few off-target effects. In the absence of light resting membrane potential and neuronal membrane resistance are unchanged (Boyden, Zhang et al. 2005), nor is there any higher incidence of neuronal mortality in cells expressing ChR2.

1.13 The rapid expansion of optogenetics

After the initial breakthrough in 2005, the use of ChR2 began to spread quickly, with many laboratories worldwide adopting ChR2 and optogenetics, and utilising it in their research. ChR2 was shown to work in brain tissue (Deisseroth, Feng et al. 2006), and the first example of ChR2 being used in a freely behaving animal appeared in 2007 (Adamantidis, Zhang et al. 2007; Aravanis, Wang et al. 2007). At the time of writing (early 2011) optogenetics has blossomed into a far more complex field, with various light-sensitive proteins being available for the researcher, transgenic animals expressing ChR2 (or a variant), and many companies are providing pre-made highly sophisticated light-delivery equipment.

1.14 The need for optogenetics

As briefly mentioned above, electrophysiology has some disadvantages. The most telling one is the lack of selectivity. Passing a current through an electrode affects any cells near the tip of the electrode. As the brain is composed of tightly packed neurones, often with radically different functions (compare say excitatory glutamatergic cells surrounded by inhibitory GABAergic neurones and their combined astrocytic partners), this lack of selectivity is experimentally undesirable. A current step delivered to the area described above would depolarise excitatory and inhibitory neurones alike, and presumably cause crosstalk within the circuit (see figure 1.9 for a diagrammatic representation of this).

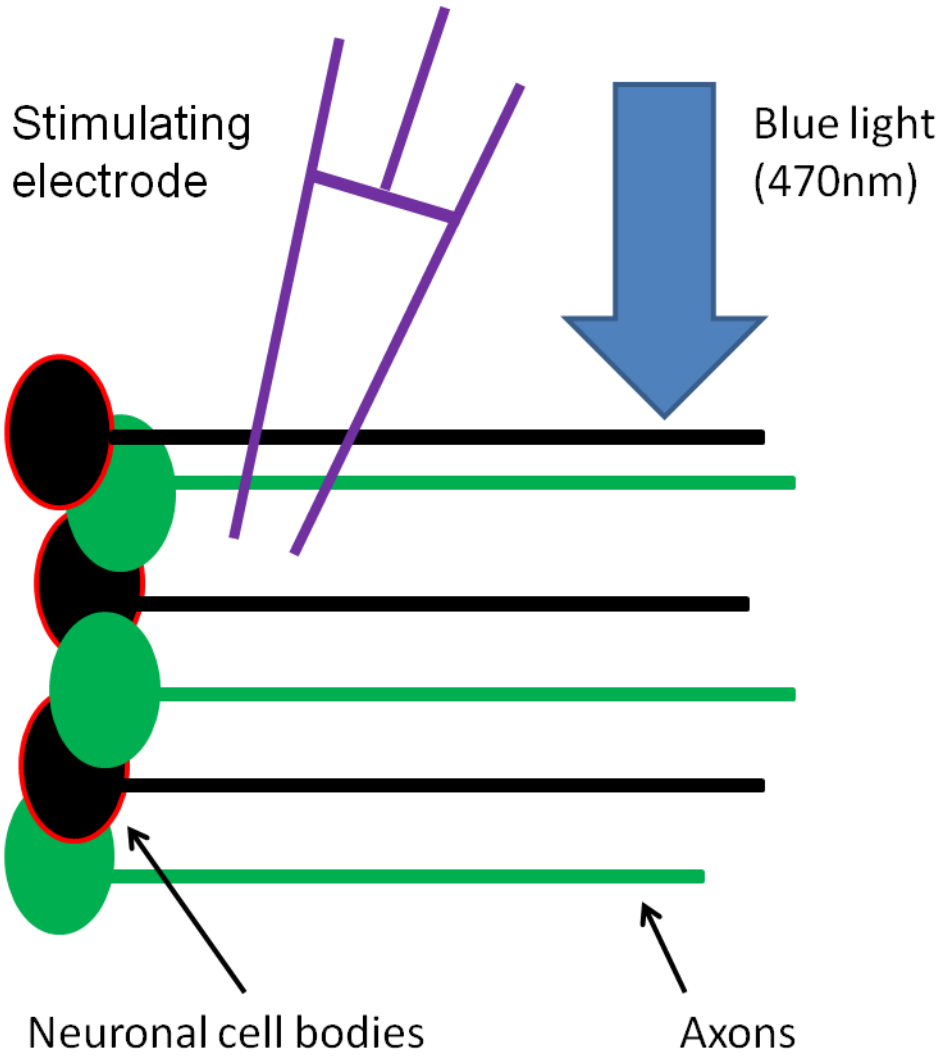

Figure 1.9 – Example of how optogenetics can target a cell type whilst leaving neighbouring cells unaffected

Neurones expressing ChR2 are depicted in green, non-expressing neurones are depicted in black. Stimulating pulse from electrode causes activation in all neurones/axons near electrode tip. Shining blue light onto region only activates green cells expressing ChR2. Adapted from (Deisseroth 2011)

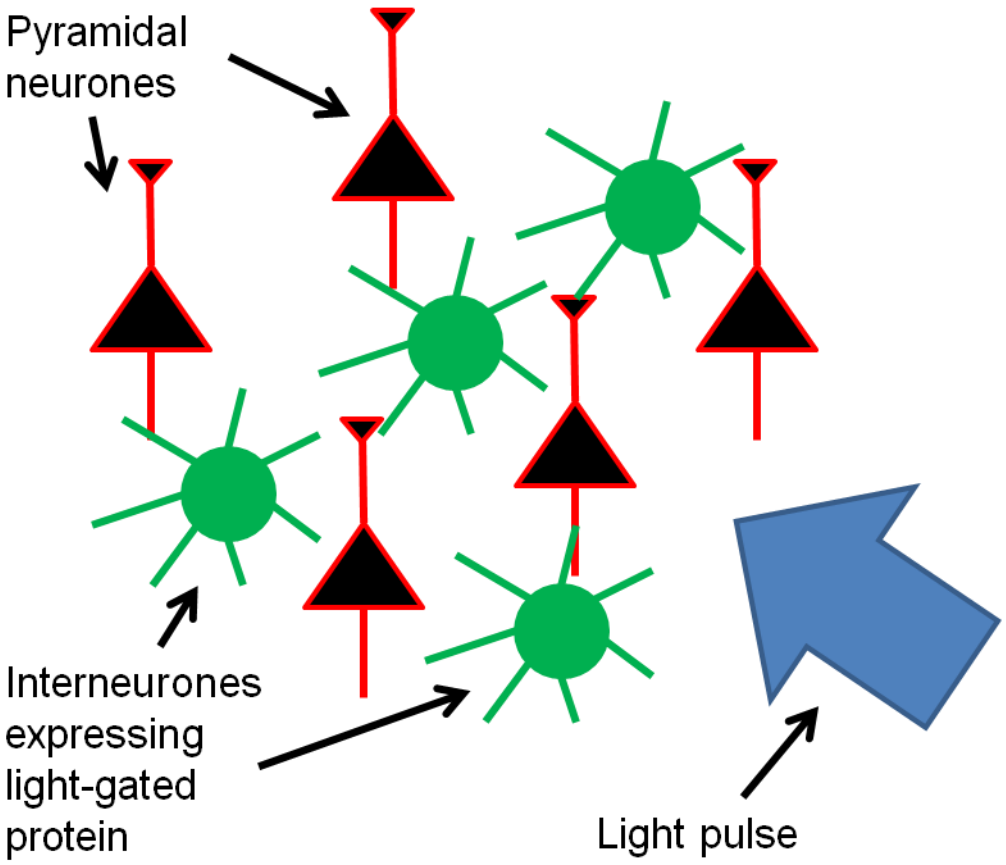

Figure 1.10 – Example of how optogenetics can target a cell type whilst leaving neighbouring cells unaffected

Green cells – interneurones, black cells – pyramidal primary neurones. In this example, ChR2 (or NpHR) has been targeted to a specific sub-class of interneurones (for example, parvalbumin-containing interneurones). By expression of the relevant light-gated protein, the inhibitory network can be silenced (NpHR activation leading to hyperpolarisation leading to silencing) or activated (ChR2 activation leading to membrane depolarisation leading to action potential generation). Notice the network is still intact, and that particular cells within the intact network can be selectively perturbed

1.15 The spread of optogenetics

Initially characterisation studies of light-gated channels were performed in classic model systems, such as xenopus oocytes (Nagel, Ollig et al. 2002; Nagel, Szellas et al. 2003; Nagel, Szellas et al. 2005), cell lines (Sineshchekov, Jung et al. 2002; Suzuki, Yamasaki et al. 2003; Zimmermann, Terpitz et al. 2006) and finally dissociated neuronal culture (Boyden, Zhang et al. 2005; Li, Gutierrez et al. 2005). Expression of ChR2 and other light-gated proteins was then moved into brain slices from intact animals expressing typically ChR2 (Ishizuka, Kakuda et al. 2006; Petreanu, Huber et al. 2007; Wang, Peca et al. 2007).

1.16 Potential disadvantages and problems with rhodopsins

1.16.1 Expression of light-sensitive proteins and their trafficking

Most uses of ChR2 and other proteins requires that the target protein is a/ targeted directly to the cell type of interest, and b/ expressed at a sufficient level in those target cells, and c/ trafficked to the appropriate location in those cells.

Various methods have been used to deliver DNA coding for rhodopsins to neuronal cells, including microinjection (Nagel, Szellas et al. 2003), transfection/ Nucleofection (Chater, Henley et al. 2010), biolistics (Zhang and Oertner 2007), and viral infection (Boyden, Zhang et al. 2005). One partial disadvantage of the use of ChR2 and its optogenetic stable mates is the need to genetically modify cells/organisms.

Expressing a protein of interest is not necessarily trivial; expressing proteins in a cell-type specific manner can be achieved by cell-type specific promoters (for example CAMKII for neurones), but access to specific intracellular sites can be more difficult. The initial version of NpHR showed significant trafficking problems (Zhang, Aravanis et al. 2007), where the protein appeared to be collecting in the endoplasmic reticulum (ER) and causing intracellular blebbing. This pathology, and the low level

of NpHR arriving at the surface of the cell, was addressed by improving the signal peptide, and adding an ER export sequence (Zhao, Cunha et al. 2008).

1.16.2 Access to tissue

Access is both an advantage and a disadvantage in the case of light-gated proteins, depending on which model organism one is working in. In optically transparent systems and organisms, illuminating the cells expressing the rhodopsin is usually easy. *C elegans* (Nagel, Brauner et al. 2005; Mahoney, Luo et al. 2008), *D melanogaster* (Schroll, Riemensperger et al. 2006; Zhang, Ge et al. 2007), and cell lines (Zimmermann, Terpitz et al. 2006; Chater, Henley et al. 2010) are all effectively optically transparent, and gross illumination of the dish containing either the cells or the animal will be sufficient to activate the light-gated proteins.

However, when working in higher organisms access is less flexible. As with *in vivo* electrophysiology, access to the brain of mammals must be gained via the skull, and long term imaging/stimulation protocols require this opening into the cranium to be kept sterile and infection free for considerable periods.

Additionally, light must be directed to the area of the brain expressing the rhodopsin of interest. This is relatively easy of the target is a cortical layer near the surface of the cortex, but deeper sub-cortical sites require the insertion of an optic fibre or some other light-delivery device to the site. As with *in vivo* electrophysiology, and other chronic implant experiments, the tract left by the insertion of the fibre/electrode/cannula is damaged and may contribute to off-target effects or increased infection risk.

This aside, there are now several companies selling ready-made devices, that can both deliver light into the brain (usually via an optic fibre connected to a light source) and record electrical activity. The arrival of the ‘optrode’ (a portmanteau of optic and electrode) has allowed light stimulation deep within the brain whilst simultaneously recording neuronal electrical activity (see (Deisseroth, Feng et al. 2006; Zhang, Laiwalla et al. 2009; Zhang, Laiwalla et al. 2009; Wang, Borton et al. 2010)).

1.16.3 Innate channel properties

The protein tools for optogenetics have come entirely from non-mammalian sources, and have evolved to do specific roles in their host cell. However undoubtedly useful ChR2 and NpHR have been when expressed in neurones, there are some aspects of channel function that are not desirable. This includes the targeting problems mentioned above, but also some more innate features of the channels and pumps. For example, ChR2 lets Ca^{2+} pass through its pore (see Nagel, Szellas et al. 2003). The ratio of Ca^{2+} to Na^{+} (I_{Ca}/I_{Na}) carried by ChR2 has been measured at 0.5, however this varies amongst mutated ChR2 variants between 0.1 and 0.8 (Kato HE, Zhang F et al., 2012) . Whilst this will contribute to the depolarisation of the cells membrane (a desired effect) it will also trigger intra-cellular calcium-dependent changes. In some cell types this may not be a problem, but in studies of synaptic plasticity at the level of dendritic spines, expression of a calcium-permeable channel in the spine head may produce off-target plasticity phenomena.

1.16.4 Choice of light wavelength

One potentially restrictive part of utilising ChR2 and other rhodopsins in an experimental context is choosing the right rhodopsin, and the right complementary fluorophore. If one is attempting to stimulate with ChR2 (optimal excitation wavelength 470nm) then this wavelength cannot be used to image and track fluorescent proteins. For example, in the case of ChR2, the excitation wavelength overlaps with the excitation spectrum of green fluorescent protein (GFP). When blue light is shone onto the sample to excite the GFP, and spatially localise the protein GFP is attached to, the blue light will also cause ChR2 opening, and membrane depolarisation. It is therefore imperative that a suitable rhodopsin/fluorophore pair is chosen. This is equally true when two rhodopsins are to be employed in the same preparation. ChR2 and NpHR are well separated in their excitation profile (ChR2 responds to blue light, NpHR to orange light), and have been successfully combined (Li, Gutierrez et al. 2005). The excitation profile of VChR1 is red-shifted, moving it

away from ChR2/GFP (Zhang, Prigge et al. 2008), making it a useful addition to the optogenetic toolbox.

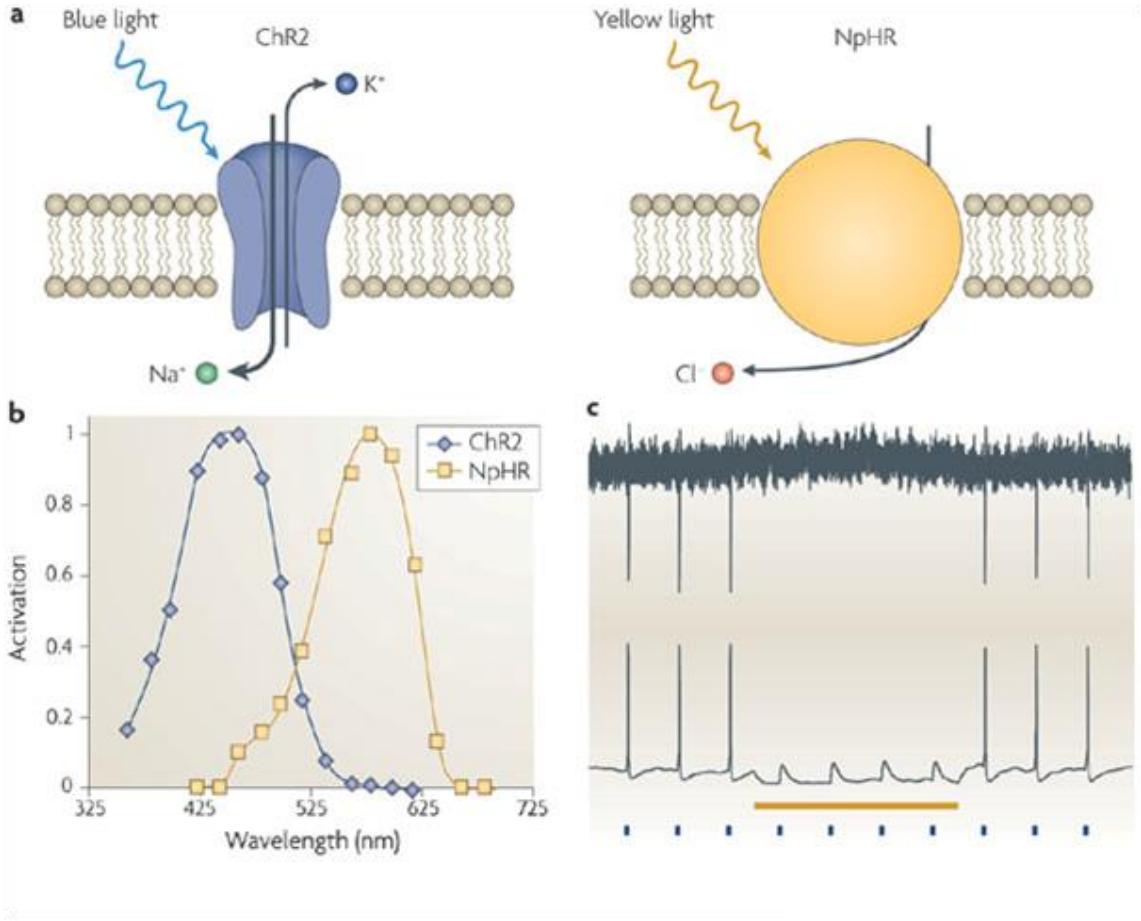

Figure 1.11 – The principle underlying neuronal excitation or inhibition with ChR2 and NpHR

a/ ChR2 is a non-selective cation channel activated by blue light, NpHR is a chloride pump activated by yellow light

b/ Comparison of the activation spectrum of ChR2 and NpHR. Notice activation peaks are well separated, and thus are capable of being switched on separately

c/ Example traces of action potential generation following blue light pulses, and action potential inhibition when yellow light is delivered to the cell. This inhibition is sufficient enough to prevent ChR2 activation (blue light) driving action potential generation

Taken from (Zhang, Aravanis et al. 2007)

1.17 The advantages of ChR2 and other light-gated proteins

The ability to target a light-gated protein to a particular class of neurone has been widely exploited by researchers. As represented in figures 1.9 and 1.10, if expression of the light-gated protein is sufficient and correctly trafficked to the cell's surface, this method allows unprecedented control over the remote activation of either single (for example Douglass AD, Kraves S et al., 2008), or groups, of neurones (for example Huber D, Petreanu L et al. 2008).

1.17.1 Spatial-temporal resolution

Optogenetics allows precise spatial and temporal control of neuronal activity in target cells expressing a particular rhodopsin (Boyden, Zhang et al. 2005; Li, Gutierrez et al. 2005). ChR2 can be switched on and off with millisecond temporal resolution (Boyden, Zhang et al. 2005), and newer rhodopsins have even faster kinetics (Gunaydin, Yizhar et al. 2010; Kleinlogel, Feldbauer et al. 2011). Spatial resolution of rhodopsin activation depends largely on the experimental set up (whether the light source is a laser beam or a LED for example), but sophisticated scanning techniques using 2-photon microscopy allow illumination of small regions of brain (sub-femtolitre excitation volumes, see (Helmchen and Denk 2005) and (Andrasfalvy, Zemelman et al. 2010)), and may be employed in the future to activate rhodopsins.

On a different note, multiple cells can be activated at once with light-based stimulation protocols. It is straightforward in an experimental context to apply whole field illumination (via LEDs or fluorescence bulbs, for example (Chater, Henley et al. 2010) and (Boyden, Zhang et al. 2005)), resulting in light-driven currents in all cells expressing the rhodopsins. Again, this widespread activation of a specific cell type is difficult to achieve with other methods.

1.17.2 Reversibility

Similar to other stimulation techniques, optogenetic activation or inhibition of cells is completely reversible. Cells are only depolarised (in the case of ChR2) when blue light is irradiating the sample. Cessation of the light stimulus leads to the ChR2 molecules closing, and ions stop flowing across the membrane. This feature of optogenetic activation allows temporally precise control of neuronal activity in a fully-reversible fashion.

1.17.3 Selective stimulation

The clearest advantage of optogenetics is the ability to selectively activate a set of neurones that are embedded in native brain tissue. Brain tissue is typically a dense mass of many cell types, (see (Ascoli, Brown et al. 2009; O'Connor, Huber et al. 2009; Otsuka and Kawaguchi 2011) as examples) and specifically targeting a subset of neurones is outside the scope of electrophysiological or drug-perfusion stimulation. However, optogenetics allows cell specific targeting (see (Katzel, Zemelman et al. 2011)), and even sub-cellular specific targeting (see (Lewis, Mao et al. 2009)). The development of rhodopsins as a neuronal control systems has not yet fully explored the possibilities for targeting of light-gated proteins to intracellular lipid bilayers (for example mitochondrial membranes) and intracellular control of function may well be possible. It is worth mentioning that light-based stimulation if cells is not restricted to neurones. Because of neurone's highly electrically active nature they are ideal candidates for rhodopsin based control systems, but other cell types may also be valid. Muscle cells have already been made to express rhodopsins in *C elegans* (Nagel, Brauner et al. 2005), with light stimulation of ChR2 producing strong contractions in these cells.

1.17.4 Light intensity

As with electrical stimulation, the level of the input into the slice/brain region can be modulated. Decreasing the light intensity will reduce the spread of light, and make smaller the cubic volume of the illuminated brain tissue, resulting in fewer and fewer neurones being activated as the light is turned down. An example of this was

shown in a study published in 2008. The group expressed ChR2 in mouse cortex, and showed that decreasing the light intensity allowed them to perturb and alter the animal's choice behaviour with optical activation of as few as 300 neurones firing a single action potential each (Huber, Petreanu et al. 2008). Decreasing or increasing stimulation intensity is possible with electrophysiological methods, but without the cell-specific targeting available to optogenetics.

1.17.5 Mapping of neuronal projections and connectivity

As stated above, stimulation based on light-gated proteins requires that those proteins be properly expressed, and trafficked, by the target cells. In neurones, with their complex dendritic arbour, and long projecting axons, this is no simple task. However, if this requirement is achieved, then shining light of the correct wavelength onto any part of the neurone expressing the light-gated protein should induce a de- or hyperpolarisation. Because of this, ChR2 has been used as a neuronal mapping tool. The flexibility and advantage of ChR2 here is the ease of moving the stimulation device, i.e. the light beam. Several groups have used this particular advantage to map neuronal circuitry and connectivity in the brain (Arenkiel, Peca et al. 2007; Petreanu, Huber et al. 2007; Wang, Peca et al. 2007). This is depicted in figure 1.12.

1.18 Diversity of light-gated proteins

Since the initial discovery of light-gated proteins (Oesterhelt and Stoeckenius 1971), and the more recent development stemming from the channelrhodopsins (Nagel, Ollig et al. 2002; Nagel, Szellas et al. 2003; Boyden, Zhang et al. 2005), the field has diversified in the amount of light-gated proteins cloned and adapted for experimental use.

At first ChR1 (a proton pump) and ChR2 (a non-selective cation channel) and NpHR/Halo (a chloride pump) were cloned and expressed in cells (Nagel, Ollig et al. 2002; Nagel, Szellas et al. 2003; Zhang, Wang et al. 2006; Han and Boyden 2007). The usefulness of this approach was immediately apparent, and labs began

searching for, and mutating, more light-gated channels. Table 1.1 provides a list of currently available rhodopsins.

1.19 Biophysics of ChR2

As stated above, ChR2 is a non-selective cation channel, able to let pass K^+, Na^+, Ca^{2+} and H^+. The individual conductance (γ) of a ChR2 molecule is low, estimated at less than 1picoSiemen (pS) (Nagel, Szellas et al. 2003; Lin, Lin et al. 2009). Because of this small unitary conductance, ChR2 molecules must be expressed in sufficient numbers to drive a sufficient depolarisation of the cell. This requires a strong promoter specific for the cell type of interest.

ChR2 is a strong inward rectifier (Chater, Henley et al. 2010). It is not yet known if this is an innate property of the rhodopsin, or if it is due to some intracellular block (e.g. similar to the amine block of certain AMPAR subunits).

The main aim of this thesis was to better understand the gating and kinetics of ChR2 when expressed in both a cell line, and in dissociated neuronal culture.

Name	Species	Reference
ChR1	*Chlamydomonas reinhardtii*	*(Nagel, Ollig et al. 2002)*
ChR2	*Chlamydomonas reinhardtii*	*(Nagel, Szellas et al. 2003)*
NpHR/Halo	*Natronomonas pharaonis*	*(Li, Gutierrez et al. 2005)*
ChR2/H134R	*Chlamydomonas reinhardtii*	*(Lin, Lin et al. 2009)*
ChETA	*Chlamydomonas reinhardtii*	*(Gunaydin, Yizhar et al. 2010)*
VChR1	*Volvox carteri*	*(Zhang, Prigge et al. 2008)*
VChR2	*Volvox carteri*	*(Kianianmomeni, Stehfest et al. 2009)*
ChR2/C128X/ D156A	*Chlamydomonas reinhardtii*	*(Lin 2011)*
ChD	*Chlamydomonas reinhardtii*	*(Lin 2011)*
ChEF	*Chlamydomonas reinhardtii*	*(Lin, Lin et al. 2009)*
ChIEF	*Chlamydomonas reinhardtii*	*(Lin, Lin et al. 2009)*
CatCh	*Chlamydomonas reinhardtii*	*(Kleinlogel, Feldbauer et al. 2011)*
OptoXRs	*Chlamydomonas reinhardtii*	*(Airan, Thompson et al. 2009)*

Table 1.1 – a list of rhodopsins currently in use

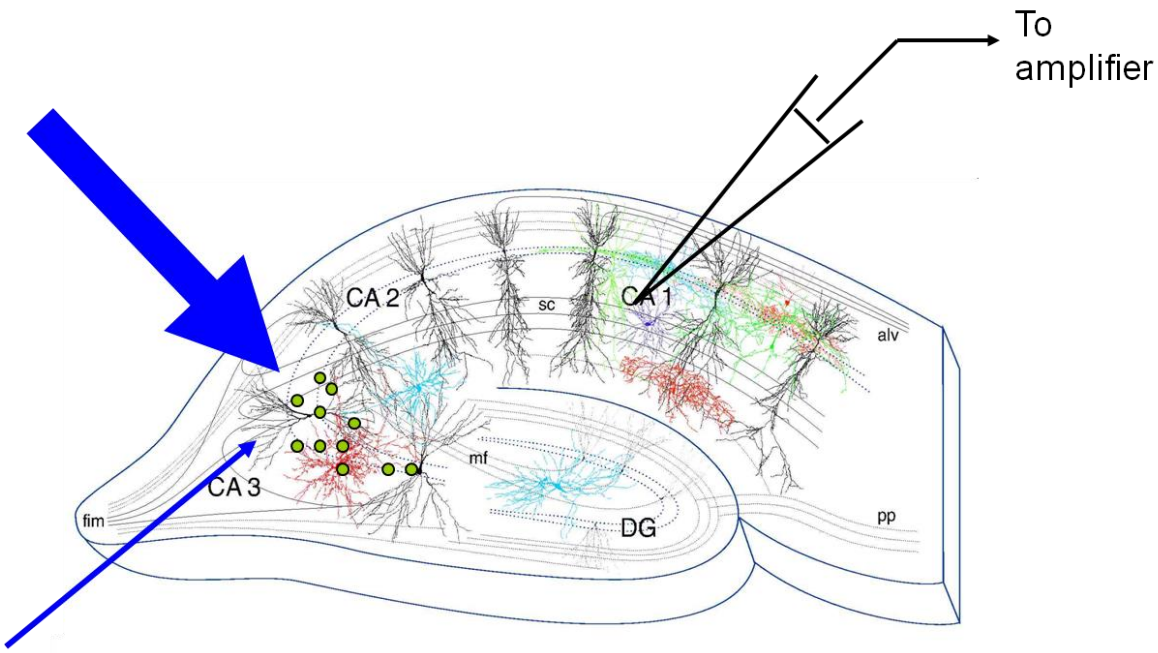

Figure 1.12 – Example of use of optogenetics in a hippocampal slice

This shows a hippocampal slice. Cells have been made to express ChR2 (green circles, left hand side) either by viral infection, biolistic transfection, or transgene expression I the intact animal.

While recording in the CA1 layer (top right), expressing cells can be activated either by whole field illumination (top left, large blue arrow) or more selective scanning via a laser beam (thin arrow, bottom left)

1.20 Future potential of optogenetics

This field of optogenetics is still extremely young, and will continue to expand over the next decade.

1.21 Channel modification and mutagenesis projects

As hinted in the table above, many labs are adapting naturally occurring rhodopsins to do particular jobs. This is typically done by either mutating particular residues in the channels pore (for example or light-sensing region, or creating chimeras by fused genes from two channels together (ChEF and ChIEF, (Lin, Lin et al. 2009)).

However mutagenesis projects as driven by the Tsien and Deisseroth labs are not the only way forward, nor in many respects are they the ideal way. Any changes to a channel or pump's sequence usually has more than one effect. Light sensitivity may be increased at the expense of opening kinetics for example. For this reason it is highly unlikely a protein such as ChR2 would be able to have the kinetics of an AMPAR conferred upon it by successive mutagenesis cycles.

One more promising strategy is the chimeric conversion of light-insensitive proteins (e.g. ionotropic membrane proteins) by the attachment of light-sensitive regions.

1.22 Human disease treatments

Karl Deisseroth, one of the main drivers of the field of optogenetics has suggested a role for optogenetics in treating human disease states. Deep Brain Stimulation (DBS) requires the insertion of an electrode into deep, sub-cortical areas, in order to treat disease such as depression, obsessive compulsive disorder (OCD) chronic pain, epilepsy and Parkinson's. Deisseroth (a qualified and practising psychiatrist) has opined that DBS could be replaced with optical-based stimulation (Zhang, Aravanis et al. 2007; Gradinaru, Mogri et al. 2009) . Underactive cells could be led to express a depolarising rhodopsin (a ChR2 variant perhaps), and their activity could be upregulated with pulses of light. Conversely, overactive cells or circuits could be quietened or silenced via the expression of NpHR/Halo. This has

some advantages over traditional DBS. Insertion of an electrode into the brain leads to glia activation, and the formation of a glial scar at the site of the electrode. Over time, this scar increases in size and means that the amplitude of the current has to be turned up and up, to achieve the same level of activation. Electrical DBS is also non-specific, with any neurones physically nearby the electrode tip being activated. Light-based activation could potentially avoid these issues. However, optical DBS would require stable gene expression deep within the human basal ganglia, and that hurdle has yet to be overcome.

1.23 Vision

One extremely promising research direction for optogenetics is in the field of visual defects. In mice models of blindness ChR2 has been used to restore sight (Thyagarajan, van Wyk et al. 2010; Tomita, Sugano et al. 2010). This is a much less challenging area to attempt to port this technology into human sufferers, due to the superficial nature of the disease site (retina vs. intracranial sub-cortical regions), and the concomitant decrease in surgical risk (no opening of skull et cetera).

1.24 Alternatives to optogenetics

As briefly mentioned previously, optogenetics is not the only method capable of remote activation of cells. Glutamate uncaging is also a remote non-invasive technique. In glutamate uncaging, a solution with ‘caged’ glutamate molecules is perfused onto the preparation. Stimulation with light (usually a UV laser) frees the glutamate from its partner cage molecule and allows it to bind to targets on nearby tissue. Glutamate uncaging has been successfully used to stimulate spine growth (Kwon and Sabatini 2011) and map connectivity (Ashby and Isaac 2011). Uncaging has some advantages over optogenetics, as there is no need to express a protein of interest in the target cell type, and the use of endogenous ligands (such as glutamate) maintains the physiology of the system to a greater extent.

Receptor proteins have also been created with a ligand attached by a short, light-sensitive tether. These are termed small molecule photoswitches. Irradiation of the molecules causes a conformational change in the tether region, which physically moves the ligand to the binding site of the receptor. Binding then occurs and the receptor is active. Examples include SPARK, a synthetic photoisomerisable azobenzene-regulated K+ channel (Chambers, Banghart et al. 2006), and LiGluR, a light-activated glutamate receptor (Volgraf, Gorostiza et al. 2006). For a fuller discussion of the current variety of light-activated tools available to the experimenter, see (Kramer, Fortin et al. 2009).

1.25 An all-optical experiment?

There is now in existence a range of tools for the neuroscientist to choose from that all rely on optical methods for both stimulation and recording. Techniques for optically monitoring changes in biological tissue are already widely used, and are become more sophisticated. Imaging of intracellular calcium levels, via a calcium-binding dye (e.g. FURA-2) can provide a readout for neuronal activity, as can the family of voltage sensitive dyes.

Reporters can either be perfused on (such as FURA-2) or genetically encoded. Both genetically encoded calcium indicators (GECIs, for example GCaMP2, see (Wilms and Hausser 2009)) and genetically encoded voltage sensors (for example FlaSh, see (Baker, Mutoh et al. 2008; Perron, Mutoh et al. 2009) for review) are currently available. For a fuller discussion of strategies to engineer light-sensitive proteins see (Moglich and Moffat, 2010).

Using ChR2 to stimulate, and one of the methods above to record, allows the entirely of the live experiment to be performed without physically touching the target tissue. With the advent of more and more powerful rhodopsins, chimeric light-sensitive proteins, and more sophisticated reporters, all-optical experiments are likely to become commonplace in the field of neuroscience.

1.26 Aims of this thesis

The main aims of this investigation was

1- to be able to express Channelrhodopsin-2 in mammalian cell lines, and characterise the behaviour of the channel in response to blue light illumination.
2- to then express ChR2 in neuronal cells and characterise the behaviour of the channel in a neuronal context
3- to use ChR2 to drive action potential generation in neurones, and to use this to explore neuronal function

Chapter 2

Materials and Methods

Unless otherwise stated, all incubators are at 37ºC and 5% CO_2.

2.1 Constructs

Unless otherwise stated, all constructs were a kind gift from Dr. Karl Deisseroth, Stanford University. Plasmids coding for ChR2-EYFP, ChR2-mCherry, and NpHR-EYFP were used in this thesis.

2.2 Coverslip preparation

Coverslips were prepared by washing in 100% ethanol, and then flaming. Dry sterile coverslips were then coated with 1mg/ml Poly-L-Lycine (dissolved in water) and left overnight in an incubator at 37ºC, 5%CO_2. The next day coverslips were washed three times with distilled water and once with plating media, then placed into 35mm wells containing 2 ml plating media.

2.3 Dissection and Neuronal Culture

Pregnant Wistar rats were overdosed with isofluorane until cardiac arrest was induced, then decapitated. E18 embryos were removed and placed in HBSS. Brains were removed from the skulls and cortex and hippocampus dissected out under a dissecting microscope. Hippocampi and cortex were pooled separately, and washed three times with HBSS (10ml and 30ml respectively). Brains were then incubated with trypsin (0.5 mg ml) in a water bath set at 37ºC for 9 or 15 minutes respectively. Brains were then washed another four times in HBSS.

Cortical samples were then suspended in 5ml plating medium (Neurobasal {Gibco}, supplemented with horse serum {10%}, B27 {Gibco}, penicillin/streptomycin and 2mM glutamine), then mechanically dissociated by repeated triturating (10-20 times) with a 5ml pipette. Samples were then made up to 20ml and then filtered through a 70µl cell strainer to remove excess debris.

Hippocampal samples were added to 1ml plating media, then mechanically dissociated by trituration with a P1000. This cell suspension was then made up to 5ml with plating media.

Cell number was then counted using a haemocytometer and diluted to 2 million cell per millilitre (cortical) and 0.5 million cells per millilitre (hippocampal). Cells were then added to pre-prepared wells contained 2ml plating media and coverslips, and placed in an incubator. 2 hours after plating cells, the media was completely replaced for feeding media (same composition as plating media described above, minus the horse serum), and the cells were returned to the incubator. Cells were then fed with 0.5ml feeding media every 5 days until they were used.

2.4 HEK293 Cell Culture

HEK293 cell lines were defrosted from a liquid nitrogen cryostore by immersion of Eppendorf in a 37^{o}C water bath. Straight after defrosting, cells were gently pipetted into a T75 flask containing warm (37^{o}C) DMEM. HEK cells were then cultured in DMEM (Lonza) containing 10% foetal bovine serum, penicillin/streptomycin and 2mM glutamine. Flasks containing cells were then kept in an incubator, and passaged approximately every 4-5 days. Passaging involved rinsing the cells with pre-warmed (37^{o}C) phosphate buffered salt solution (PBS) then replacing this with 2 ml of trypsin. The trypsin was left on for 2 minutes, then aspirated and replaced with 10 ml DMEM (as described above). Trituration ensured even dispersal of now detached HEK cells, and they were counted using a standard

haemocytometer. Cells were then replated at a concentration of 1 million cells per T75 flask.

2.5 Amaxa Nucleofection

Cells were passaged 2 days prior to transfection. Cells were transfected with the Amaxa Nucleofection device as per the manufacturers instructions. Briefly, cells were resuspended in solution from Nucleofector Kit V following the Amaxa guidelines for cell-line transfection. 100 µl of 2-5 x 10^6 cell suspension mixed with 3µg DNA was transferred to the supplied cuvette and nucleofected with an Amaxa Nucleofection device (Amaxa). Post transfection, cells were plated onto PLL-coated coverslips at a density of 100 cells per mm^2. Cells were then used for experiments 2-5 days later.

2. 6 Lipofectamine Transfections

To induce ChR2 expression in neurones, cells were transfected using Lipofectamine^{2000} (Invitrogen) with 2-5µg DNA per dish, and used in experiments 2-5 days later. Briefly, 2 eppendorfs were prepared, both containing 100 µl Neurobasal. Tube 1 had between 1-5 µg DNA , and tube 2 had Lipofectmaine^{2000} at the ratio 1µg DNA to 1.5 µl Lipofectmaine^{2000}. Tubes were briefly vortexed, and then left for 5 minutes. Then tube 2 was added to tube 1, and the mixture was vortexed again and left for 20 minutes to allow DNA-Lipofectamine complexes to form. Meanwhile coverslips with neurones for transfection were moved from their standard feeding media to feeding media without penicillin/streptomycin with a brief rinse in unadulterated Neurobasal. After 20 minutes the 200 µl of DNA-Lipofectamine mix was added dropwise to each coverslip, and returned to the incubator for 45 minutes to an hour. Then the coverslips were again briefly rinsed in plain Neurobasal (to remove any remaining DNA-Lipofectamine) and returned to their original dishes.

Depending on construct, expression of proteins coded for in added plasmids was seen 24-72 hours later.

2.7 Electrophysiology

For all the electrophysiological recording the patch-clamp rig was set up as shown below.

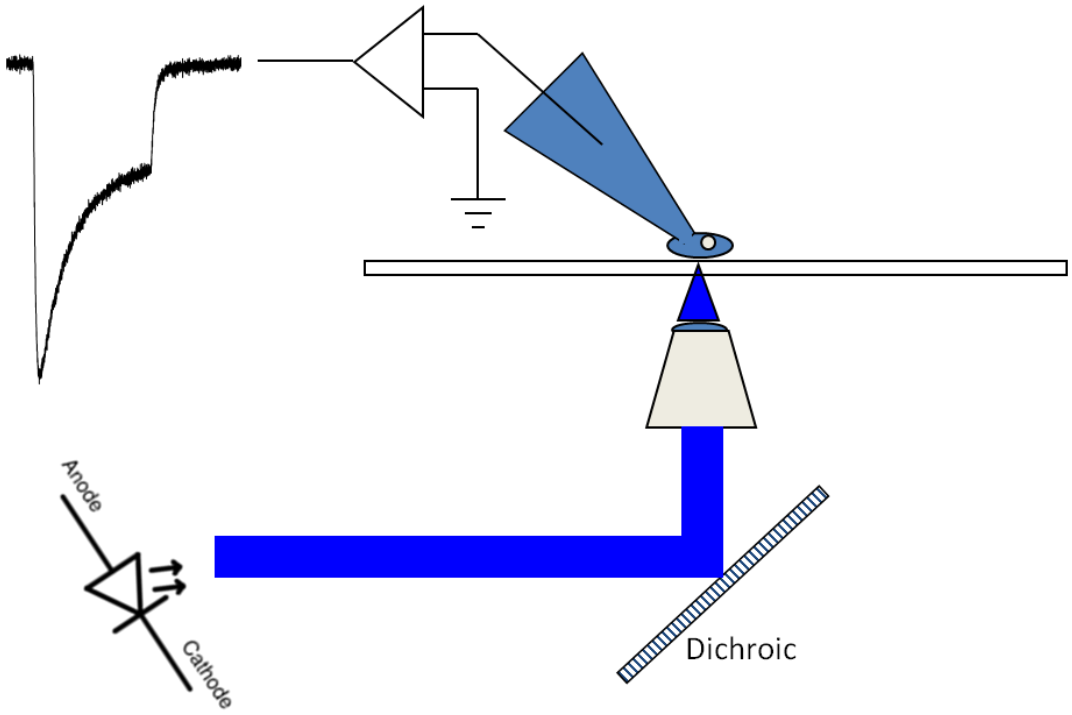

Figure 2.1 – electrophysiological set up

A transfected cell (on a glass coverslip) is placed in the chamber and whole-cell patch-clamped. Light from an OptoLED device (Cairn) is shone up through the objective via a dichroic mirror. Current responses are recorded on a computer running pClamp (Axon Laboratories)

2.7.1 Intracellular recording solutions.

Intracellular solutions were made up according to these recipes.

Potassium Gluconate (KGlu)

Molecule	Mr	mM	g/L	mg/100ml
K Gluconate	234.2	130	30.446	3044.6
KCl	74.6	20	1.492	149.2
HEPES free acid	238.3	10	2.383	238.3
EDTA	380	0.2	0.076	7.6
GTP Na salt	523	0.3	0.1569	15.69
ATP Mg salt	507	4	2.028	202.8

Caesium Gluconate (CsGlu)

Molecule	Mr	mM	g/l	mg/100ml
CsMeSO4	228	130	29.64	2964
NaCl	58.44	20	1.1688	116.88
HEPES free acid	238.3	10	2.383	238.3
EGTA	380	0.2	0.076	7.6
GTP – Na salt	523	0.3	0.1569	15.69
ATP – Mg salt	507	4	2.028	202.8

pH both to 7.3 with CsOH

2.7.2 Extracellular Solution

Whole cell patch clamp recordings were made from single cells visualized using an inverted microscope (Nikon TE300). Experiments were performed at room temperature (~22ºC) or 37ºC. The bath contained a HEPES-buffered saline solution containing (mM) NaCl, 135; KCl, 5; HEPES, 10; MgCl2, 1; CaCl2, 2; d-glucose, 30; ～310mOsm, and pH to 7.3 with NaOH.

Patch pipettes were filled with a potassium gluconate-based solution of the following composition (mM) K-Gluconate, 130; KCl, 20; HEPES, 10; EGTA, 0.2; GTP-Na salt,0.3; ATP Mg salt,4; ～295mOsm, and pH7.3 with KOH;

All voltage-clamp potentials have been corrected for a 15mV liquid junction potential.

Channelrhodopsin 2 was activated with a Cairn OptoLED 'Royal Blue' light source The OptoLED device was attached to the epifluorescence port of the microscope. The Cairn device was controlled by Axon Laboratories pClamp software, which allowed control of the intensity and duration of the light pulses produced by the LED. Light intensity was varied by changing the amount of current passing through the LED between 0 and 1.1 Ampere. Using an optical power meter (Spectra Meter 407A) we confirmed that the LED current was proportional to the light intensity in our sample plane. Unless otherwise stated, all experiments use a 1A LED current to elicit ChR2 responses.

For all the data collected from HEK293 cells, current responses to light pulses were recorded in voltage clamp using pClamp software .

Neuronal current responses to light pulses were recorded in voltage clamp for the majority of the experiments, but some employed the whole cell current clamp configuration.

Some recordings used the loose-patch configuration in voltage clamp to non-invasively characterise ChR2-mediated action potential responses. In these

recordings pipettes were filled with standard extracellular solution, as described above. This configuration is explained in more detail in Chapter 4

Sample frequencies were 10 or 20 kHz and data were filtered at 3 or 5 kHz using the 4 pole Bessel characteristic filter inherent to the patch clamp amplifier (Axon Instruments, Axopatch 200B).

2.8 Transformation of DH5α competent cells

Chemically competent *E.coli* (DH5α) prepared by the Inoue method (Sambrook and Russell, 2001) were thawed on ice. Next a mixture of 1µl cDNA and 10 µl DH5α was kept on ice for 30 minutes. The mixture was then heat shocked at 42^{o}C for 90 seconds and placed back on ice for 5 minutes. To this mixture 100 µl of SOC was added, and then 10 µl of this mixture was pipetted onto a pre-warmed LB agar plate containing ampicillin. The mixture was spread across the plate and incubated overnight at 37^{o}C to allow colony growth.

2.9 Mini-prep

The appropriate amount of colonies were picked and mini-prepped according to the manufacturer's instructions (either Quiagen or Sigma)

2.10 DNA sequencing

All DNA sequencing was performed by the sequencing facility at the University of Oxford (Department of Biochemistry)

2.11 Sub-cloning

2.11.1 Ethanol precipitation

To the DNA solution I added 0.1 x the volume of 5 M NaOAc (pH 5.2) and 2.5 x of 100% EtOH. Then the solution was mixed by inverting the tube 10-20 times. 10 µl of linearised polyacrylamide was added and then the tube was vortexed for 10 seconds. Next the solution was centrifuged for 15 minutes at 13,000 rpm (all room temperature). After spinning, a small pellet was formed. The supernatant was the removed (being careful not to disturb the pellet) and replaced with 800 µl 70% EtOH. The tube was briefly vortexed and then again centrifuged for 1 minute at 13,000 rpm. Finally the supernatant was discarded and the DNA re-suspended in the desired volume of TE buffer.

2.11.2 Insert fragment purification

DNA that had been previously digested and purified was run on an agarose gel. The insert fragment band was cut out of the gell carefully with a scalpel, and the slab of gel placed into a filter barrel. The filter barrel was then centrifuged at 10,000 rpm for 10 minutes at room temperature. Next, 150 µl of TE buffer was added to the filter barrel and spun again at the same speed but for 5 minutes. The eluate was transferred to a fresh Eppendorf and made up to 300 µl with TE buffer ready for ethanol precipitation.

2.11.3 Quantitation

To estimate volumes required for subsequent ligations etc, varying amounts of insert and vector were run on agarose gels.

2.11.4 Agarose gel electrophoresis

Agarose gels were made with molecular biology grade agarose (Type I, low EEO, Sigma) at either 0.8% or 1.5% (w/v). Briefly, agarose was mixed with 50 x TAE buffer and dH_20 to a final concentration of 0.5 x (working conc., 40 mM Tris-Acetate 0.1 mM EDTA, pH8). The solution until completely dissolve3d, and subsequently cooled to less than 60^{o}C. Ethidium bromide (10mg/ml stock solution) was added (4 µl per 100 ml solution) and the mixture was poured into moulds and cooled.

DNA sample were loaded with loading dye (6 x, 0.25% (w/v) bromophenol blue, 0.25% (w/v) xylene cyanol FF, 30% (w/v) glycerol, 6 mM EDTA). Smartladder (Eurogentec) was used as a running marker. Typically, electrophoresis was run for 20-35 minutes at 125 V in 0.5 x TAE buffer, using an i-Mupid gel electrophoresis system.

2.11.5 Ligation

After DNA quantitation, a ratio of 1 insert : 3 vector was placed in an Eppendorf tube. Added to this was an equal volume of Ligation Solution1 (Takara). As negative controls, Eppendorfs with no insert and no ligase were also prepared, to help define the efficiency of the ligation. Tubes were incubated on ice for 5 minutes, then at room temperature for a further 30 minutes. The contents were then transformed (see below). Post transformation and plating, colonies were counted on

all plates, and if less colonies were seen on the negative control plates the ligation was considered to have been successful.

2.12 Immunocytochemistry

Dispersed cortical and hippocampal neurones were grown on glass coverslips and transfected or infected as described above. After enough time for protein expression (typically 12-72 hours depending on construct and method of transduction) coverslips were processed for immunocytochemistry. Coverslips were removed from their plating media and placed into new 35 mm dishes. They were then washed twice with pre-warmed (37^{o}C) Earle's buffer (140 mM NaCl, 5 mM KC, 25 mM HEPES, 5 mM D-glucose, 0.8 mM $MgCl_2$, 1.8 mM $CaCl_2$, pH 7.5). Next pre-warmed (37^{o}C) paraformaldehyde (3.7%) was added to the cells to fix them, for 10 minutes. Again the coverslips were washed twice in Earle's buffer, and then the paraformaldehyde was quenched with one incubation of 50 mM NH_4Cl (10 minutes). Again the coverslips were washed twice in Earle's buffer, and then permeabilised in 0.1% TX-100 (Sigma) for 10 minutes. Again coverslips were washed twice in Earle's buffer, before being incubated in primary antibody (40 µl antibody, 5% horse serum) for 1.5 hours. Again coverslips were washed 3 times in Earle's buffer before being incubated with secondary antibody (in 5%, for 1 hour). Finally coverslips were washed 6 times in Earle's buffer, once in dH_20, and then inverted onto Mowiol (Sigma).

2.13 Fluorescence imaging

Cells were imaged on an Zeiss confocal (LSM 510 UV META Axiovert 200M, Oberkochen, Germany) laser scanning microscope. Fluorophores were excited with a 488 nm laser light and emission was detected through a 505 long pass filter (also Zeiss).

2.14 Analysis

Data was analysed in Excel and figure and tables were made in Excel or Origin. All error

Chapter 3

Results

Biophysical characterisation of Channelrhodopsin-2 in HEK293 cells

3.1 Aims

In the first chapter of this thesis I introduced optogenetics in a broad overview, covering many aspects of the use of ChR2 and its variants in neuronal systems. However I thought it sensible to initially attempt to characterise the basic aspects of ChR2 currents in a non-neuronal system. For this I choose HEK293 cells. These are well-characterised workhorses of cellular biology, and have the advantage of being mammalian in origin. Moreover, I attempted to look at the properties of ChR2 at room temperature, (RT ≈22^{o}C) and at a more physiologically relevant temperature (37^{o}C). The results in this chapter demonstrate that ChR2 expresses well in HEK293 cells, is surface trafficked, and retains its sensitivity to light. It is capable of being activated at a wide range of frequencies (10 Hz up to 500 Hz) with our experimental set up. Channel gating is both voltage- and temperature-sensitive, and displays similarities with some other well-characterised ion channels.

3.2 Introduction

Channelrhodopsin-2 (ChR2) is a light-activated channel originally isolated from algae that is now being widely used as a tool to non-invasively stimulate neurones, both in the intact animal, and *in vitro*. Despite this widespread use across several fields of neuroscience, some aspects of their biophysical properties have not been fully characterised.

Channelrhodopsins are light-activated ion channels that allow green algae species to phototaxically respond to light stimuli (Harz and Hegemann, 1991; Sineshchekov et al., 2002; Suzuki et al., 2003). The genes encoding these channels were cloned (see Nagel et al., 2002, 2003; Zhang et al., 2008) and the subsequent expression of ChR2 and its variants in various host cells has provided a selection of new experimental tools to manipulate membrane potential by exposure to light (see Nagel et al., 2003, 2005a).

Channelrhodopsin-2 (ChR2) is a non-selective cation channel from *Chlamydomonas reinhardtii* that opens when exposed to blue light (≈470nm) (Nagel et al., 2003). Before beginning to using this protein in neurones we characterised the macroscopic kinetics and voltage-dependence of ChR2 channels expressed in HEK293 cells. I performed experiments under conditions that closely resemble physiological ion concentrations and temperatures. Previous studies have reported that recovery from desensitisation is faster at more negative membrane potentials (Nagel et al., 2003). I confirmed this observation and also identified additional voltage-dependent modulation of ChR2 gating. These new observations should be taken into consideration when employing ChR2 in cell types where the membrane potential is not always stable, for example neurones.

3.3 Results

Initially we overexpressed ChR2 in HEK293 cells using Amaxa Nucleofection. Our ChR2 plasmid also coded for *enhanced yellow fluorescent protein* (EYFP) (fused to the rhodopsin), a common fluorescent protein that allows identification of successfully transfected cells. Cells were then transferred to the recording chamber and whole-cell patch-clamped. Cells were then illuminated with a Blue LED (470 nm, Cairn) unless otherwise stated.

3.3.1 Basic Channelrhodopsin-2 induced current and the effect of varying light source

Figure 3.1A shows an example confocal microscope image of a group of HEK293 cells overexpressing ChR2-EYFP (*left*), and the far right cell in close up (*right*). Figure 3.1B shows an example trace from a HEK293 cell expressing our ChR2-EYFP construct. The membrane current is stable, until blue light is shone onto the cell. At the onset of light, a sharp inward current is produced of about 400 pA. This peak rapidly decays to a steady state current, which remains stable until the light is switched off. On cessation of light, the membrane current rapidly returns to baseline. Experimentally cells were first identified by fluorescence, and then whole cell path clamped. If a cell exhibited a characteristic light-evoked inward current then I continued to record from that cell. Non-fluorescing cells never exhibited a light-evoked current, suggesting that ChR2-expression was indeed responsible for these currents. We can therefore identify at least five components of the ChR2 signal, an activation rising to a peak, immediately followed by desensitisation to a steady state, which deactivates to baseline once the light ceases. This pattern of response to light is highly reproducible, with some caveats that will be discussed later.

While the blue LED is optimised for ChR2 activation, we wondered whether ambient light in our laboratory might be sufficient to activate ChR2. If this was the case, experiments would have to be performed under dark conditions, to prevent off-target effects (spatially and temporally). We therefore monitored membrane current whilst exposing ChR2-expressing cells to different light sources. This is presented in Figure 3.2. All parts A-C are from the same ChR2-EYFP expressing HEK293 cell. 3.2A shows the membrane potential of a ChR2-expressing cell when exposed to room light. 3.2B is the response when the episcopic light of the microscope was used to illuminate the cell. There is a small depolarisation without any sharp initial peak. Presumably the white light source of the episcopic light contains enough blue light to partially activate and open the ChR2 molecules in the cell's membrane. 3.2C shows the response to a mercury bulb passing through a FITC filter cube. This experiment satisfied us that ambient room light in the laboratory would not affect our continuing experiments.

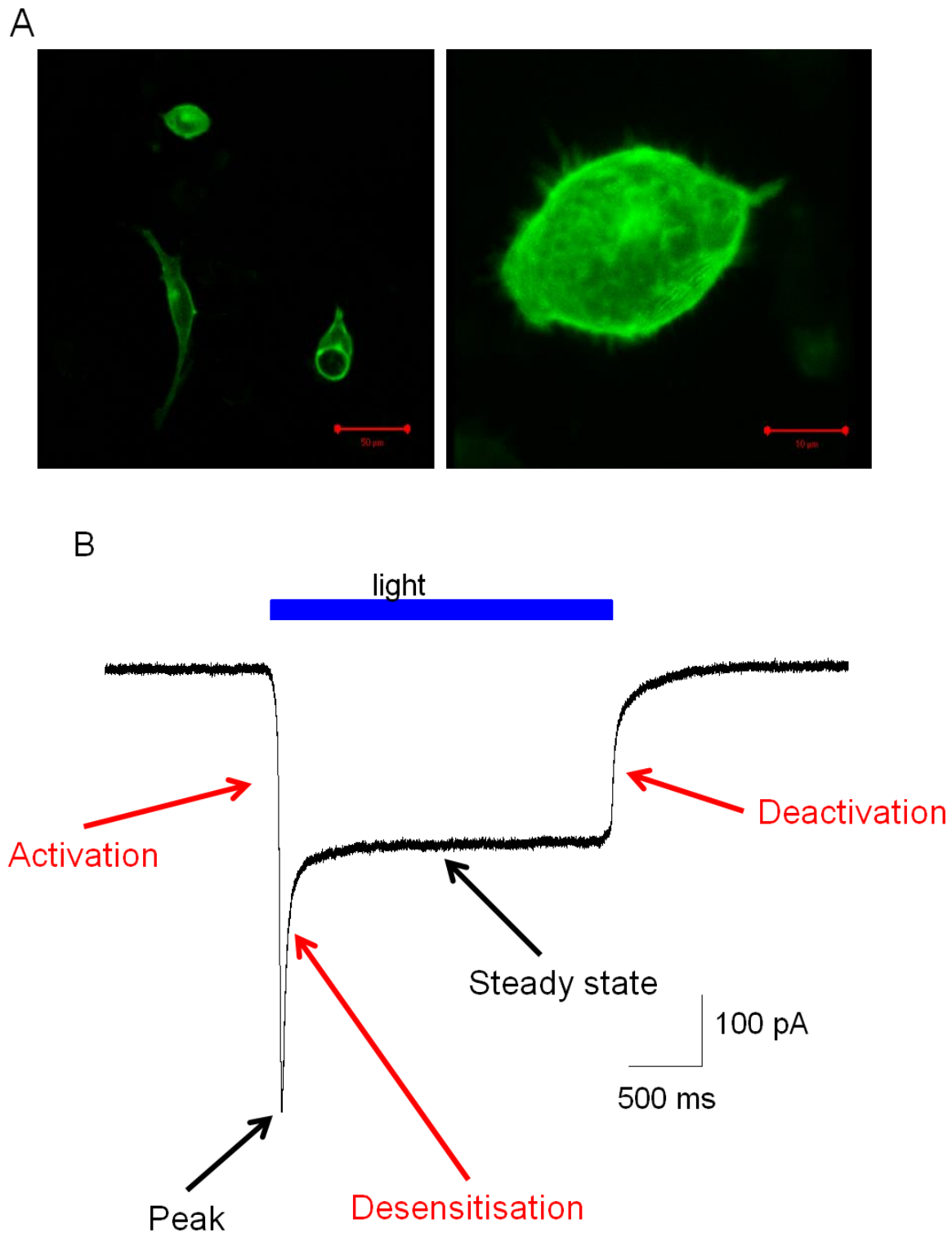

Figure 3.1 – Basic ChR2 current

HEK 293 cells were transfected with ChR2-EYFP, and cells exhibiting yellow fluorescence were whole-cell patch-clamped.

A –ChR2-EFYP expressing HEK293 cells imaged by confocal microscopy (scale bar 50 µm, left, 10 µm right)

B – Example ChR2 current induced by blue light flash. Notice fast rise to peak and immediate desensitisation to steady state current

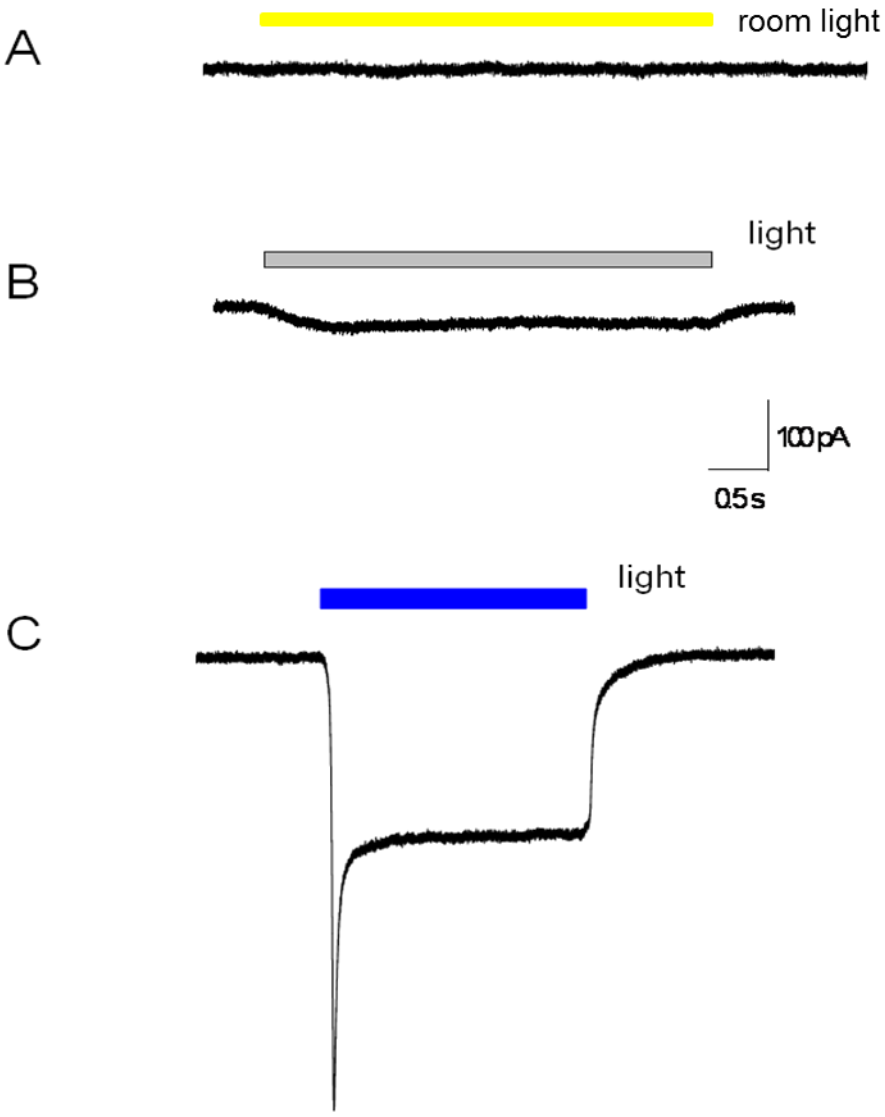

Figure 3.2 – Comparison of light sources

HEK 293 cells were transfected with ChR2-EYFP, and cells exhibiting yellow fluorescence were whole-cell patch-clamped.

A - room light

B - microscope episcopic light

C - with Hg bulb and FITC filter set (blue light, ≈470 nm)

3.3.2 Intensity *versus* response

Next we approached the issue of by how much current was produced across the cell membrane relative to the light intensity. By altering the current through the LED I could change the light intensity emitted, and the amount of light emitted by the LED varied linearly with current (data not shown). I therefore patch-clamped a ChR2-expressing cell, and increased the current through the LED in 0.1A steps from 0A to 1.1A. This is plotted in figure 3.3A. LED flash intensity is at the top, with the cells response to each light step below. As expected, increased light produces larger currents in the target cell. Figure 3.3B *left* shows the current produced in a cell voltage clamped at -70 mV, as light intensity varies. These factors are not linearly related. Figure 3.3B *right* shows the same data normalised. Figure 3.3C shows example traces from the same ChR2-expressing HEK293 cell responding both to a 0.1A light flash (black) and a 1.1A flash (red) scaled for comparison. There is a less defined peak at the lower light intensity. Figure 3.3D shows how both the 10-90% activation (*left*) and the time constant of desensitisation (*right*) also varies with increasing light intensity. I did not perform experiments using a LED current than 0.1A, although it is likely that the channels behaviour at lower light intensities would follow a similar pattern to the data presented here.

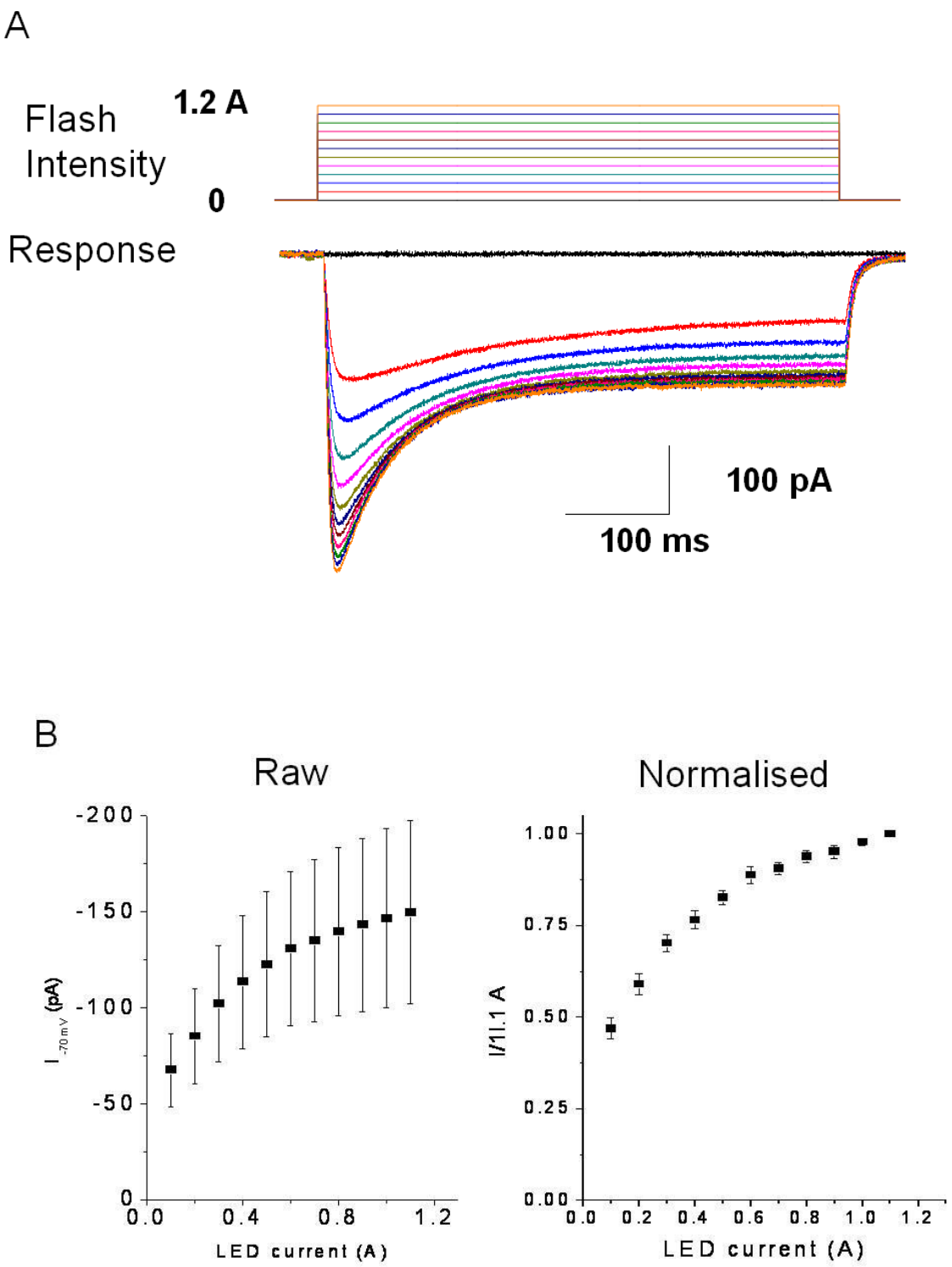

Figure 3.3 – Intensity dependent kinetics in HEK293

HEK 293 cells were transfected with ChR2-EYFP, and cells exhibiting yellow fluorescence were whole-cell patch-clamped.

A - Currents evoked by 500 ms flashes of various intensities. Current through the LED was raised in 0.1A steps

B - Pooled data plotting the relationship between peak ChR2 current and LED current. *Left*, raw data, *right* normalised data

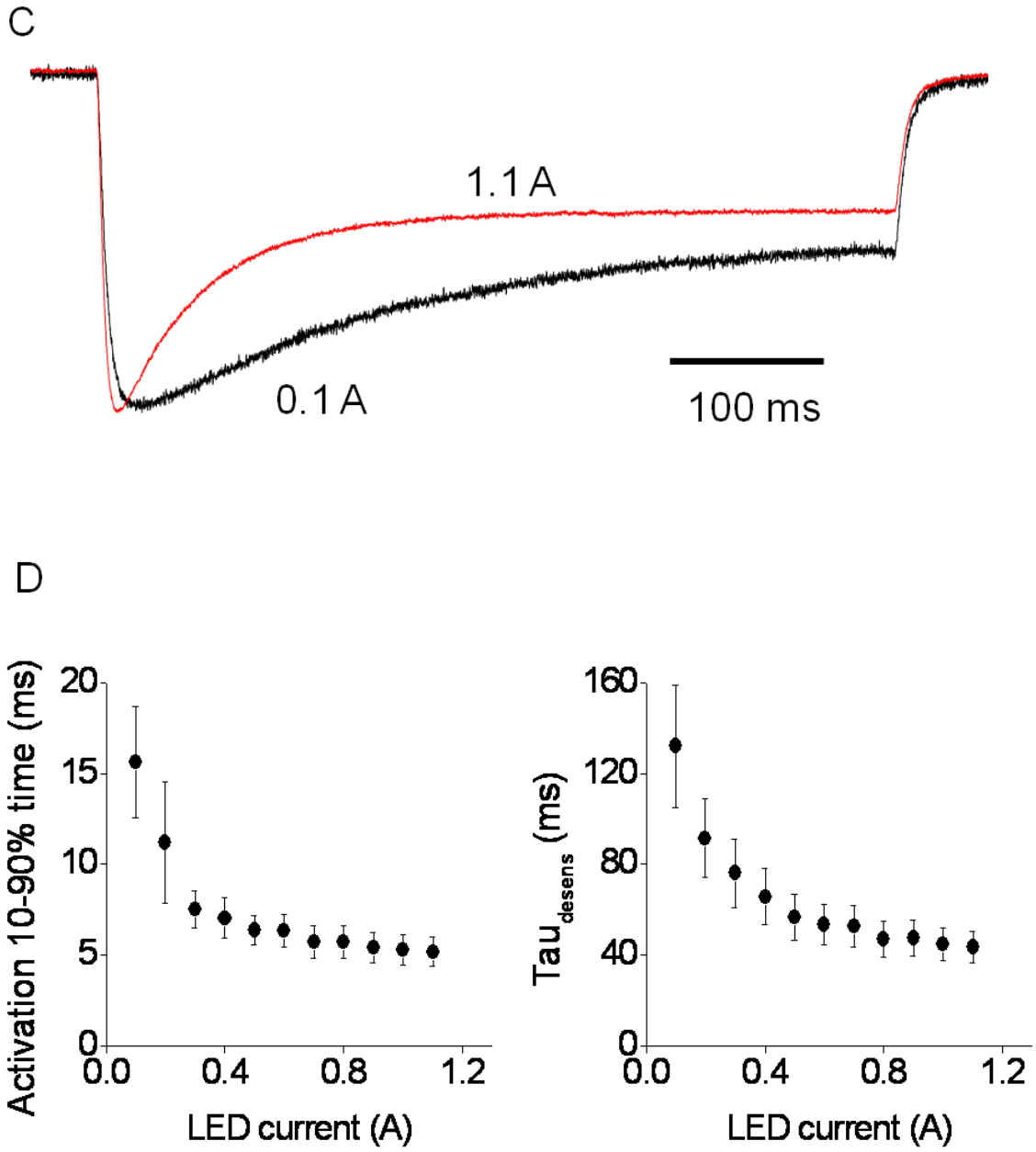

Figure 3.3 Intensity dependent kinetics in HEK293 continued -

C - Peak scaled responses to a low (0.1A) and high (1.1A) intensity flash from the same cell.

D - Pooled data describing the dependence of ChR2 activation (*left*)

and desensitisation kinetics (*right*) on light intensity (n=8).

3.3.3 Trial-to-trial reproducibility

An extremely important consideration with using any stimulating technique is whether or not it is stable. Modern patch-clamp amplifiers are capable of injecting precise amounts of current into biological tissue repeatedly, and to be useful optogenetics and ChR2 specifically must be capable of the same. To check whether this was the case, we subjected cells expressing ChR2-EYFP to a paired flash protocol. We subjected cells to 2 successive flashes, separated by a brief interval, and compared trial-to-trial performance, see figure 4A. Each pair of flashes was separated from the next pair by a period of 20 seconds with no light. Twenty seconds allows recovery of the channel between trials. We then compared peak and sustained current, the ratio of peak to sustained, and the 10-90% rise time of the initial current (to peak) over 60 trials (figure 3.4B-E). Rundown over the whole experiment was negligible (p=0., and the initial fall noted is due to the initial desensitisation of the channel and resultant reduction in magnitude of peak current. These data indicate that response of ChR2 is relatively stable over the time scales of short experiments. This does not tell us anything about chronic *in vivo* expression of ChR2 and its response to stimuli in the intact animal; however this is beyond the scope of this thesis.

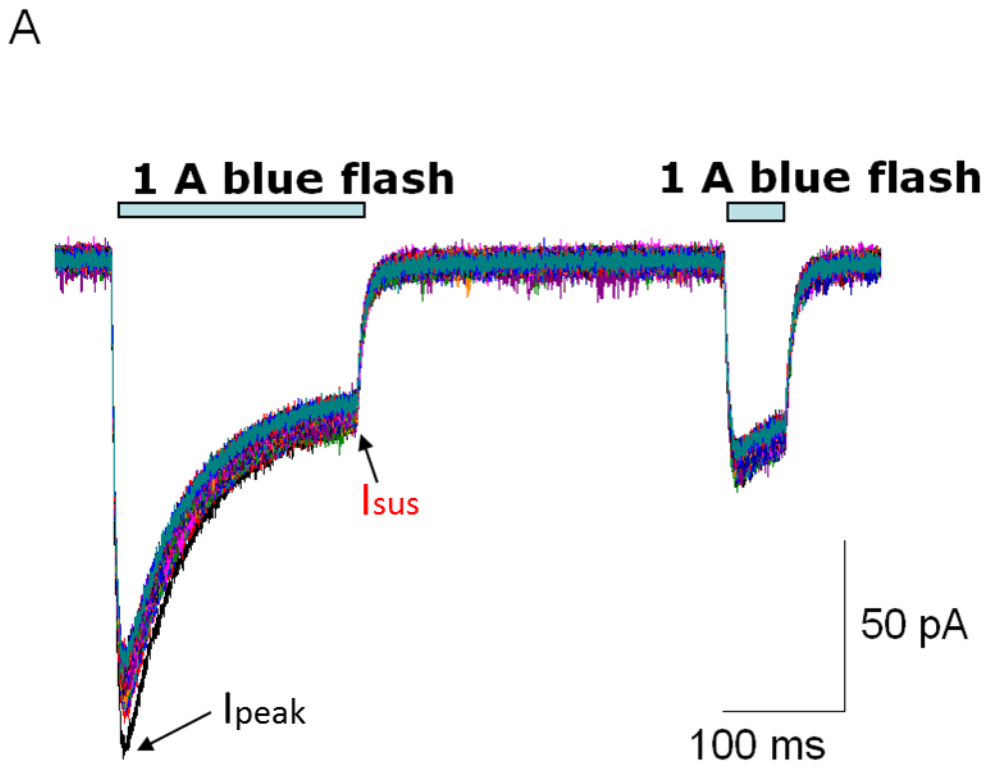

Figure 3.4 – Trial to trial reproducibility

HEK 293 cells were transfected with ChR2-EYFP, and cells exhibiting yellow fluorescence were whole-cell patch-clamped.

A - An example recording in which 60 paired flashes were applied to a ChR2 expressing cell at 0.05 Hz.

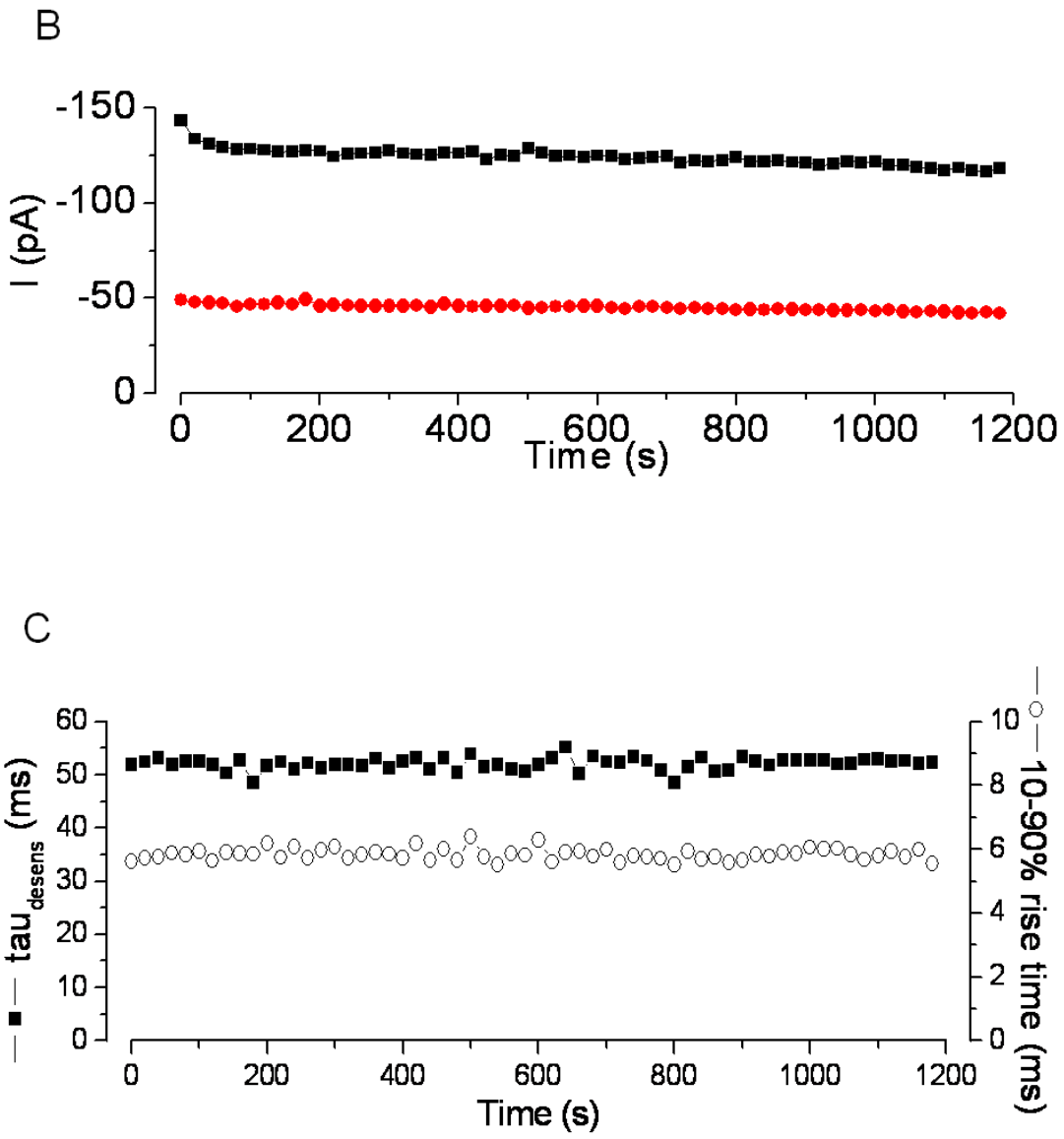

Figure 3.4 continued – Trial to trial reproducibility

B - A plot of peak (black) and sustained current (red, second flash) *versus* time for the cell in A

C - A plot depicting the timecourse of activation and desensitisation kinetics of ChR2 responses

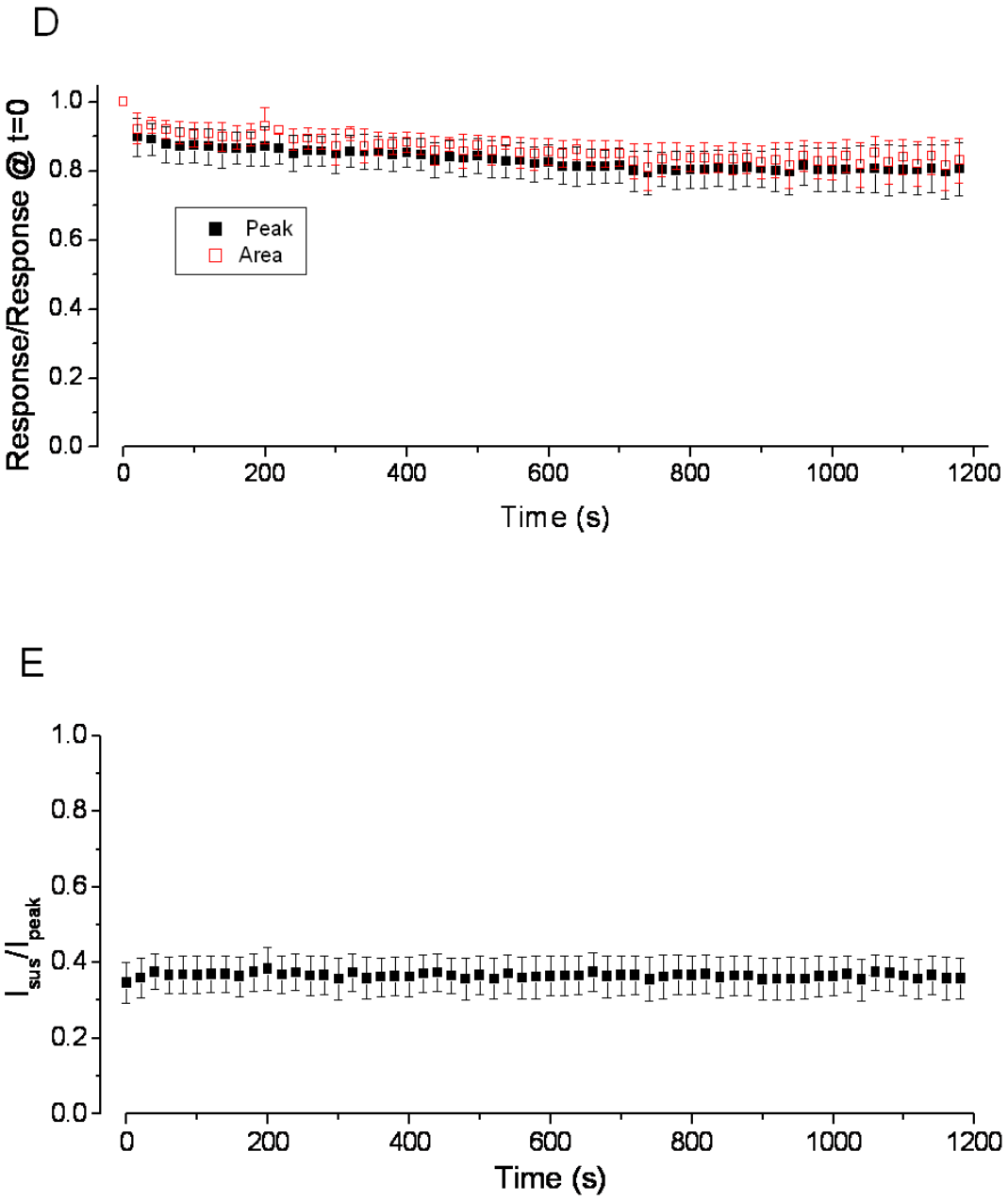

Figure 3.4 continued– Trial to trial reproducibility

D -Pooled data from 5 recordings like that in (A) illustrating the stability of response amplitude (area, p=0.60, peak p=0.63, ANOVA)

E - A graph illustrating the ratio of peak to sustained current for the same 5 recordings.

3.3.4 Duration versus response

Next we investigated how the duration of a light flash changed the response in the cell. Cells expressing ChR2-EFYP were whole-cell patch clamped, and different durations of light flashes were delivered, from 1 ms up to 300 ms. See figure 3.5A for example traces reflecting the membrane's response to flashes of varying durations, and figure 3.5B for a plot of the overlaid traces from one cell. Figure 3.5C shows the relationship between duration of light flash and peak current amplitude (*left*, filled squares) and charge transfer (*right*, open circles, both n=10). Figure 3.5D plots the same parameters but normalised. Figure 3.5E shows a biexponential fit (*red*) to a 330 ms flash response (*black*), and figure 3.5F shows pooled data from 9 such recordings describing the two time constants of desensitisation. Finally, figure 3.5G depicts a scatter plot showing that there is no correlation between the peak current amplitude and the extent of desensitisation generated during a 300 ms light flash, and its resulting depolarisation.

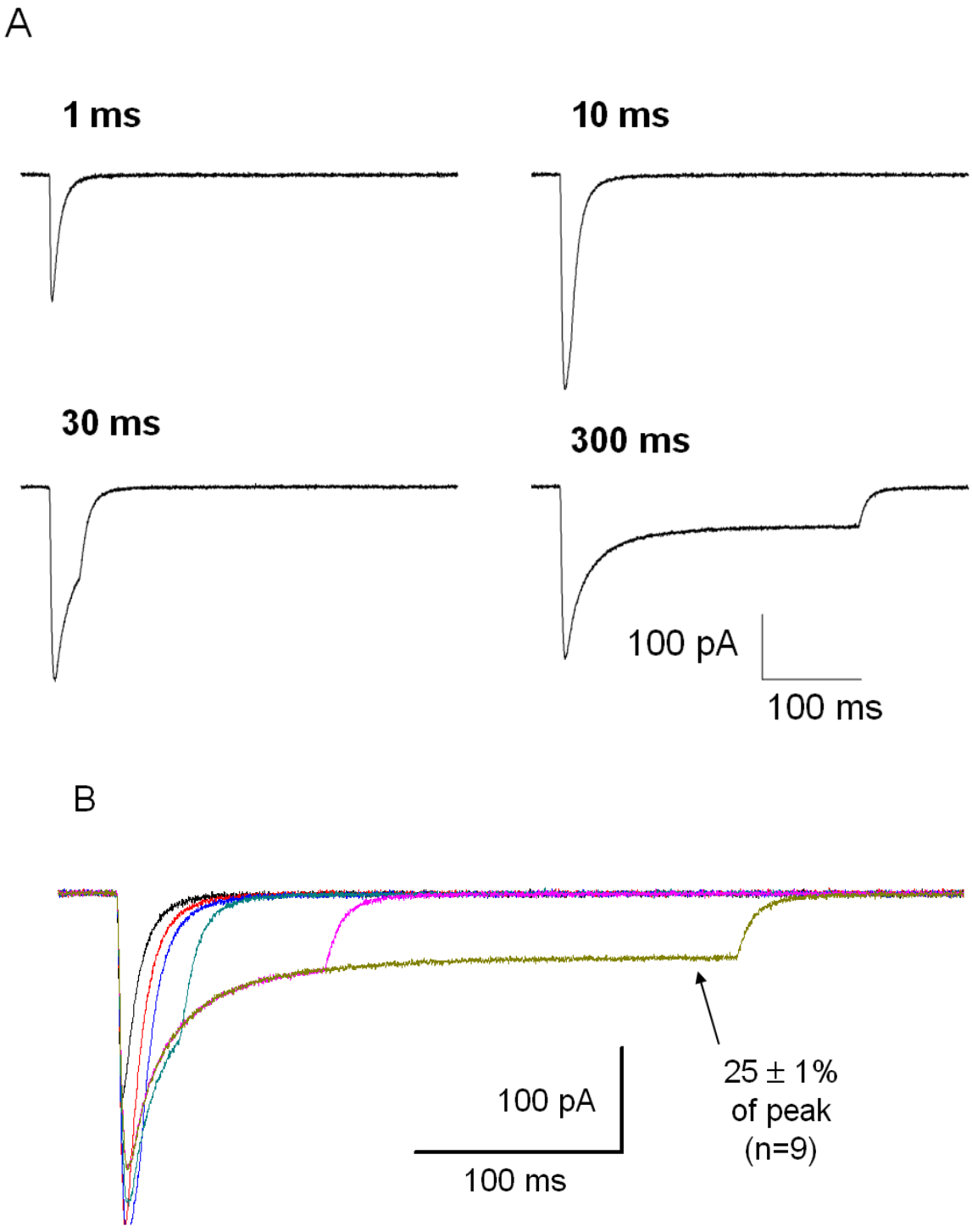

Figure 3.5 – Flash duration vs. ChR2 response relationships

HEK 293 cells were transfected with ChR2-EYFP, and cells exhibiting yellow fluorescence were whole-cell patch-clamped.

A - An example recording in which a ChR2 expressing cell was exposed to light flashes (1 A LED current) of 1,3, 10, 30, 100 and 300 ms duration.

B – Individual examples of membrane responses to 1, 3, 10 and 300 ms light flashes

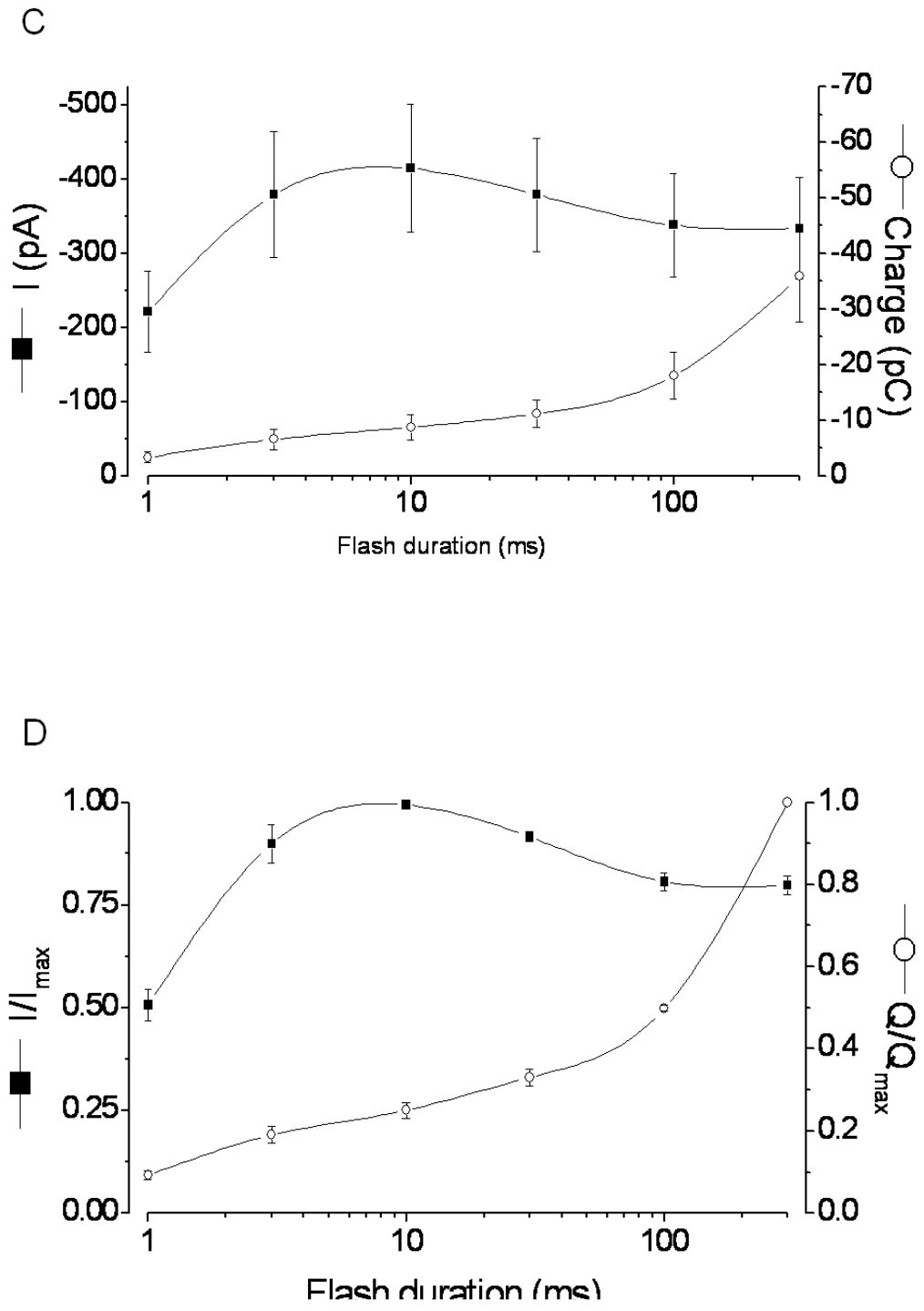

Figure 3.5 continued – Duration vs. response

C - Pooled raw analysis of 10 such recordings plotting the relationship between flash duration and either current amplitude (filled squares) or charge transfer (open circles)

D - Peak normalised analysis of 10 such recordings plotting the relationship between flash duration and either current amplitude (filled squares) or charge transfer (open circles)

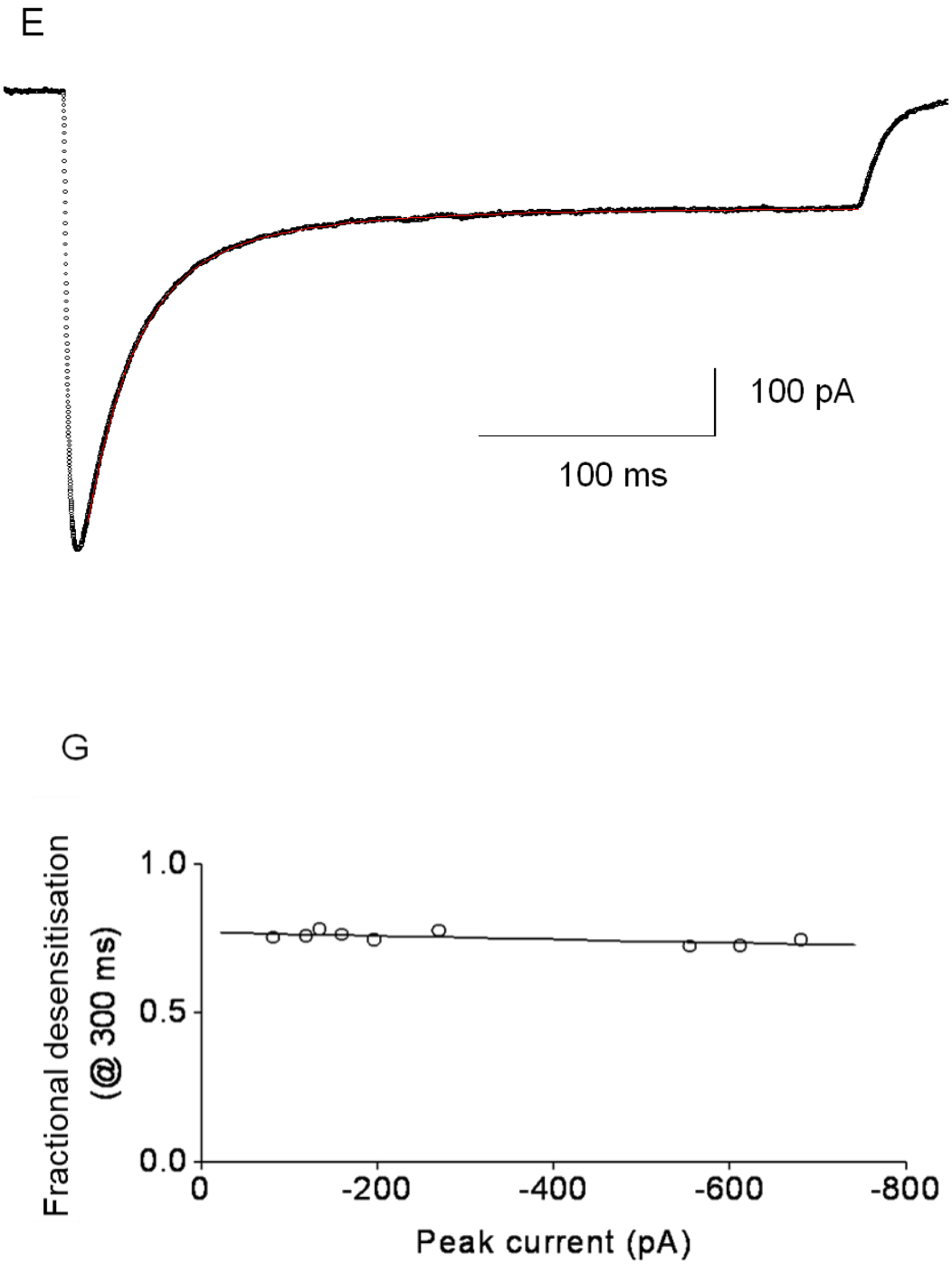

Figure 3.5 continued – Flash duration vs. response

E - A biexponential fit (red) to a 330 ms flash response (black)

F - Pooled data from 9 such fits describing the two time constants of desensitisation.

G - A scatter plot showing the lack of correlation between the peak current amplitude and the extent of desensitisation generated during a 300ms light stimulus ($r^2 = 0.1$)

3.3.5 Recovery from Desensitisation

The inward currents produced by the opening of the pore of ChR2 quickly rise to a peak, as we have already showed (Figure 3.1B). However this peak is lost if another flash is given immediately afterwards. This is due to desensitisation of the ChR2 molecules in the membrane, and their resulting inactivation. To investigate this we designed a paired flash protocol. One flash of light was given, which was followed by a shorter second flash after a variable delay. The first flash induced desensitisation, and the second flash allows monitoring of the kinetics of recovery from desensitisation. Figure 3.6A shows example membrane responses to a series of such paired flashes. Figure 3.6B plots the degree of recovery of the peak amplitude against the interflash interval. Filled black squares correspond to recordings at room temperature (≈22^{o}C), and open triangles correspond to recordings made at physiological temperature (37^{0}C). Presumably, upon an initial (faux-naïve) flash, all or a large majority of the ChR2 molecules respond by opening. However, in a cell or patch of membrane that has recently seen a light flash (less than 20 seconds ago), not all of the ChR2 molecules are available for opening, due to some being currently in an inactive form.

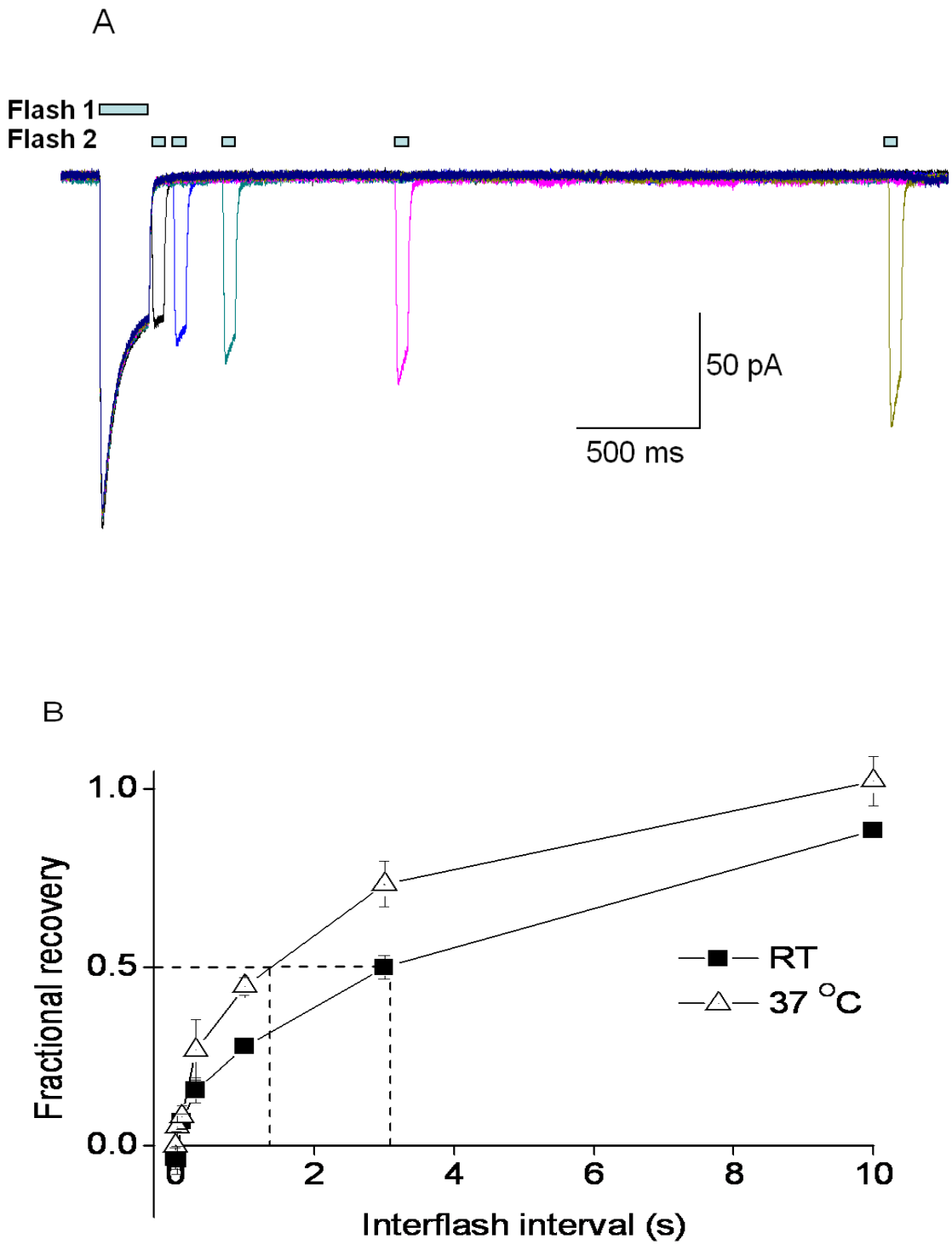

Figure 3.6 – Recovery from desensitisation

HEK 293 cells were transfected with ChR2-EYFP, and cells exhibiting yellow fluorescence were whole-cell patch-clamped.

A - An example dual pulse experiment used to characterise the kinetics of recovery from desensitisation of ChR2. Flash one induced desensitisation and was followed at a variable latency by a second briefer flash to assess the degree of recovery of the peak

B – Pooled data showing fractional recovery *versus* interflash interval. Room temperature (n=7, filled squares), and 37ºC (n=7, open triangles)

3.3.6 Voltage-dependent properties of ChR2

Next we investigated the effect of membrane voltage on ChR2. Cells were subjected to symmetrical voltage ramps, running from -85 mV to +55 mV, (changing at 17.5V/sec), and back down to -85 mV. These ramps were run either in the presence of absence of blue light. A schematic of the experiment is seen in figure 3.7A. In figure 3.7B we present subtractively determined traces from 6 recordings like that in 3.7A, demonstrating the membrane's current responses. Figure 3.7C shows a plot of the current-voltage relationship of the response to light. These data have been averaged, and then normalised to the current at -85 mV

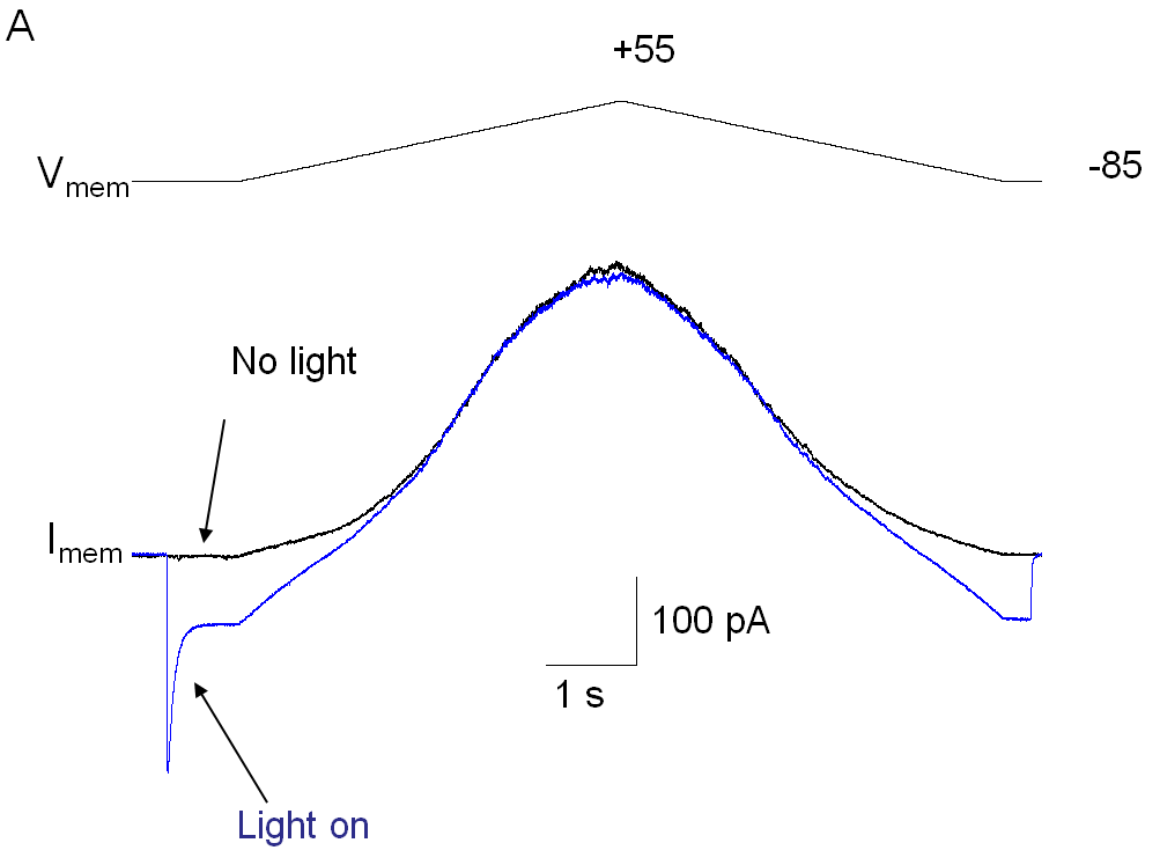

Figure 3.7 – Voltage-dependent properties of light-induced responses

HEK 293 cells were transfected with ChR2-EYFP, and cells exhibiting yellow fluorescence were whole-cell patch-clamped.

A - Current responses to symmetrical voltage ramps

(−85 mV to +55 mV to −85 mV) delivered either during a light pulse (intensity, 1A; blue trace) or in the absence of light (black trace).

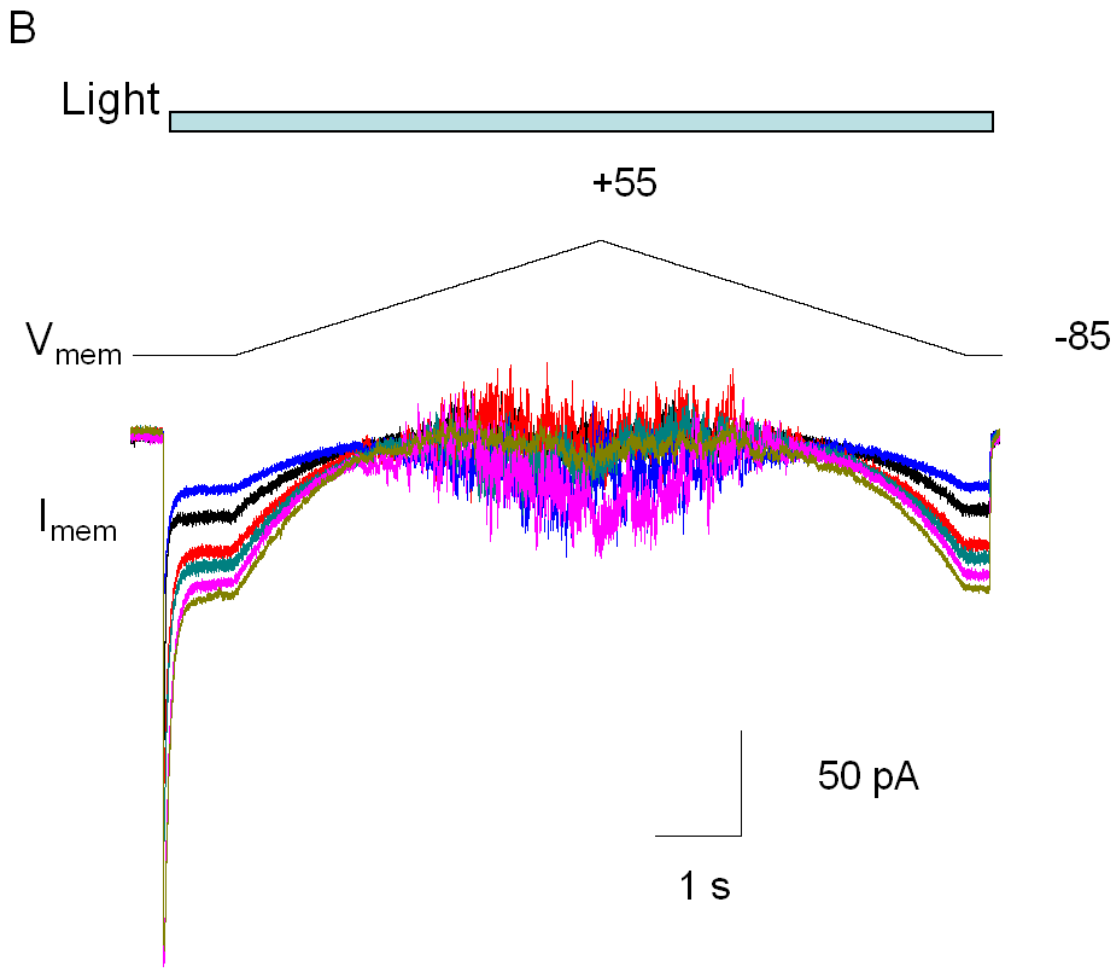

Figure 3.7 continued – Voltage-dependent properties of light-induced responses

B - Subtractively determined light-activated current responses from 6 recordings like that shown in A

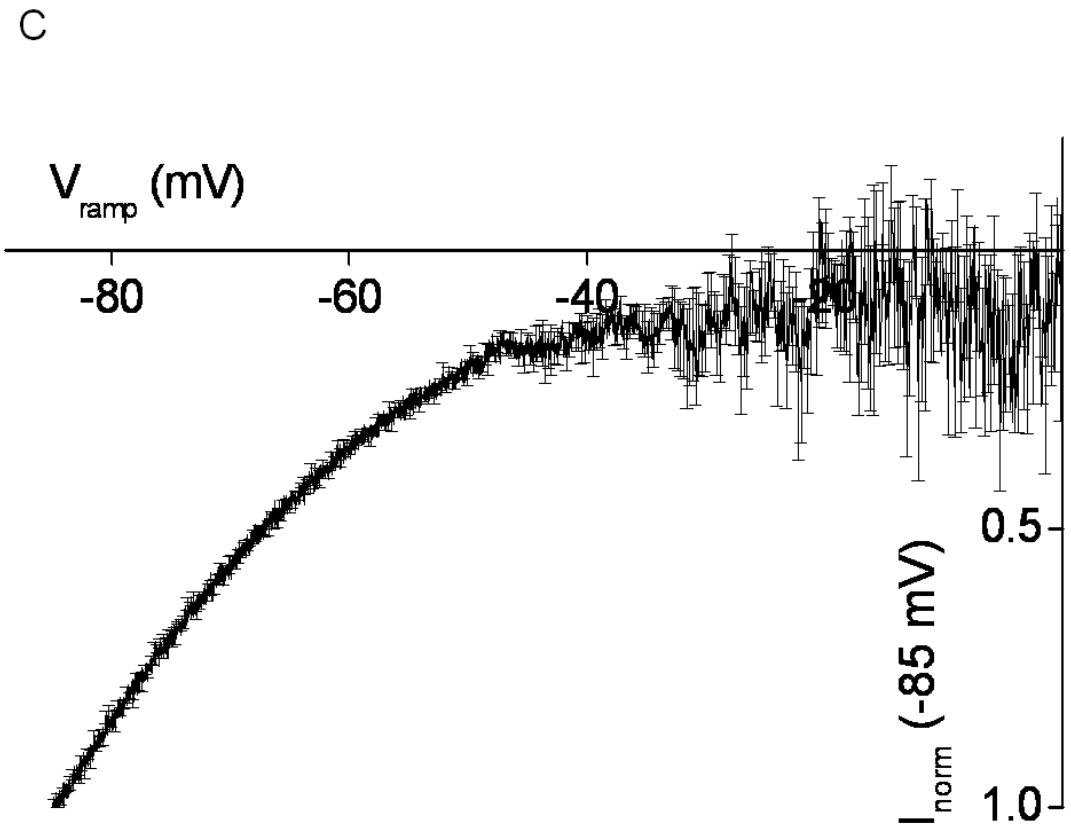

Figure 3.7 continued

C – Averaged and normalised current –voltage relationship of ChR2 (n=6)

We also examined the voltage-dependence of ChR2-mediated currents and their kinetics at both ≈22ºC and 37ºC. By holding the cells at a range of different membrane potentials (-85 mV to +25 mV, in 10 mV increments), and exposing the cells to a 250 ms light flash, we were able to investigate if ChR2 exhibits any voltage-dependent gating. An example of the traces recorded is shown in figure 3.8A, and the pooled current-voltage (I-V) relationships for both temperatures are shown in figure 3.8B. Figure 3.8C shows the same set of data but normalised to the current response at -85 mV before any averaging. The largest currents passing through ChR2 were observed at the most negative membrane potentials (i.e. -85 mV) and the I-V relationships for ChR2 show strong inward rectification. At both room temperature and 37ºC the reversal potential of ChR2 was slight positive to 0 mV (figure 3.8B). We were then able to also analyze the voltage-dependence of four other factors at both temperatures; activation, deactivation, desensitisation, and the steady state extent of the desensitisation (see figure 3.9A-D). All four were significantly faster at 37ºC compared to room temperature ($p<0.05$, ANOVA). Activation and deactivation were both faster at more negative membrane potentials (3.9A and D, respectively). In comparison the rate of desensitisation is not dependent on membrane voltage, but there are effects on the level of desensitisation when compared to peak current as the membrane become more depolarised. This is illustrated in figure 3.9E by overlaying responses normalised to their peak currents at -25 mV and -85 mV, at room temperature (*left*, n=8) and 37ºC (*right*, n=6)

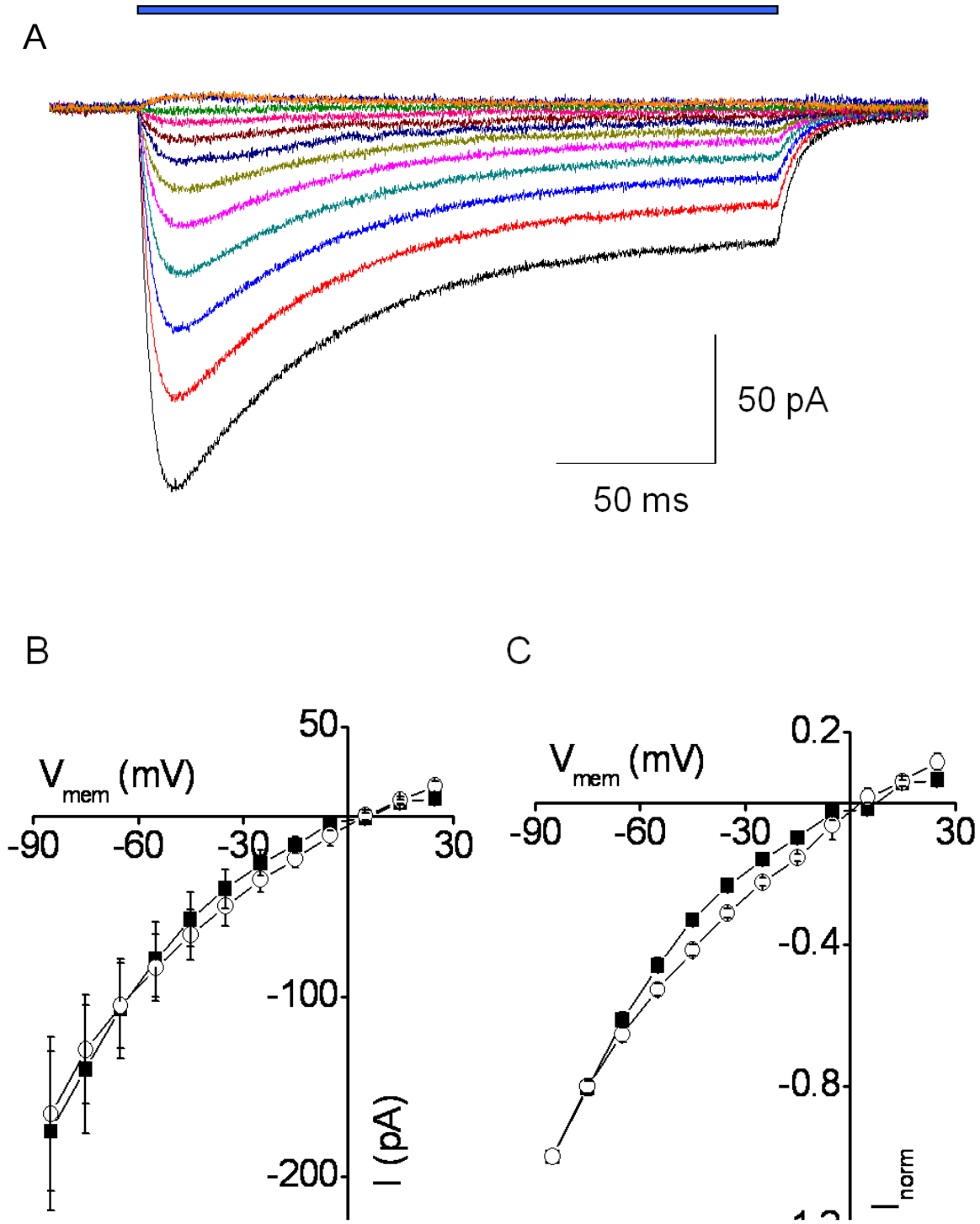

Figure 3.8 – Voltage-dependent properties of light-induced responses

at room temperature and 37 ◦C

HEK 293 cells were transfected with ChR2-EYFP, and cells exhibiting yellow fluorescence were whole-cell patch-clamped.

A - Current responses to 250ms light pulses (intensity, 1A) in a cell voltage-clamped at membrane potentials between −85mV to +25 mV, in 10mV intervals. The largest currents were evoked at the most negative potentials.

B - Pooled I–V relationships at room temperature (filled symbols; n = 8) and 37 ◦C (open symbols; n = 6).

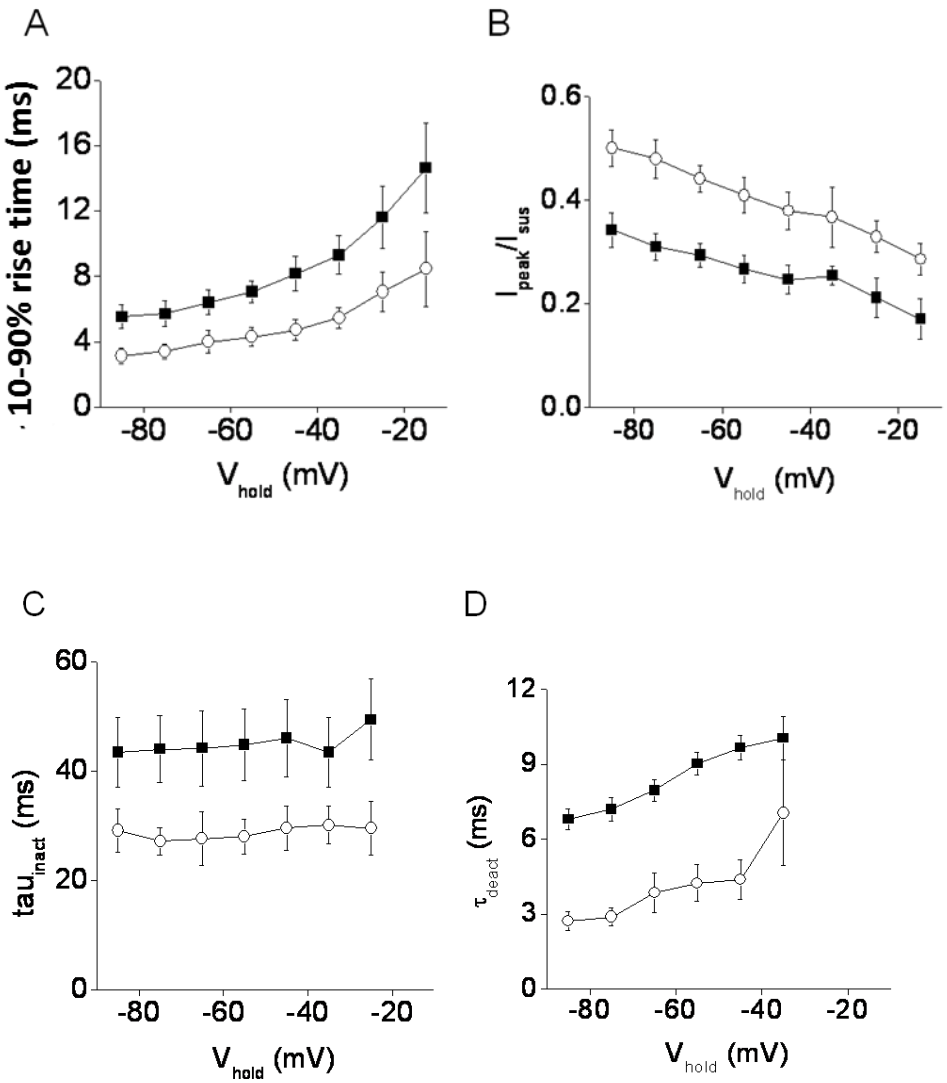

Figure 3.9 – Voltage-dependent kinetics of light-induced responses at room temperature and 37^{0}C.

HEK 293 cells were transfected with ChR2-EYFP, and cells exhibiting yellow fluorescence were whole-cell patch-clamped.

A - Pooled data showing the 10–90% rise time

B – Pooled data showing the ratio of the sustained current to the peak current (I_{sus}/I_{peak})

C – Pooled data showing the time constant of inactivation (Tau_{inact})

D – Pooled data showing the time constant of deactivation (Tau_{deact}).

Data from cells recorded at room temperature (≈22 ◦C) are represented by filled symbols (n = 8). Data from cells recorded at 37 ◦C are represented by open symbols (n = 6). In all cases there was a significant difference ($p<0.05$, ANOVA) between data acquired at 37 and 22◦C

E

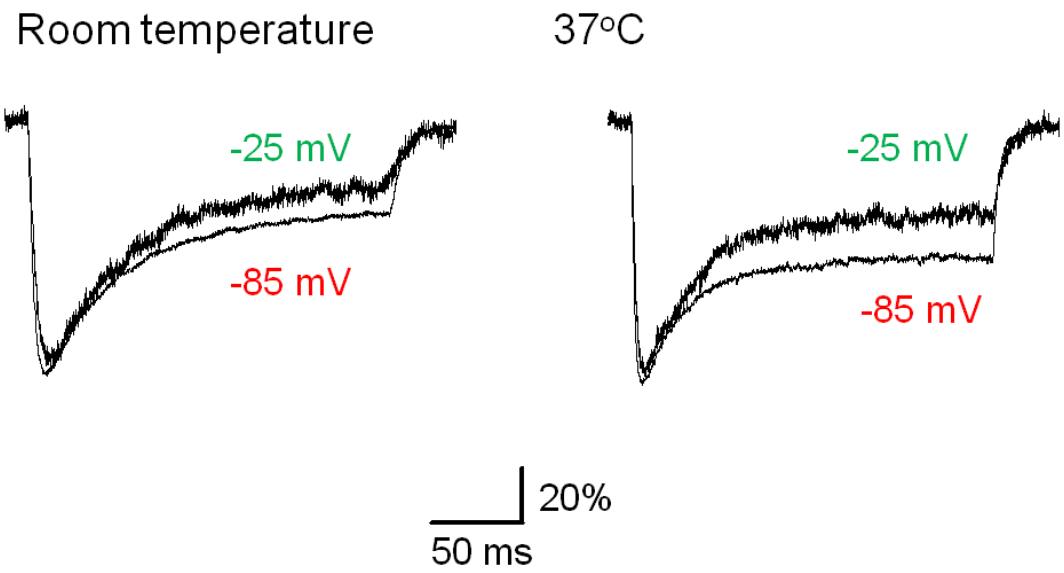

Figure 3.9 continued – Voltage-dependent kinetics of light-induced responses at room temperature and 37^0C.

E - *Left*: peak-normalised average current responses compiled from 8 cells recorded at ≈22◦C and stimulated with 250ms light pulses.

Traces recorded at voltage-clamp potentials of −85 and −25mV are shown. *Right*: identical pooled data sets for recordings from 6 different cells made at 37 ◦C.

3.3.7 Responses to trains of light flashes

Having investigated several aspects of ChR2 biophysical function, we finally looked at how well ChR2 could follow high-frequency trains of brief light flashes. One potential issue was the slow recovery of the peak current from desensitisation (> 10 seconds, see figure 3.6A and B), and how this would affect light flashes at high frequencies. As the key use of ChR2 in a neuronal context is to drive neuronal action potential firing, this particular question is key to the whole utilisation of ChR2 (see next chapter). As stated at the beginning of this chapter, it is technically simpler to investigate these properties in non-neuronal cells before moving into them. Therefore, we transfected HEK293 cells with ChR2-EYFP, and exposed them to trains of 2 ms light flashes whilst whole-cell patch-clamping them. Figure 3.10A shows examples of trains delivered at 10, 20, 40 and 80 Hz (top to bottom) at room temperature. Notice that the loss of the peak current caused by desensitisation is affecting all frequencies, and begins to become clearly apparent in trains at 20 Hz and above, and that summation of responses starts to become apparent at higher frequencies. Figure 3.10B shows pooled data for 10 such recordings at each frequency as shown in 3.10A, plotting amplitude (normalised to the first response in a train) against stimulus number (filled circles) and mean latency to peak (filled circles). Notice desensitisation at all frequencies. In every case this loss of peak amplitude is significant ($p<0.05$, student's t test), however latency to peak does not experience any change between first and last response ($p>0.1$ in all cases, student's t test).

As neurones *in vivo* can fire at much higher frequencies than 80 Hz, we investigated whether our experimental setup could drive light-induced trains of depolarisation at faster rates. Figure 3.10C shows overlaid example traces from one such experiment where the flashes of 2 ms light were given at 100, 150, 200, 300 and 400 Hz respectively (all at ≈22^{o}C). At these frequencies it becomes increasingly harder to resolve individual membrane responses to individual light flashes, due to summation, but performing a Fourier transform enables us to pick out the underlying

oscillations of the membrane (figure 3.10D). Trains of brief light stimuli performed at 37°C show less summation than at room temperature, (Figure 3.10E, *top* 10 Hz, *bottom* 80 Hz) but notice that desensitisation is still clearly apparent ($p < 0.05$, student's t test).

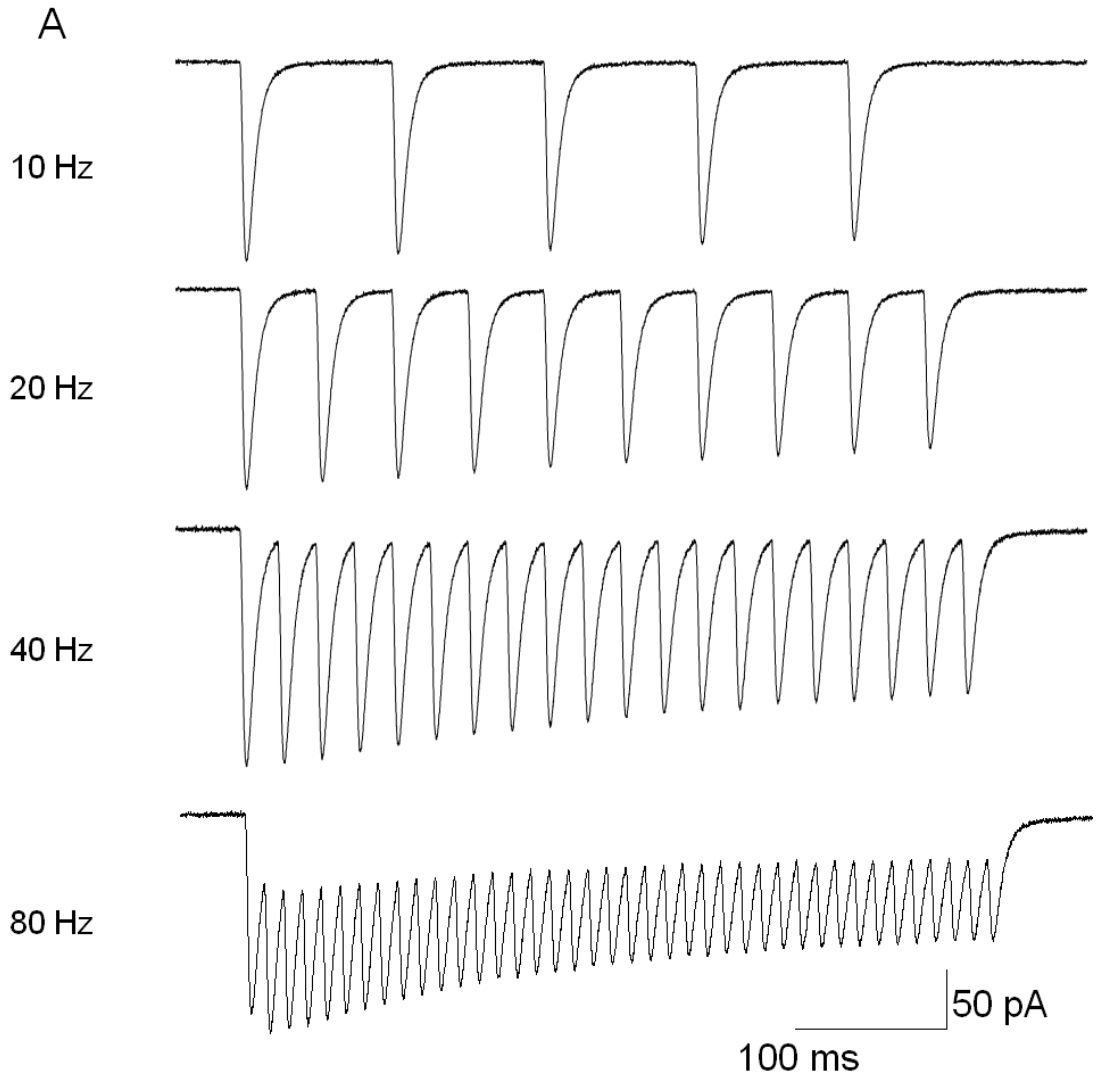

Figure 3.10 – Responses to trains of light flashes

HEK 293 cells were transfected with ChR2-EYFP, and cells exhibiting yellow fluorescence were whole-cell patch-clamped.

A - Responses to trains of 2 ms flashes applied at 10, 20, 40 and 80 Hz as indicated. Note that desensitisation accumulates at all frequencies, and becomes more obvious as frequency increases.

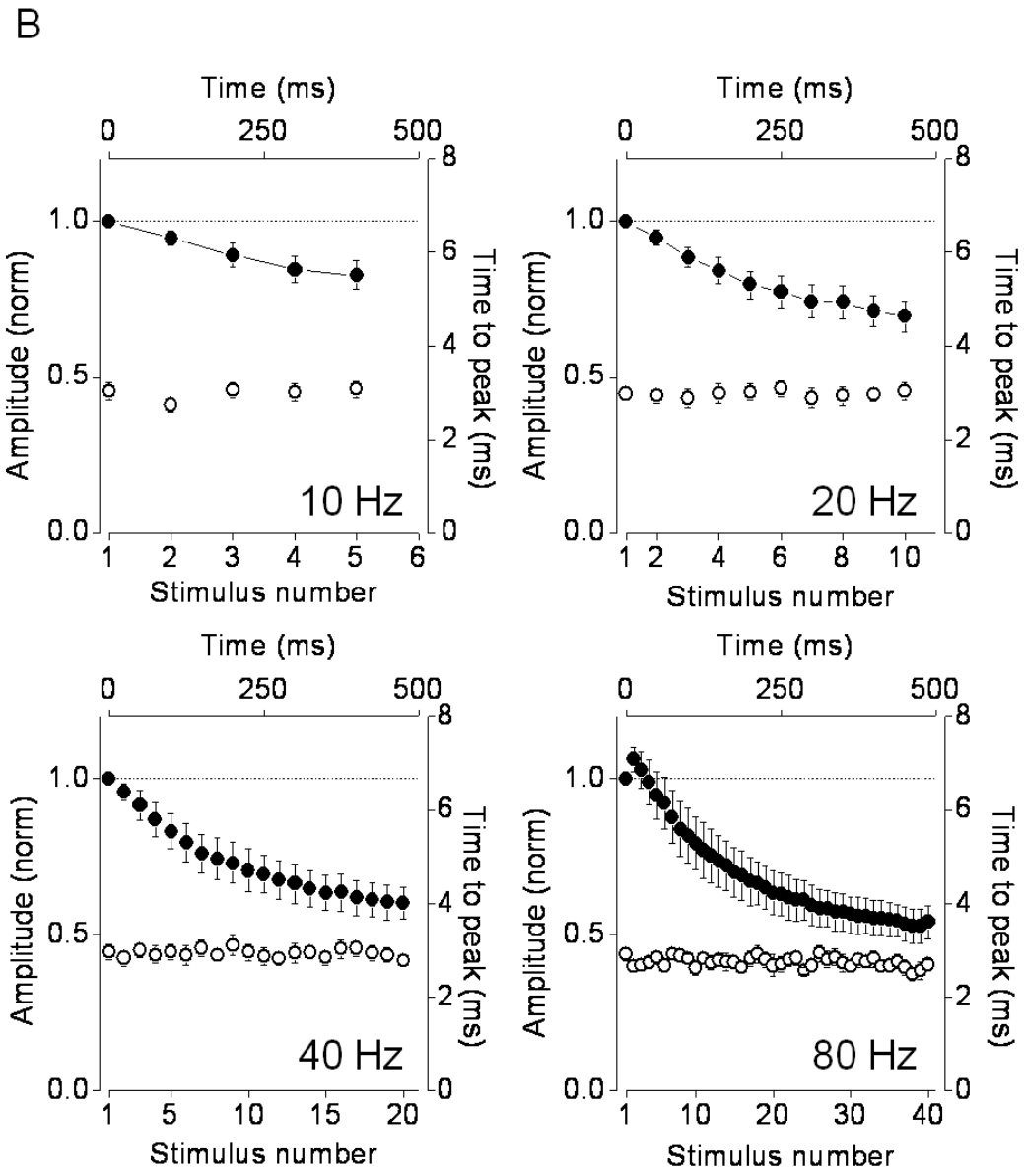

Figure 3.10 continued – Responses to trains of light flashes

HEK 293 cells were transfected with ChR2-EYFP, and cells exhibiting yellow fluorescence were whole-cell patch-clamped.

B - Pooled data plotting the amplitude (filled symbols) of each response in a stimulus train normalised to the amplitude of the first response in a train=10 for each of the four frequencies illustrated in (A). Notice significant fall in peak normalised amplitude across the 4 frequencies ($p<0.05$ in all 4 cases, student's t test). Also shown is the mean latency to peak for each response (open symbols) which remains stable ($p>0.1$ in all cases)

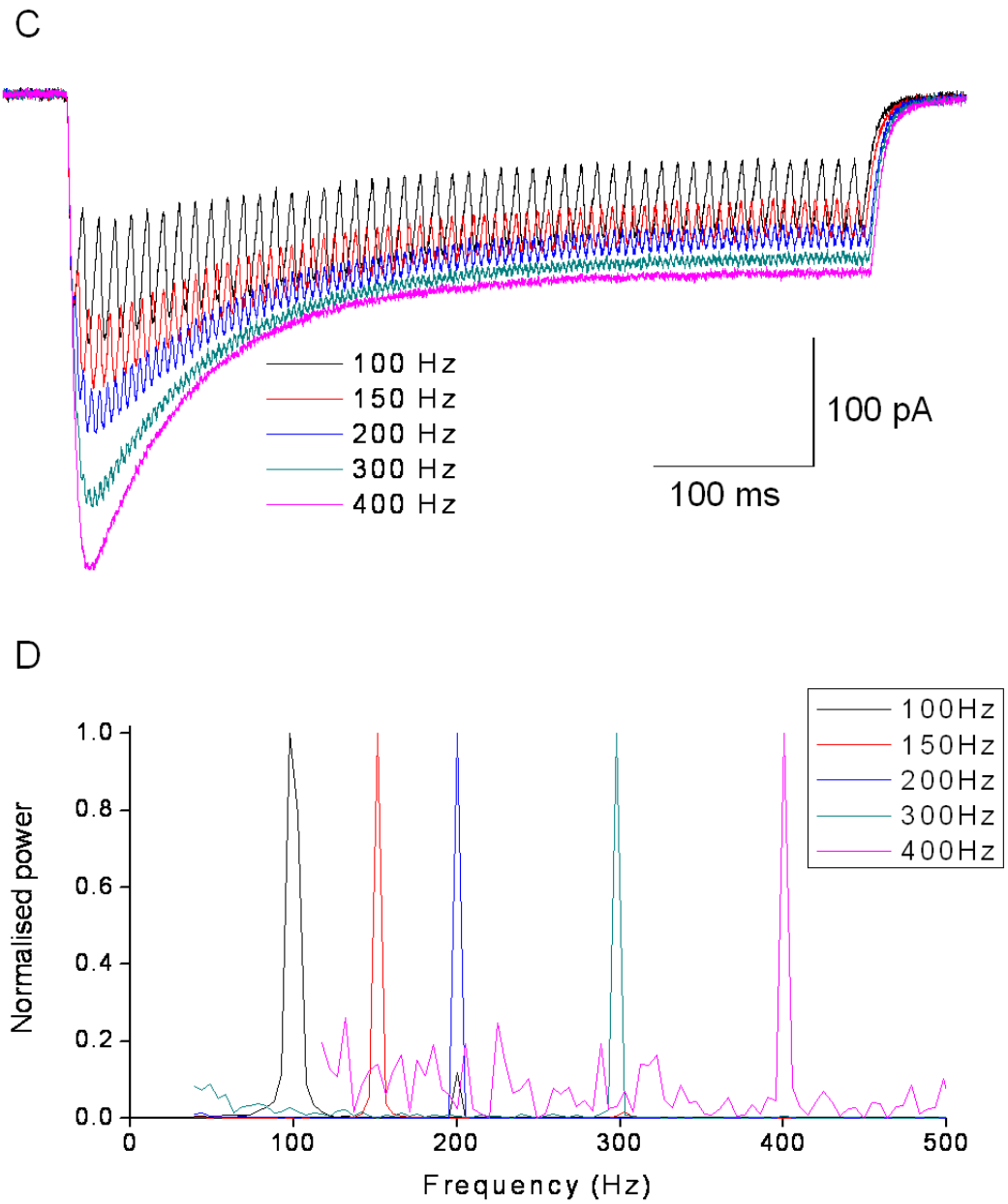

Figure 3.10 continued – Responses to trains of light flashes

C - Responses to trains of 2 ms flashes delivered at 100, 150, 200, 300 and 400 Hz. Above 200 Hz it becomes increasingly hard to resolve membrane fluctuations caused by individual light flashes.

D - Peak normalised power spectra of (C) illustrating the preservation of the activation frequency within the current responses.

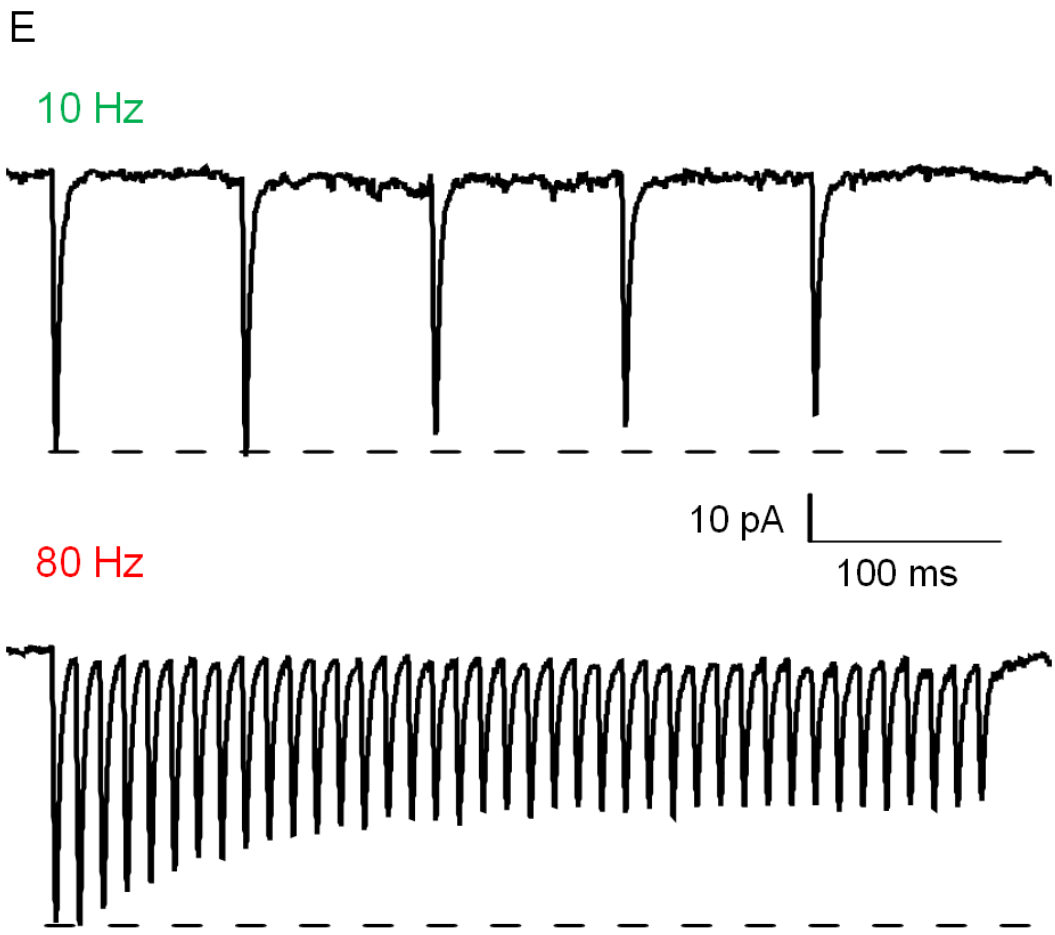

Figure 3.10 continued – Responses to trains of 2 msec light flashes at 37ºC

E- Examples of traces with 10Hz (top) and 80 Hz (bottom) stimulation. Notice how mild desensitisation is apparent at even 10Hz, and this effect is much more exaggerated at 80Hz. Comparing the first and last 5 responses at 80Hz gives $p<0.05$ (student's t test)

3.3.8 Slowly increasing light intensity avoids peak

Under some experimental conditions it might be useful to avoid the large transient peak current that ChR2 exhibits. By increasing light intensity gradually, we were able to lose the peak completely. This is illustrated in figure 3.11. Part A shows pooled data of a rectangular light step, which results in the characteristic ChR2 current, which rises quickly to a peak, and then desensitises to a steady state current. By ramping up light intensity, this peak is avoided but the steady state current is not affected (Figure 3.11B).

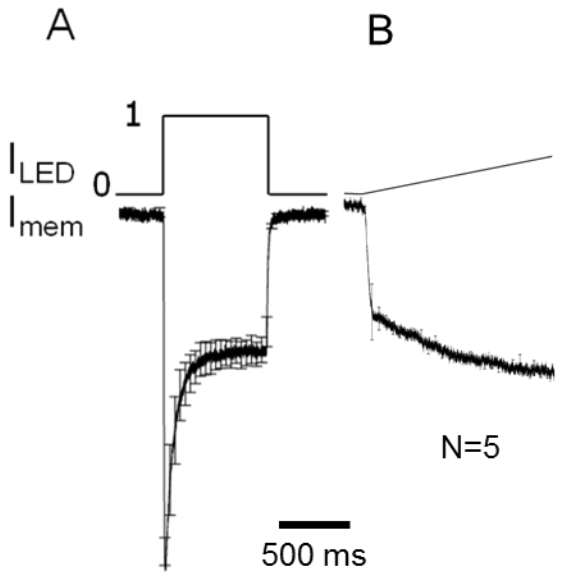

Figure 3.11 – Loss of peak

HEK 293 cells were transfected with ChR2-EYFP, and cells exhibiting yellow fluorescence were whole-cell patch-clamped.

In some preparations it might be advantageous to avoid the large peak produced by ChR2 activation. We noted that it is possible to avoid this by steadily ramping up light intensity, as opposed to the more typical ‘rectangular wave’ light flash

A - Light step induces sharp inward current rising to a noticeable peak (n=5)

B – Steadily rising light intensity abolishes peak (n=5)

3.4 Discussion

Channelrhodopsins (and the other members of the light-activated cohort of ion channels and pumps) have been introduced to the field of neuroscience as a set of tools to stimulate and control neurones. However it is important to understand the behaviour of ChR2 and its macroscopic kinetics and voltage-dependence in a simpler mammalian cell line than primary neuronal culture. Previously, several labs have investigated the biophysical properties of ChR2 in a variety of systems (including xenopus oocytes and HEK293 cells, (see Nagel et al., 2003, Bamann et al., 2008, Zimmermann et al., 2006) but in an incomplete fashion, focussing mainly on channelrhodopsin-2's photocycle, permeation properties and channel protonation/deprotonation.

In order to characterise the biophysical properties of channelrhodopsin-2 we overexpressed a fluorescently tagged version of ChR2 in HEK293 cells, then using whole-cell patch-clamp investigated several aspects of its function at room temperature (22^{o}C) and at a temperature more physiologically relevant to mammalian cells (37^{o}C). Under these conditions, ChR2-EYFP expresses well and is trafficked to the surface of the cell, as shown by our combined confocal and electrophysiological data. HEK293 cells tolerate the rhodopsin well, and require no extra factors (i.e. retinal) to mediate the channel's function (see figures 3.1 and 3.2)

The recovery from desensitisation of ChR2 is a relatively slow process, which is further slowed by depolarisation (see Nagel et al., 2003; and Fig. 10). At ≈22^{o}C and a membrane potential of −85 mV, the majority of the peak is recovered after 10 seconds, but complete recovery takes ≈20 seconds. This may be a disadvantage when aiming to use ChR2 to repeatedly stimulate cells at high frequencies. Our experiments at ≈22^{o}C (using trains of 2ms flashes applied at 10, 20, 40 and 80 Hz) show that even a single 2 ms flash triggers ≈5% desensitisation (Fig. 3.10B). This desensitisation is seen in the reduced peak amplitude of the next response in the stimulus train. As ChR2 has a slow rate of recovery from desensitisation this means that little recovery can occur in the short time period between stimuli when they are applied at frequencies of 10 Hz or higher.

Recovery from inactivation remains slow at physiological temperatures (see figure 3.10), with similar decreases in trains of flash responses. Conversely, deactivation is faster at these temperatures, leading to less summation of responses at faster frequencies (for example 80 Hz), but there is still a significant decrease in peak amplitude (see fig. 3.9).

One possible way around this is to increase ChR2 expression to higher levels. However, ChR2 lets a significant amount of calcium into the cell through its pore region, and this may have implications for the study of plasticity in certain cell types, neurones being a prime example (see Caldwell et al., 2008).

Previous work has utilised ChR2 in both warm and cold-blooded species (see Aravanis et al., 2007) including studies performed *in vivo*. With this in mind we compared ChR2 responses at ≈22ºC and 37ºC. ChR2 activation, deactivation, desensitisation and recovery from desensitisation are all quicker at 37ºC than ≈22ºC. At 37ºC the increase in rate is approximately double that of ≈22ºC at all membrane potentials examined (Fig 3.9).

Current *versus* voltage relationships reveal that ChR2 is a strong inward rectifier (see Nagel et al., 2005a; Bamann et al., 2008; Zimmermann et al., 2006). We used both voltage ramps (fig 7) and varying steady state voltage-clamp potentials (fig 8) to examine ChR2s voltage dependence, and our data corroborates previous studies. Our data show that at ≈22ºC and 37ºC both activation and deactivation were significantly slowed by depolarisation (Fig. 9) and there is a voltage-dependence in the extent of desensitisation generated at steady state (Fig. 9). These voltage-dependent changes may have functional consequences in experimental involving neuronal cell types. For example the voltage-dependence of activation means that in a neurone with a membrane potential of −55mV ChR2 will take approximately 30% longer to activate than in a neurone at −85mV (Fig. 9). On the same lines, the voltage-dependence of deactivation will cause responses to brief light flashes to be approximately 30% longer in cells at −55 mV than cells at−85 mV.

Our results also show that we can drive ChR2 at frequencies in HEK cells above and beyond what would likely to be needed in a neuronal stimulation

paradigm (see figure 3.10).There is no reason to think this would differ significantly in a neuronal cell.

Here we describe various aspects of the gating of ChR2 expressed in a mammalian cell-line which indicate that a number of different factors determine the effectiveness and timecourse of activation. A variety of factors that will influence the response to ChR2 activation include the type of light illumination, the intensity of light illumination, when ChR2 was previously activated (and the duration of the last activation), the membrane potential of the cell, and the extracellular pH. These are all also sensitive to temperature.

In several experiments a degree of rundown was noticed when comparing the initial ChR2 light evoked responses and responses elicited seconds to minutes later. The cause of this rundown is not entirely clear. In some case (see figure 3.5C and D) channel desensitisation may be responsible, as the inter-flash interval was not sufficient for full recovery from desensitisation. It is also possible that other factors were at play, such as changes in series resistance.

Chapter 4

Results

Utilising Channelrhodopsin-2 in a dispersed neuronal culture model

4.1 Aims

Chapter 3 described overexpression of the ChR2-EYFP construct in HEK293 cells, and the subsequent characterisation of ChR2 response's to various light stimuli whilst varying temperature and voltage. Satisfied that we had determined the basic biophysical parameters of ChR2, I moved onto neurones. The aim was to use ChR2 to noninvasively drive action potential generation in neurones. This chapter explores overexpression of ChR2 in dispersed hippocampal neuronal cell culture, and raises some points about the usage of ChR2 in certain experimental paradigms.

4.2 Introduction

As detailed in previous chapter, over-expressed fluorescently tagged Channelrhodopsin-2 trafficks to the surface and forms functional channels in HEK293 cells. I therefore next investigated their properties in dispersed hippocampal neuronal cultures. These represent a simplified neuronal assay system that has both advantages, and disadvantages over other neuronal models (Banker and Cowan 1977; Banker and Cowan 1979). Access to cells is extremely easy in these cultures, both in an imaging context and an electrophysiological context, as cells are lying flat

in a layer on a coverslip. These cultures are also relatively easy to transfect with plasmids, using (in this case) Lipofectamine ^{2000}, a commercially available transfection agent. Alternatives to dispersed cultures (for example organotypic slices, semi-acute slices) while potentially more physiologically relevant, are more difficult to culture, and typically require either viral or biolistic techniques to express exogenous protein.

Our previous data show that ChR2-EYFP expresses well in HEK293 cells, and is capable of trafficking to the surface, and depolarising the plasma membrane in response to flashes of blue light. Initially we hoped to confirm that this was also the case in our dispersed hippocampal cultures. We also examined whether our neurones could tolerate ChR2 activation, and that the responses were stable in neuronal cells, as they were in HEK293 cells.

One of the key properties of neurones is their ability to generate the tightly controlled waves of depolarisations know as action potentials (APs). ChR2 can initiate APs, via the opening of the channel pore in response to blue light, and the subsequent ion entry and depolarisation of the cells membrane (see (Zhang, Wang et al. 2006; Zhang, Aravanis et al. 2007; Gunaydin, Yizhar et al. 2010). The data presented in the previous chapter show that the experimental setup is capable of delivering short blue light flashes at frequencies up to 400 Hz, and that the membrane depolarisations of HEK293 cells could follow these light flashes. I therefore set out to determine if Lipofectamine-mediated expression of ChR2 in dispersed hippocampal neuronal was sufficient to drive and control spiking in neurones.

4.3 Methods

4.3.1 Dissection and Neuronal Culture

Pregnant Wistar rats were overdosed with isofluorane until cardiac arrest was induced, then decapitated. E18 embryos were removed and placed in HBSS. Brains were removed from the skulls and the cortex and hippocampus removed under a dissecting microscope. Hippocampi and cortex were pooled separately, and washed three times with HBSS (in 10ml and 30ml volumes respectively). Brains were then incubated with trypsin (0.5 mg ml) in a water bath set at 37^{o}C for 9 or 15 minutes respectively. Brains were then washed another four times in HBSS.

Cortical samples were then suspended in 5ml plating medium (Neurobasal {Gibco}, supplemented with horse serum {10%}, B27 {Gibco}, penicillin/streptomycin and 2mM glutamine), then mechanically dissociated by repeated triturating (10-20 times) with a 5ml pipette. Samples were then made up to 20 ml and then filtered through a 70 µl cell strainer {Millipore} to remove excess debris.

Hippocampal samples were added to 1ml plating media, and then mechanically dissociated by trituration with a P1000 pipette. This cell suspension was then made up to 5 ml with plating media.

Cell number was then determined using a haemocytometer and diluted to 2 million cell per millilitre (cortical) and 0.5 million cells per millilitre (hippocampal). Cells were then added to pre-prepared wells contained 2 ml plating media and coverslips, and placed in an incubator. Two hours after plating cells, the media was completely replaced with feeding media (same composition as plating media described above, minus horse serum), and the cells were returned to the incubator. Cells were then fed with by removing 0.3ml and adding 0.5ml feeding media every 5 days until they were used.

4.3.2 Lipofectamine Transfections

To induce ChR2 expression in neurones, cells were transfected using Lipofectamine^{2000} (Invitrogen) with 2-5 µg DNA per dish, and used in experiments 2-5 days later. See Chapter 2 (Materials and Methods) for more detail.

4.3.3 Electrophysiology

Except where stated below, all electrophysiology was performed as in Chapter 2 (Materials and Methods). Intracellular solution contained (in mM) K-Gluconate, 130; KCl, 20; HEPES, 10; EGTA, 0.2; GTP-Na salt, 0.3; ATP Mg salt, 4; pH adjusted to 7.3 with KOH; ~295 mOsm.

Neuronal current responses to light pulses were recorded in whole-cell voltage clamp for the majority of the experiments, but some employed the whole-cell current clamp configuration. Finally, some recordings used the loose-patch configuration in voltage clamp to non-invasively characterise ChR2-mediated action potential responses. In these recordings, pipettes were filled with standard extracellular solution, as described above.

4.4 Results

4.4.1 Expression of ChR2 in dispersed hippocampal neuronal cultures

DIV 12-14 hippocampal cultures were transfected with ChR2-EYFP using Lipofectamine 2000 as previously described. Figure 4.1 shows example images of neurones (*left*) and astrocytes (*right*) expressing ChR2-EYFP. The fluorophore-tagged protein is clearly present throughout the dendritic arbour and axon without obvious clustering in specific cell compartments.

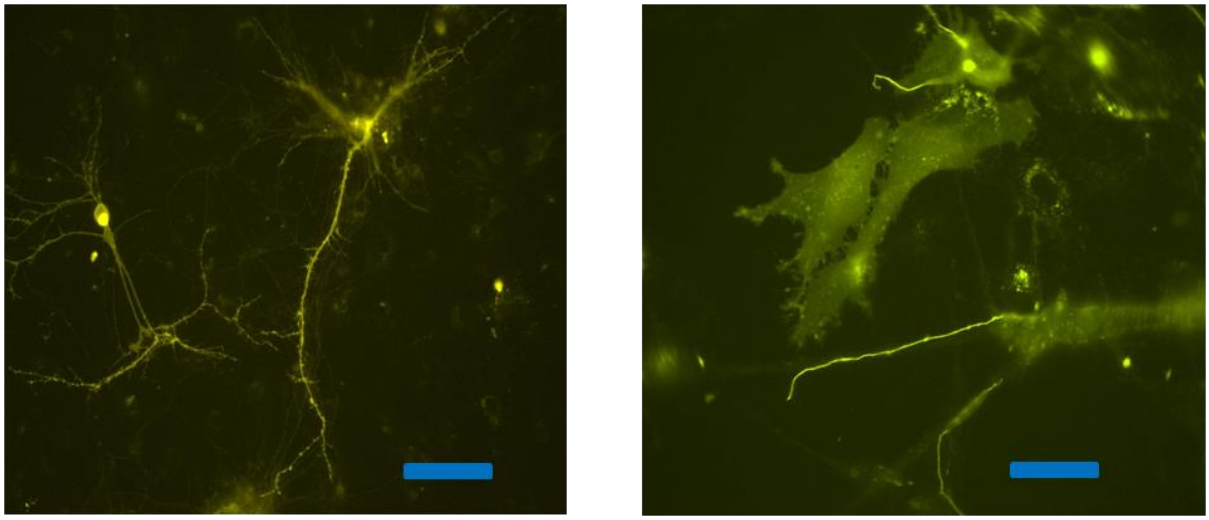

Figure 4.1 Example wide field images of cultured E18 cells expressing ChR2-EYFP

Dispersed hippocampal cultures were transfected at between DIV 12-14 with ChR2-EYFP. 72 hours later cells were imaged on a widefield microscope. *Left*, a neurone, and *right* an astrocyte, both expressing ChR2-EYFP. Scale bar is 100 µm

4.4.2 Trial-to-trial reproducibility

An important consideration with using any stimulating technique is whether or not it is stable. To check this was the case, we subjected dispersed hippocampal neurones expressing ChR2-EYFP to a paired flash protocol. We subjected cells to 2 successive flashes, separated by a brief interval, and compared trial-to-trial performance, see figure 4.2A. Each pair of flashes was separated from the next pair by a period of 20 seconds with no light, to allow full recovery of the peak current. We then compared peak and sustained current, see figure 4.2B. Rundown over the whole experiment was significant ($p<0.05$ for both peak and sustained current, comparing first and last responses, student's t test), and the initial fall noted is due to the initial desensitisation of the channel and resultant reduction in magnitude of peak current. These data indicate that use of ChR2 is relatively stable in hippocampal neurones over the time scales of short experiments, but rundown of the response must be taken into account.

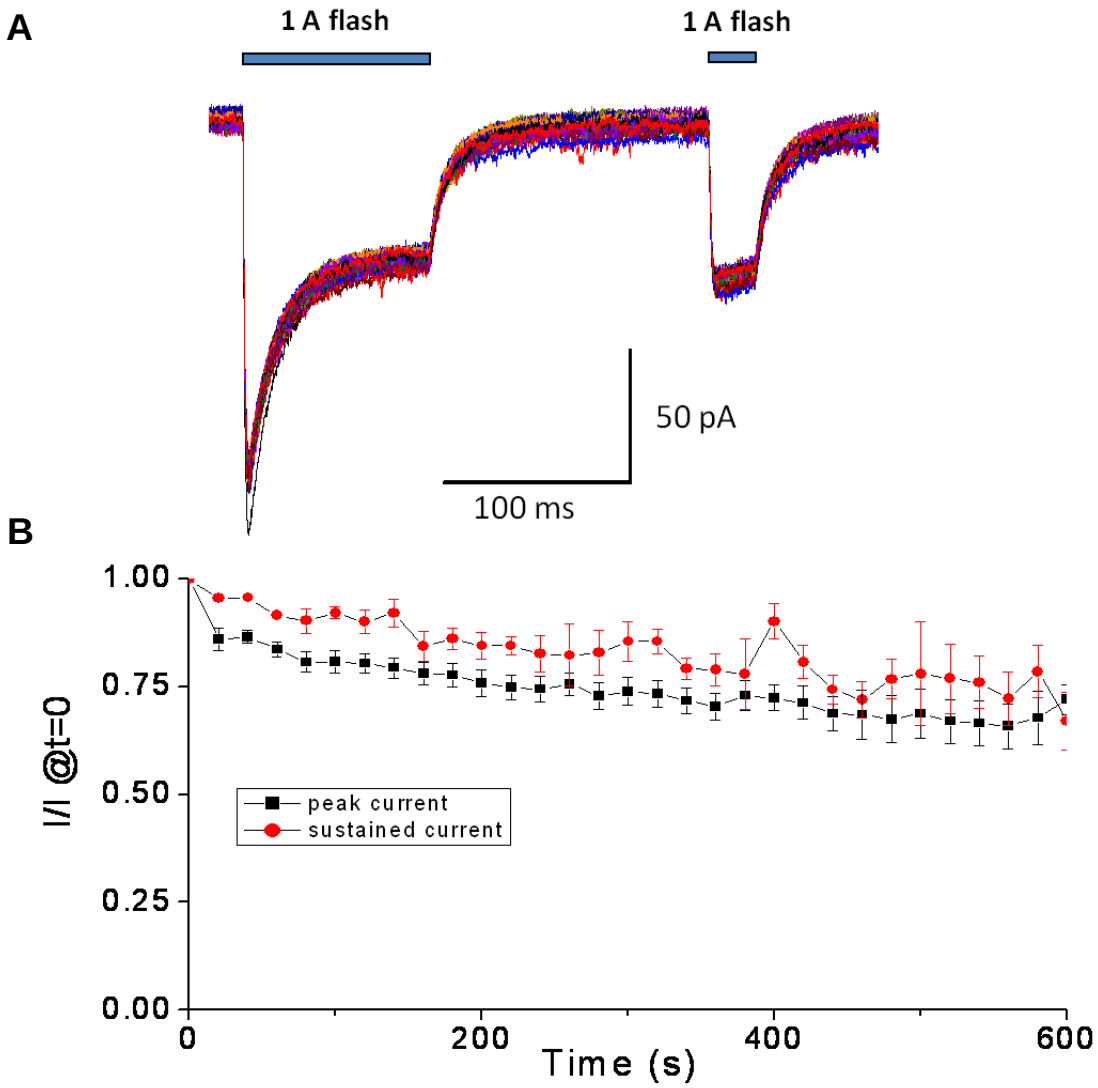

Figure 4.2 - Trial to trial reproducibility

Hippocampal cells were transfected with ChR2-EYFP, and cells exhibiting yellow fluorescence were whole-cell patch-clamped.

A - An example recording in which 60 paired flashes were applied to a ChR2 expressing cell at 0.05 Hz.

B – Plot of pooled peak current (black squares) and sustained current (red circles) data against time. Both decrease significantly over time ($p<0.05$ comparing first and last responses, student's t test)

4.4.3 Response to trains of light flashes

Our experimental setup is capable of inducing trains of light-induced membrane depolarisations in excess of 300 Hz in HEK293 cells expressing ChR2 (see figure 3.10). Figure 4.3A shows example traces from a neurone expressing ChR2-EYFP that has been whole-cell patch-clamped and exposed to a train of 2 ms flashes at various frequencies (figure 4.3A). As in the HEK data, a loss of peak amplitude caused by the desensitisation of ChR2 is clearly apparent, as is summation above 20 Hz. This aside, the membrane response of the neurones is closely time-locked to the light stimuli. Differences between trains recorded in HEK293 cells and neurones may be explained by incomplete space clamp in the neuronal recordings, and other intrinsic neuronal membrane properties such as the preponderance of membrane channels.

So far in this body of work, all the electrophysiological data has been recorded in the voltage clamp configuration. However, in order to record neurones firing action potentials the current clamp configuration must be used. We first briefly tried this in HEK293 cells. Figure 4.3B shows two traces recorded from a HEK293 transfected with ChR2-EYFP. *Top* is in the current clamp configurations, and *bottom* is in the voltage clamp configuration.

Next we tried to record from hippocampal neurones in current clamp. Figure 4.3C shows 4 overlaid example traces from a neurone subjected to trains of light flashes at varying frequencies (10, 20, 40 and 80 Hz). Notice membrane oscillations but no action potential generation. This particular cell did not fire any action potentials. This may have been because ChR2 expression was not high enough to sufficiently depolarise the cell, or because the cell was initially too hyperpolarised to reach threshold upon light stimulus. We are able to say this conclusively as we are whole-cell in this case, but when stimulating *in vitro* or *in vivo* this could be an issue, as you cannot be sure your light flash stimuli are necessarily inducing action potentials in the target cells.

Fortunately, this was not true of all the neurones expressing ChR2. Figure 4.3D shows example traces recorded in current clamp from a ChR2 expressing

neurone in which the light flashes induced the cell to fire action potentials at a range of frequencies from 10 Hz to 80 Hz. At lower frequencies each stimulus was sufficient to generate a corresponding action potential but, at higher frequencies failures begin to appear. Figure 4.3E summarizes the ratio of success to failures from a single cell in response to trains of various frequencies

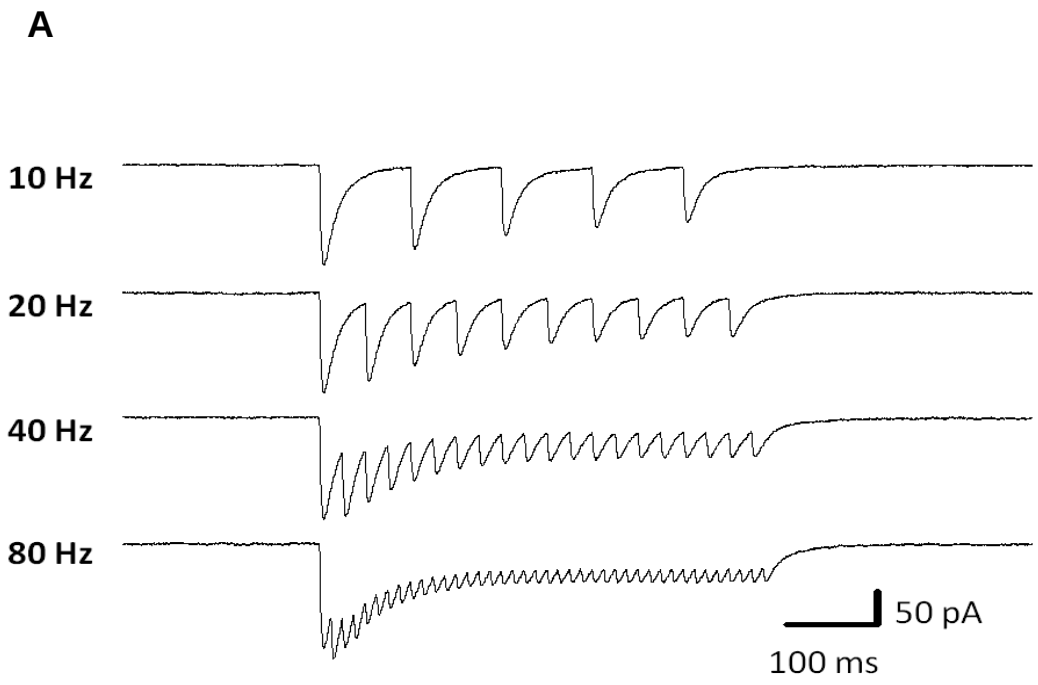

Figure 4.3 Responses to trains of light flashes in hippocampal neurones at room temperature

Dispersed hippocampal cultures were transfected between DIV 12-14 with ChR2-EYFP, and recorded from 48-72 hours later.

A - Responses to trains of 2 ms flashes applied at 10, 20, 40 and 80 Hz as indicated. Note that desensitisation accumulates at all frequencies, and becomes more obvious as frequency increases.

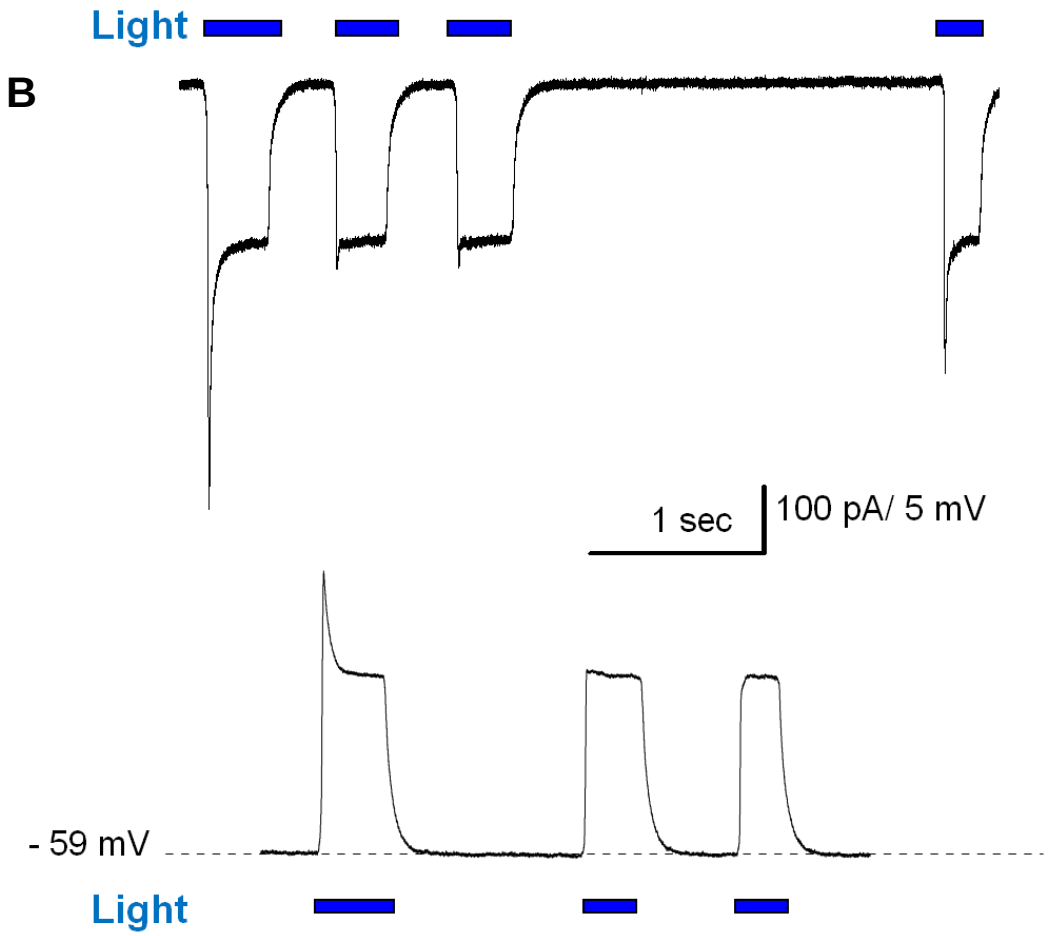

Figure 4.3 continued Responses to trains of light flashes hippocampal neurones

Dispersed hippocampal cultures were transfected between DIV 12-14 with ChR2-EYFP, and recorded at room temperature from 48-72 hours later.

B - Example traces in HEK293 cells showing recordings in current clamp (*top*) and voltage clamp (*bottom*)

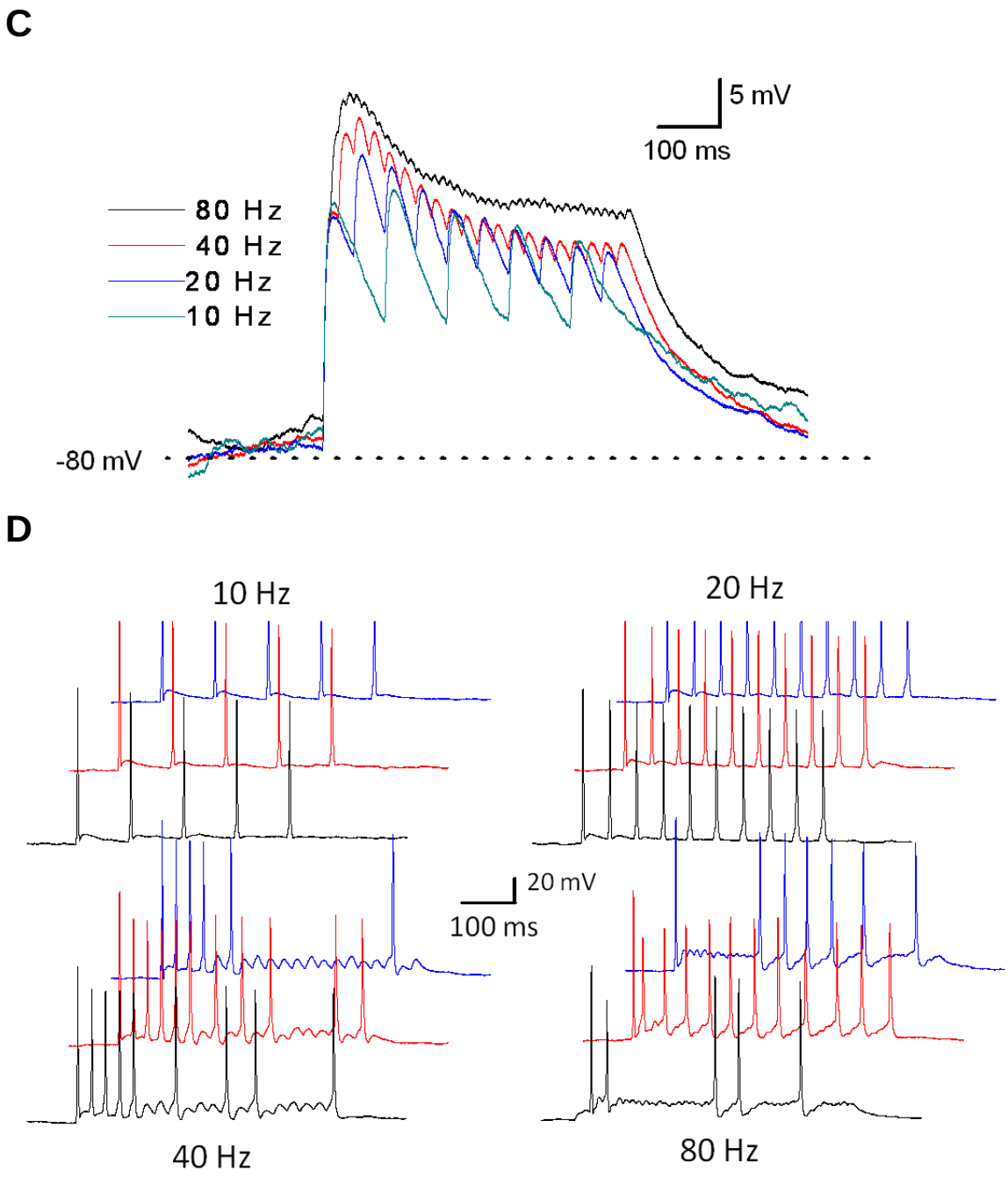

Figure 4.3 continued Responses to trains of light flashes hippocampal neurones

C - Voltage recording from a ChR2 transfected hippocampal neurone flashed with 1A LED current, 2 ms duration, light flashes at the indicated frequencies. In this cell the summating depolarisations were sub-threshold for action potential activation

D - Recordings from a different cell in which ChR2 activation with 2 ms flashes elicited action potential firing. For each activation frequency tested three separate trials are shown. Vrest was ~-75 mV. Note the inability to follow 40 and 80 Hz stimulation.

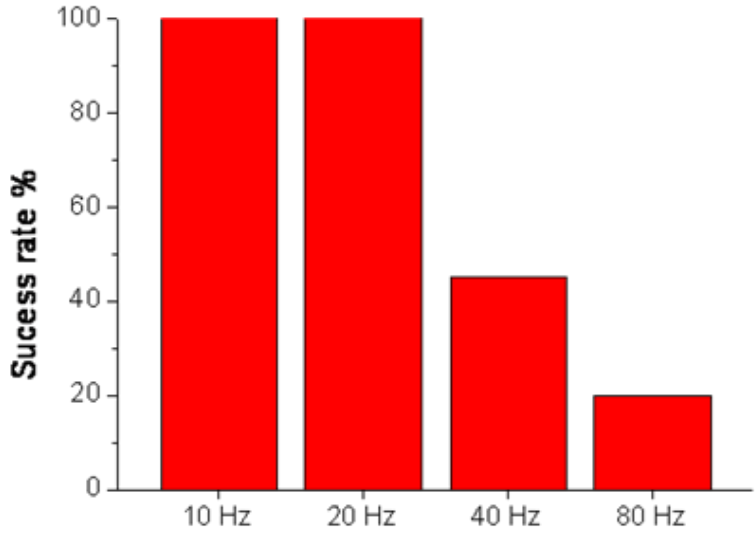

Figure 4.3 continued Responses to trains of light flashes in hippocampal neurones

E – Ratio of successes to failures of the cell shown in D

4.4.4 Latency of action potentials in the loose patch configuration

Dispersed hippocampal neurones were grown for between 10 and 12 days in culture then transfected using Lipofectamine ^{2000} with ChR2-EYFP. Cells were left for 2-3 days to allow for ChR2 expression, then transferred to an extracellular recording solution, and placed in the patch clamp rig chamber.

For the loose patch configuration the solution inside the glass electrode was the same as the ECS. The electrode was manoeuvred until it lightly touched the outside of a ChR2-expressing neurone, but no tight seal or effort to break in was made. Cells were then exposed to brief light flashes and current deflection recorded. Figure 4.4A shows a schematic of the experimental set-up, with an example trace visible on the top left. This method is advantageous as it is non-invasive, with none of the associated problems of washout and it stays as close to physiological conditions as possible when working in culture. Conversely, the loose-patch technique cannot tell us anything about the size of the generated action potential, just information about the latency. Responses induced by light in the loose patch configuration were blocked by TTX (data not shown).

Cells were exposed to trains of 20 5 ms light flashes, at 0.5, 2, 10 and 20 Hz, illustrated in figure 4.4B. The latency from exposing the cell to a light flash to the generation of an action potential by the neurone becomes increasingly longer as the train of 20 stimuli progresses. For all frequencies tested, latency was significantly longer for the final response than the first ($p<0.01$, student's t test). This is shown in figure 4.4E. This was true at all frequencies. At frequencies above 10 Hz failures started to appear in the action potential train, with the neurone failing to follow the light flashes. On average the action potential latency for first stimulus was 3.3 ± 0.2 ms from the onset of the 5 ms light pulse, whereas the action potential latency for the last (20th) spike was 5.3 ± 0.5 ms. The increase in latency from start to finish was significantly different between groups except for at 0.5 and 2Hz ($p=0.14$, and $p<0.05$ in all other cases, student's t test).

Once a spike train was finished, re-stimulating the same cell with another 5 ms light flash triggered an action potential with a latency of 3.4 ± 0.3 ms, which is not

significantly different to the first (naïve) response in the stimulus train (3.3 ± 0.2 ms, as stated above, p=0.2, student's t test).

This result suggests that when repeatedly stimulating hippocampal neurones the onset of the action potential will be different between the first flash in a sequence and subsequent flashes. At 0.5 Hz this difference is less than 2 ms when comparing first to last response, but when the frequency increases to 10 Hz this difference is over 15 ms. Therefore there is a reversible short-term change in the firing pattern of the neurone when stimulating with ChR2 in this way. This could either be a property of the neurone, perhaps a form of short term intrinsic plasticity, or alternatively it could be a property of the rhodopsin. Marrying this data with some of the data gathered from the previously described HEK293 studies suggests an explanation. The desensitisation of the peak current seen upon repeated activation of ChR2 is likely responsible for this effect. An initial light stimulus opens ChR2 molecules sitting in the neuronal plasma membrane. The channels open, and let ions through (predominately Na^+). As ions pass, the membrane depolarises and moves towards the threshold for action potential generation. As it passes threshold, the action potential is triggered and the neurone fires a spike. On the next light stimulus light stills opens the rhodopsins, but due to desensitisation the peak amplitude of the current is reduced. Consequently less ions pass in the same period of time, and the neuronal membrane takes longer to charge, and therefore longer to reach threshold. The end result is an increase in the latency to peak. This has some implications for the usage of ChR2 to drive activity in neurones (and perhaps other cell types). Effectively the cell is never experiencing the same stimulus twice in a train of stimuli. However the effect is small and will only be a concern in certain types of experiment. For example, experiments requiring that a neurone receives a very precise amount of depolarisation several times in succession may be compromised by this property of ChR2.

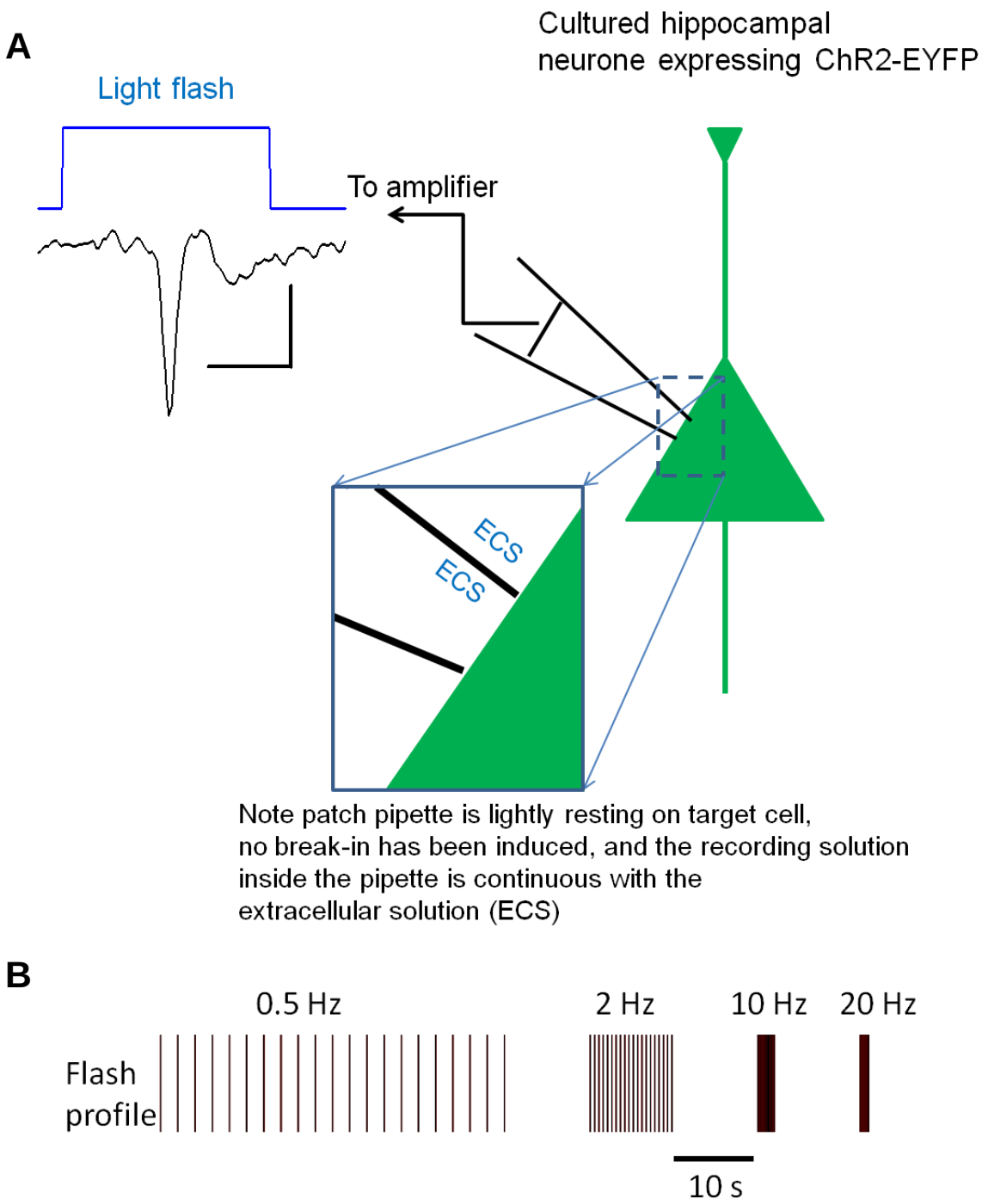

Figure 4.4 Action potential latency in the loose patch configuration

Dispersed hippocampal cultures or HEK293 cells were transfected between DIV 12-14 with ChR2-EYFP, and recorded from 48-72 hours later.

A – Experimental set-up for the loose patch configuration. Recording pipette is filled with extracellular solution (ECS) and gently lowered onto the outside of the neurones cell body. 5 ms light flashes were delivered by our Cairn OptoLED light source. An example light step and recorded response can be seen on the top left.

B – Schematic illustrating flash profile delivered to cells. All cells received the same number of flashes, but delivered at different frequencies

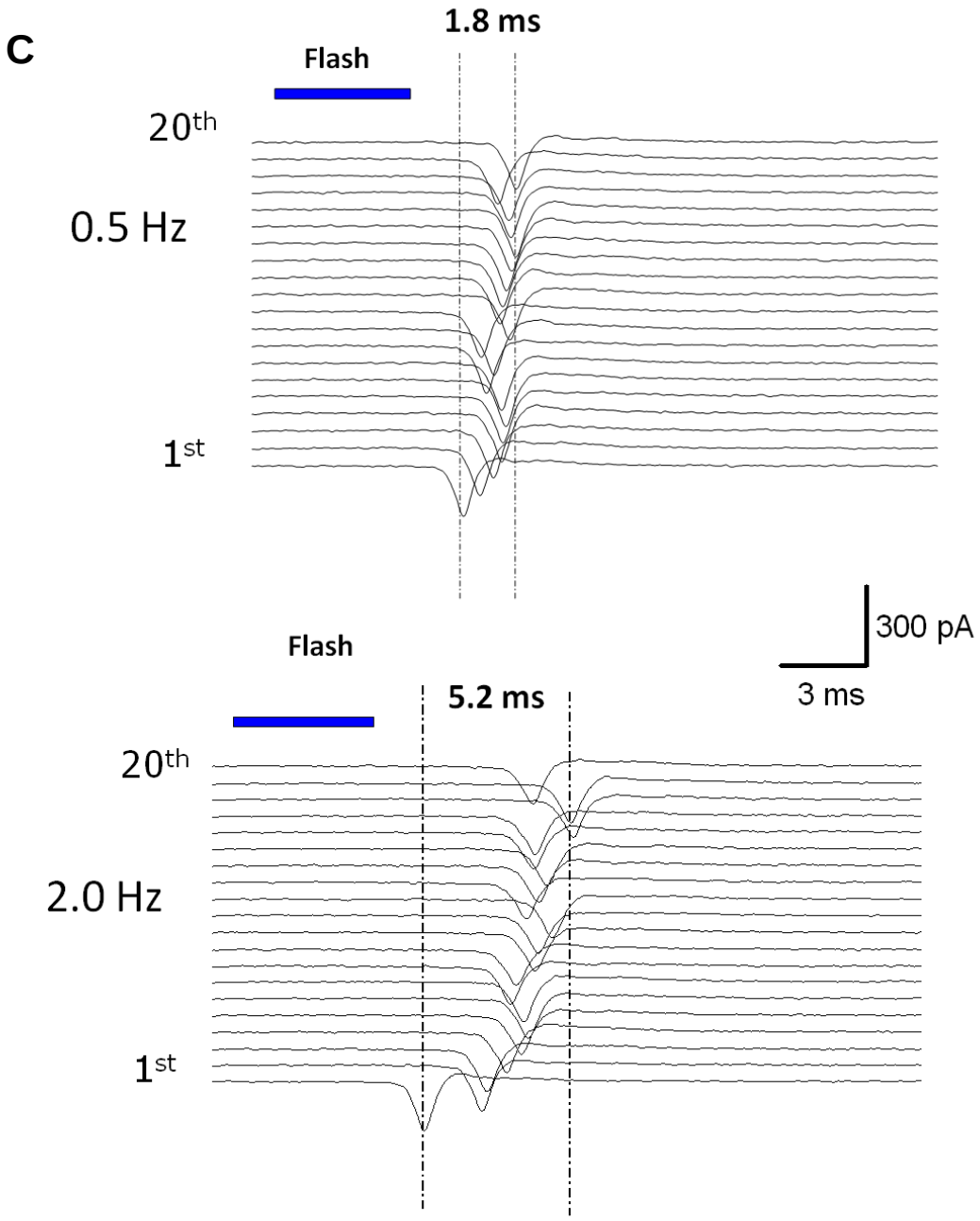

Figure 4.4 continued - Action potential latency in the loose patch configuration

C – Traces recorded in loose patch configuration from 0.5 Hz (*top*) and 2 Hz (*bottom*) flash trains.

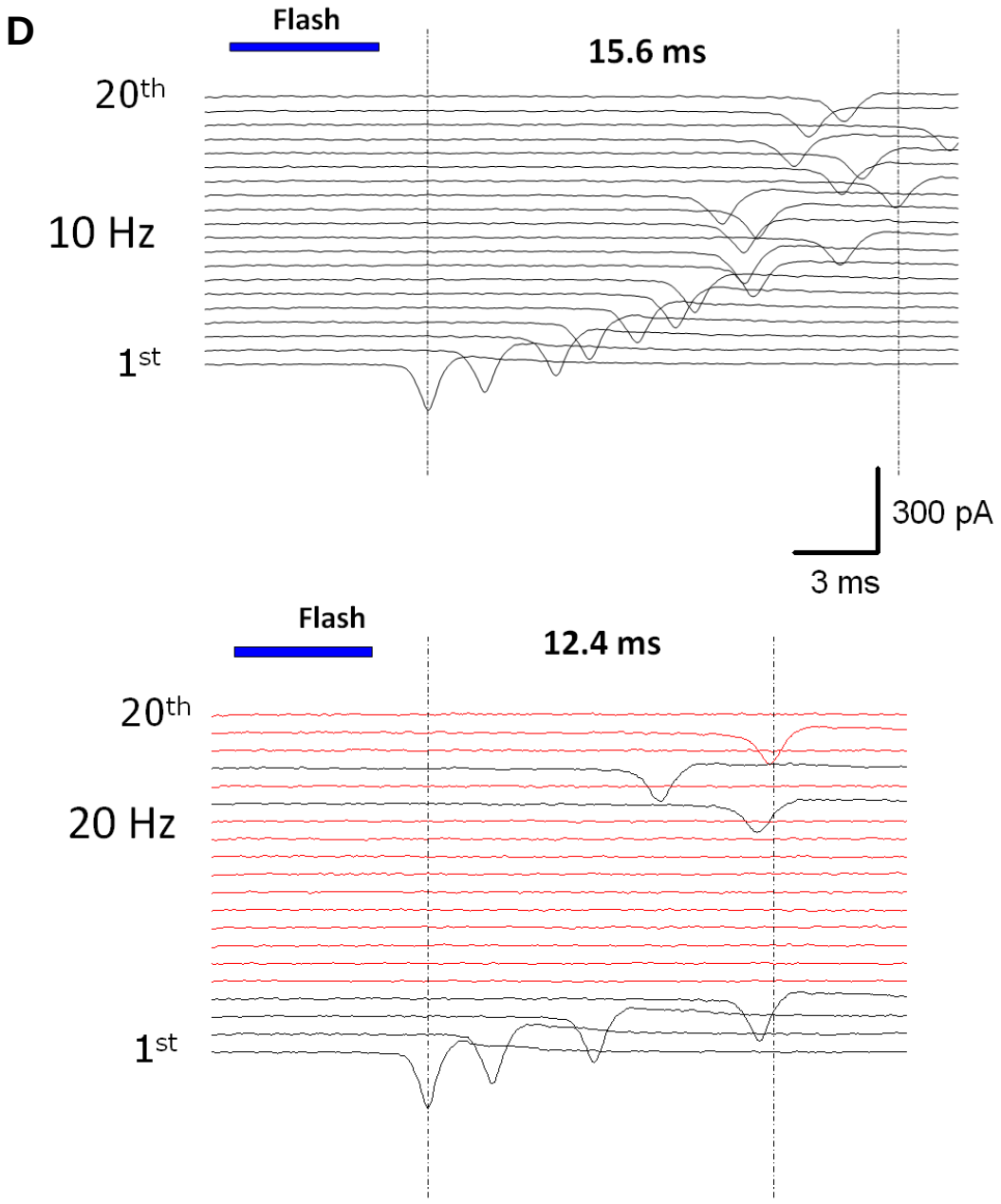

Figure 4.4 continued Action potential latency in the loose patch configuration

D - Traces recorded in loose patch configuration from 10 Hz (*top*) and 20 Hz (*bottom*) flash trains. Notice failures in 20 Hz flash train.

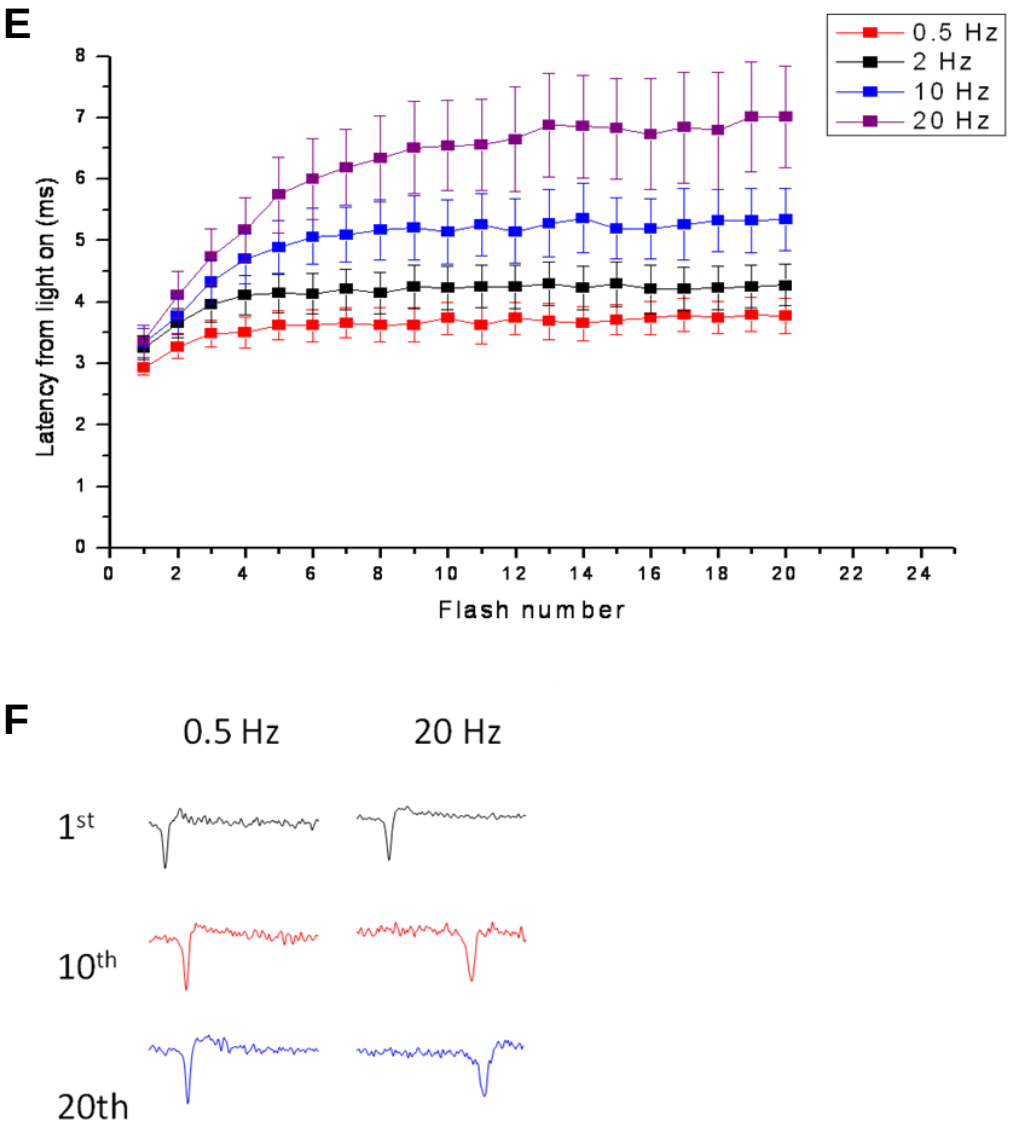

Figure 4.4 continued Action potential latency in the loose patch configuration

E – Plotted data showing flash number plotted against the average latency between light on and peak deflection. Failures are not plotted. There is no significant difference at the start between any frequencies ($p>0.1$) but at the twentieth light flash all groups are significantly different from one another except 0.5 Hz and 2 Hz ($p<0.05$, student's t test)

F – Example traces comparing the first and the last (twentieth) responses to light flashes in the slowest (0.5 HZ) and fastest (20 Hz) flash profiles.

4.4.5 Epileptiform activity in cultures triggered by light flashes

Dispersed hippocampal neuronal cell cultures transfected via Lipofectamine ^{2000} typically have fairly low expression levels. In our hands, cell transfection efficiency with ChR2-EYFP is between 2 and 5%. This means on a 15mm coverslip with approximately 70,000 neurones as few as 1400 will be expressing ChR2. Even with these low levels of ChR2 expression, we still noticed that activity in this small subset of the neuronal population could have effects upon much of the network. One example is the generation of epileptiform activity in the network. In the presence of a GABA antagonist, flashes of blue light could trigger self-perpetuating waves of activity in the dish. These are possibly analogous to seizures in intact brain tissue. Whilst patch-clamping multiple cells was beyond the scope of this investigation, patching a single cell and delivering light to the preparation was possible. An example of this is shown in figure 4.6. A single 2 ms flash was sufficient to trigger large waves of depolarisation that on occasion lasted more than 5 minutes. This is likely partly due to the hyperwired nature of cultures, and in the absence of GABA antagonist this epileptiform activity was never seen. Removing the cultures inhibitory input destabilises the network, and then an input of activity (occurring at several sites at once, viz. at each ChR2-expressing cell) is sufficient to trigger the ‘seizure’. The gradual reduction over time may be due to the desensitization of synaptic receptors.

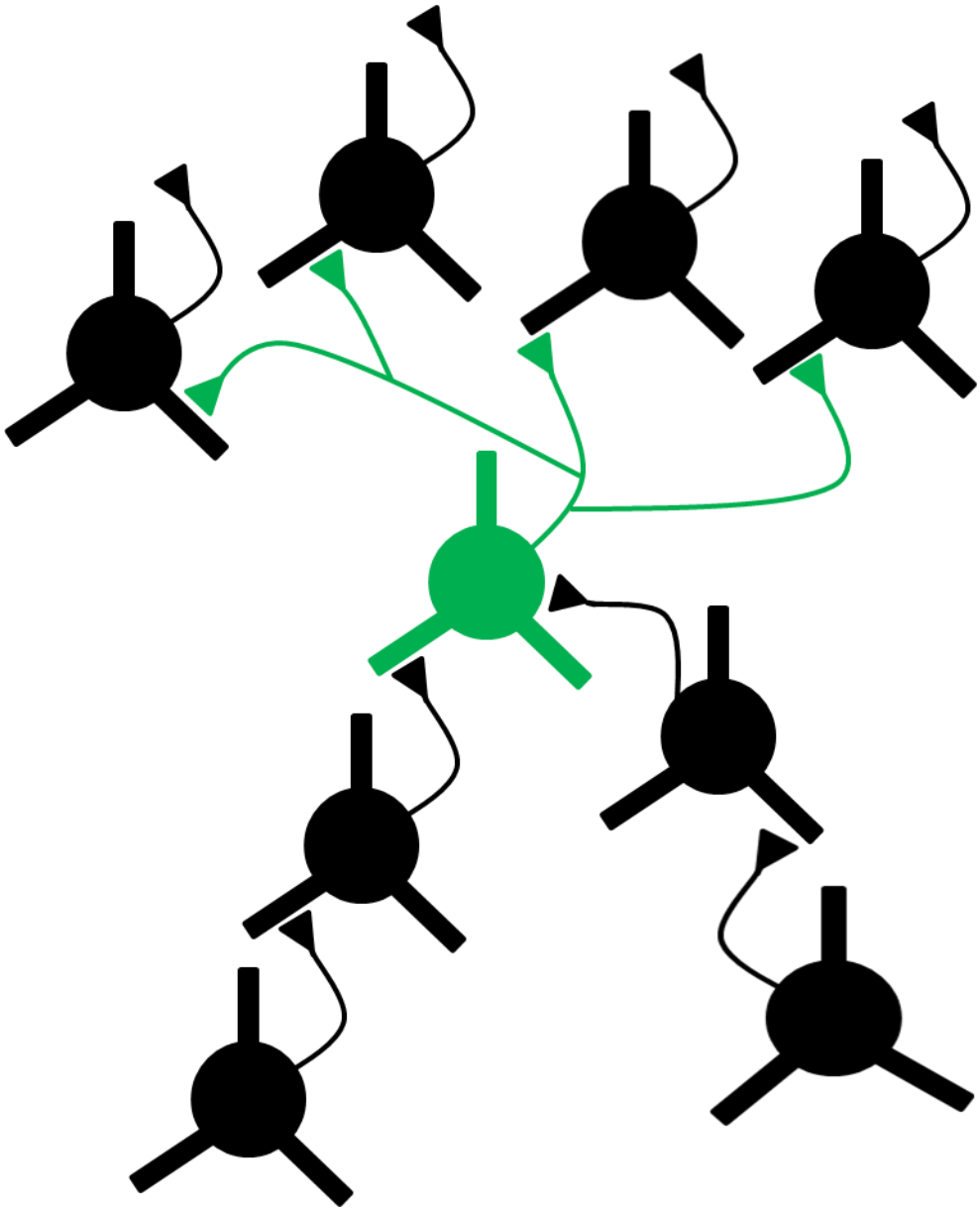

Figure 4.5 Schematic of ChR2-expression in dispersed hippocampal cultures

Transfection efficiency of ChR2-EYFP using Lipofectamine 2000 is between 2 and 5%. This results in a fairly low number of ChR2-expressing neurones in our cultures, perhaps as low as ≈1400 cells out of 70,000 cells on a single 13mm coverslip. This is illustrated above. A ChR2-expressing neurone (in green) is surrounded by non-transfected cells, and the vast majority of its synaptic partners will not be expressing the light-sensitive rhodopsin.

(Black, untransfected cells also synapse onto each other, not shown for clarity)

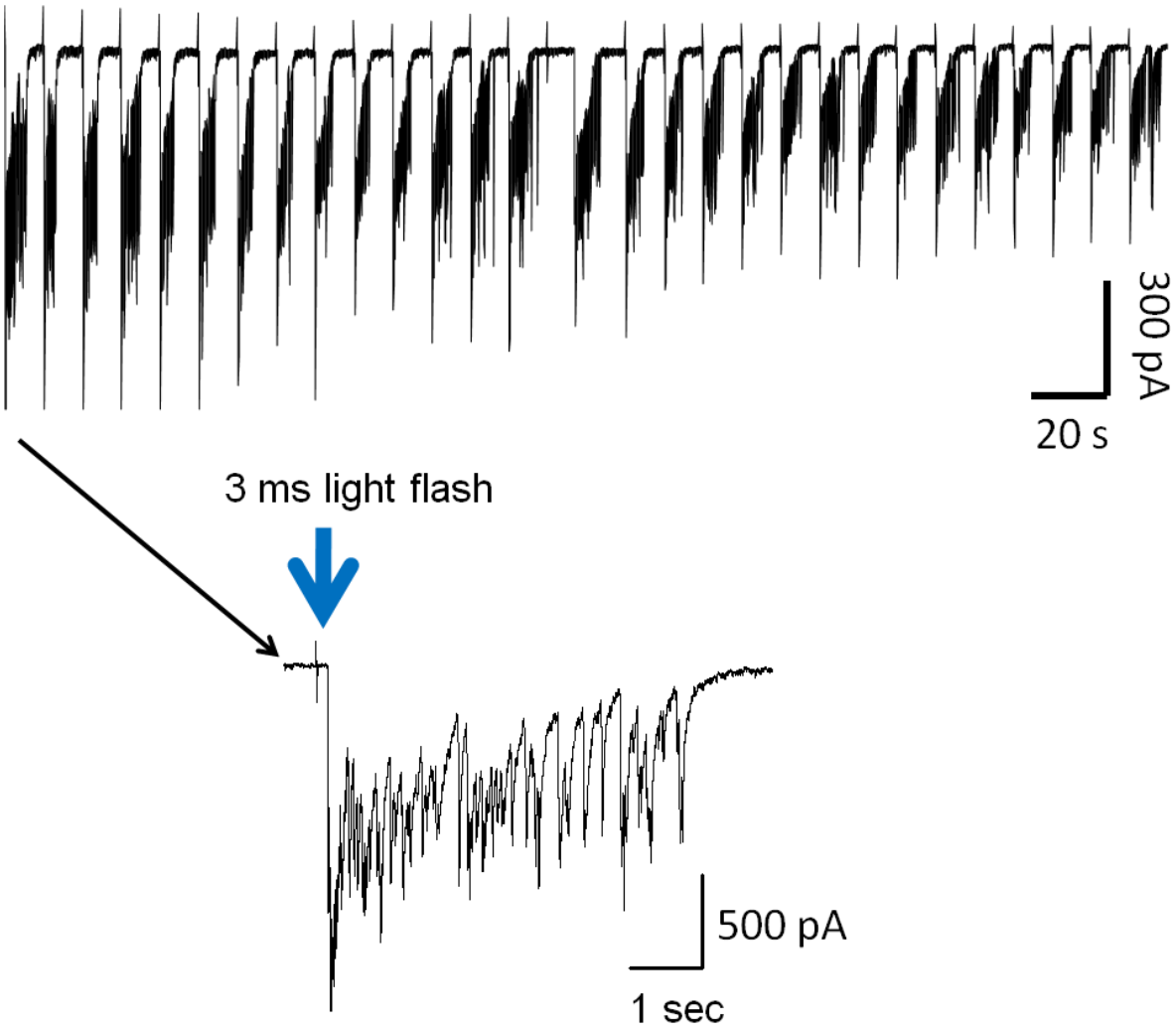

Figure 4.6 Light-driven epileptiform activity in dispersed hippocampal culture

Dispersed hippocampal cultures or HEK293 cells were transfected between DIV 12-14 with ChR2-EYFP, and recorded from 48-72 hours later. A non-transfected cell was chosen to patch-clamp. In this figure gabazine was added to the ECS at 10 µM.

Top, an example trace recorded from a cell *not* expressing ChR2 (a black cell in figure 4.5), but situated in a culture dish that has been transfected with ChR2-EYFP. Individual 3 ms light flashes initiate large and long-lasting waves of depolarisation in the culture.

Bottom, a magnified view of one of the bursts of depolarising activity

4.4.6 Post-synaptic responses to pre-synaptic ChR2 activation

There are two basic experimental conditions available in our dispersed hippocampal culture expressing ChR2, either choosing to patch a cell expressing ChR2 or patch a non-transfected cell in a dish with other cells that *are* expressing ChR2. As our ChR2 is fused to an EYFP molecule we can choose to patch cells that exhibit no fluorescence. However this technique could fail to detect cells that are expressing ChR2-EYFP, but only at a low concentration. Fortunately, it is also possible to assess the patched cell for the presence of ChR2 by the shape and latency of a response to a light flash. Before commencing a particular experiment or protocol, a trial flash is given to the cell. If no characteristic inward current with the shape and latency of ChR2 activation is seen, (along with the lack of fluorescence), we can be satisfied that the target cell is not expressing the light sensitive rhodopsin.

We can now look for pre-synaptic innervation from ChR2-expressing neurones onto our post-synaptic non-expressing neurone. Pre/post connectivity can be divided into three categories; 1- no pre-synaptic ChR2 input, 2 - one pre-synaptic ChR2 input, and 3 - multiple pre-synaptic ChR2 inputs. These three potential conditions are illustrated in figure 4.7. We in fact saw all three of these conditions in our transfected cultures; Condition 1 was the most common, with most non-transfected cells showing no change in membrane potential in response to the culture dish receiving light flashes. There could still be connectivity between these pairs of cells, but it is not strong enough to depolarise the post-synaptic cell enough for us to record a response. Various observations of conditions 2 and 3 are described below. All of these are recorded from a non-transfected cultured hippocampal neurone.

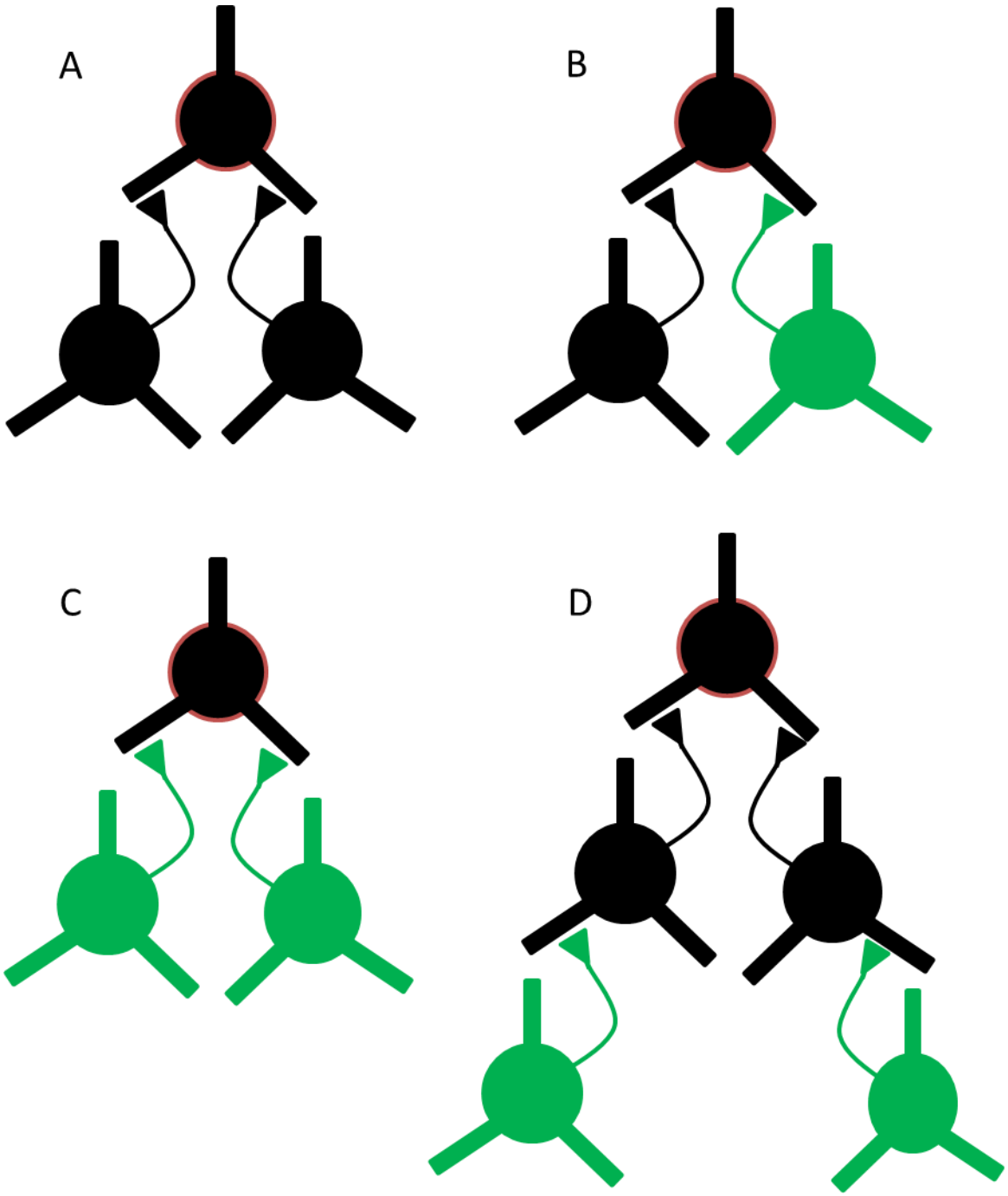

Figure 4.7 Schematic illustrating possible wiring configurations of inputs into non-transfected cells

Target cells (black with red outline) are whole-cell patch-clamped. Light flashes are then delivered to the dish. A target cell could have no ChR2 inputs (A), a single ChR2 input (B), or multiple ChR2 inputs (2 or more, C). Alternatively, poly-synaptic ChR2 inputs may be available to the target cell (D)

4.4.6.1 Excitatory post-synaptic currents in response to pre-synaptic ChR2 activation

Figure 4.8A shows EPSCs recorded from four different neurones. That follow the dish receiving a 10 ms light flash. These are all presumably mono-synaptic based on the latency between blue light on, and depolarisation in the patched cell. These four examples are clear, and show no contamination from multiple inputs. Presumably these four are examples of a single pre-synaptic ChR2 input being able to activate a post-synaptic partner. Figure 4.8C shows example traces where the response in the post-synaptic cell is much less clear, with evidence of poly-synaptic contamination. On the left, the initial EPSC is sometimes followed by a secondary EPSC. Perhaps this is an example of a bi-synaptic response to ChR2 input (part D in figure 4.7). On the right are example traces showing more poly-synaptic contamination, with secondary EPSCs being common and often much larger than the initial mono-synaptic response. To check these responses are indeed AMPA receptor-mediated, we washed on the drug NBQX (5 µM). In the presence of NBQX the response were abolished, and return upon wash-out of the drug (figure 4.8B).

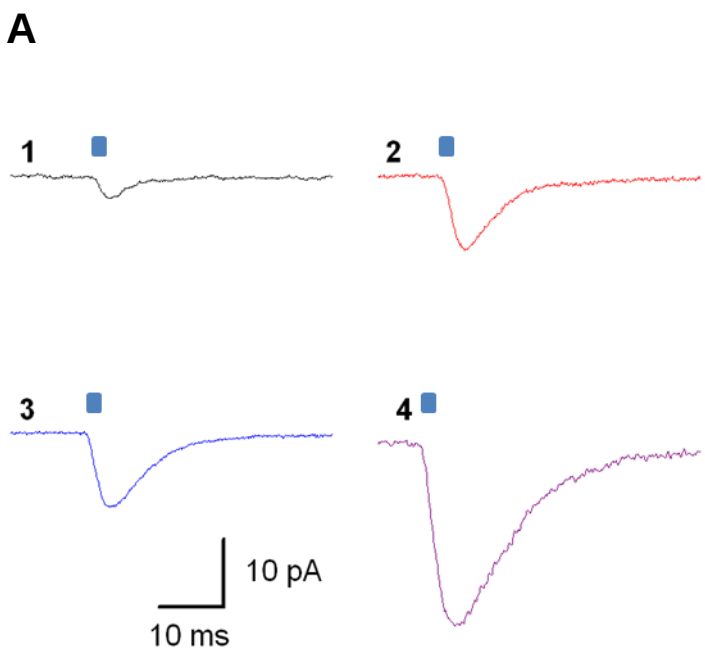

Figure 4.8 Excitatory post-synaptic currents in response to pre-synaptic ChR2 activation

Dispersed hippocampal cultures were transfected between DIV 12-14 with ChR2-EYFP, and recorded from 48-72 hours later. A non-transfected cell was chosen to patch-clamp In this figure gabazine was added to the ECS at 10 µM.

A – Examples of (presumably) mono-synaptic EPSCs recorded from 4 different cells in response to a single light flash

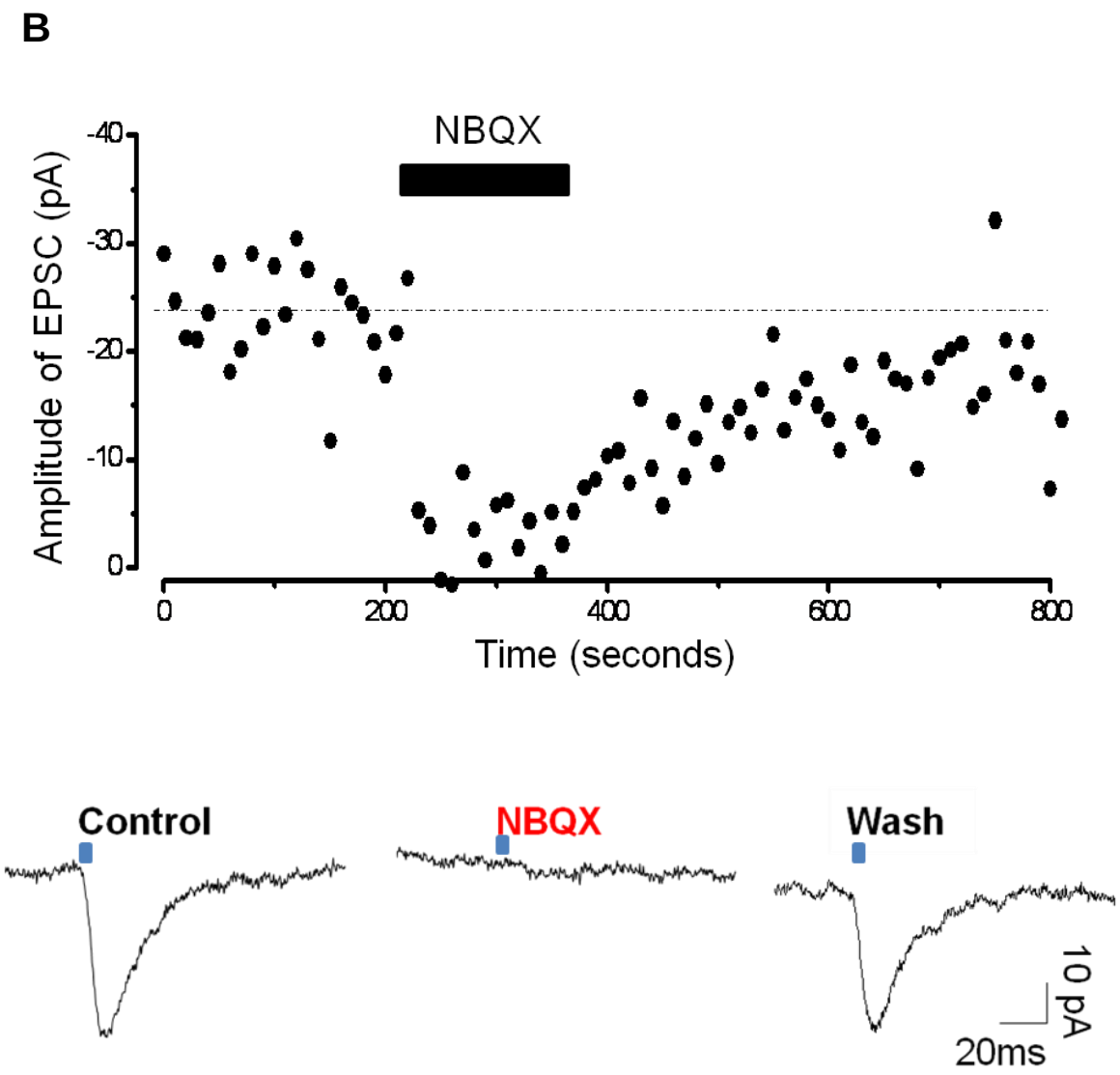

Figure 4.8 continued - Excitatory post-synaptic currents in response to pre-synaptic ChR2 activation. Dispersed hippocampal cultures were transfected between DIV 12-14 with ChR2-EYFP, and recorded from 48-72 hours later. A non-transfected cell was chosen to patch-clamp. In this figure gabazine was added to the ECS at 10 µM.

B – An experiment showing EPSCs are AMPA mediated. Recorded EPSCs were blocked upon application of NBQX. *Top*, plot of EPSC amplitude *vs*. time. *Bottom*, example traces showing block of EPSC upon NBQX wash-on, and the return of EPSCs following washout

C

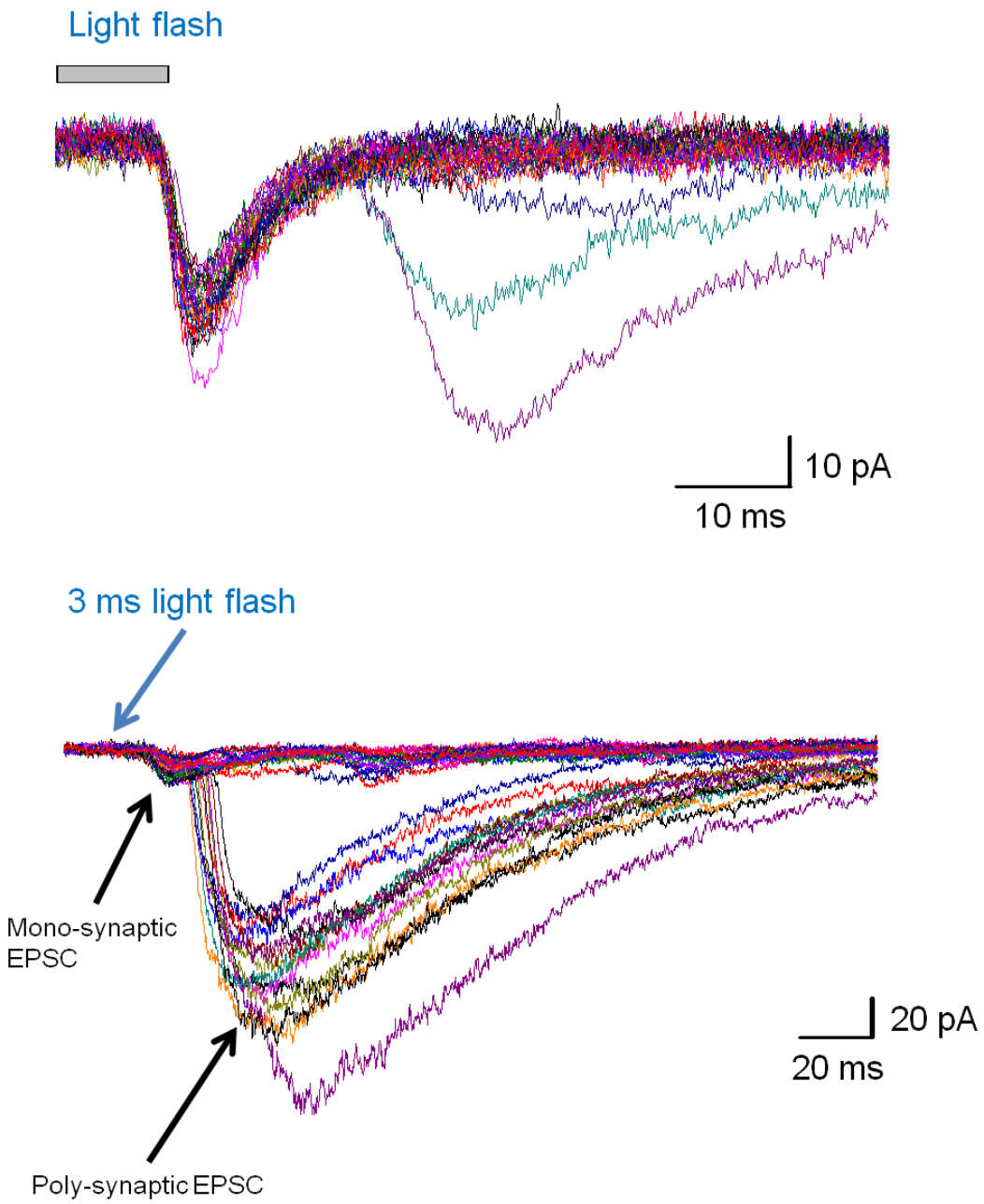

Figure 4.8 continued Excitatory post-synaptic currents in response to pre-synaptic ChR2 activation Dispersed hippocampal cultures were transfected between DIV 12-14 with ChR2-EYFP, and recorded from 48-72 hours later. A non-transfected cell was chosen to patch-clamp

C – examples of poly-synaptic EPSCs. *Top*, recording of secondary EPSCs a similar size to the primary, mono-synaptic EPSCs. *Bottom*, large secondary EPSCs following a single 3 ms light flash

4.4.6.2 Short term synaptic plasticity

Figure 4.9 shows a trace from a neurone not expressing ChR2-EYFP. The entire coverslip was flashed with 2 paired 10 ms light flashes 50 ms apart. The flashes have depolarised a presynaptic partner of our patched cell, and caused excitatory post-synaptic currents (EPSCs) in our patched cell. Not only that, the response in the post-synaptic partner exhibits classic paired-pulse depression, with the second response being less than half the amplitude of the first.

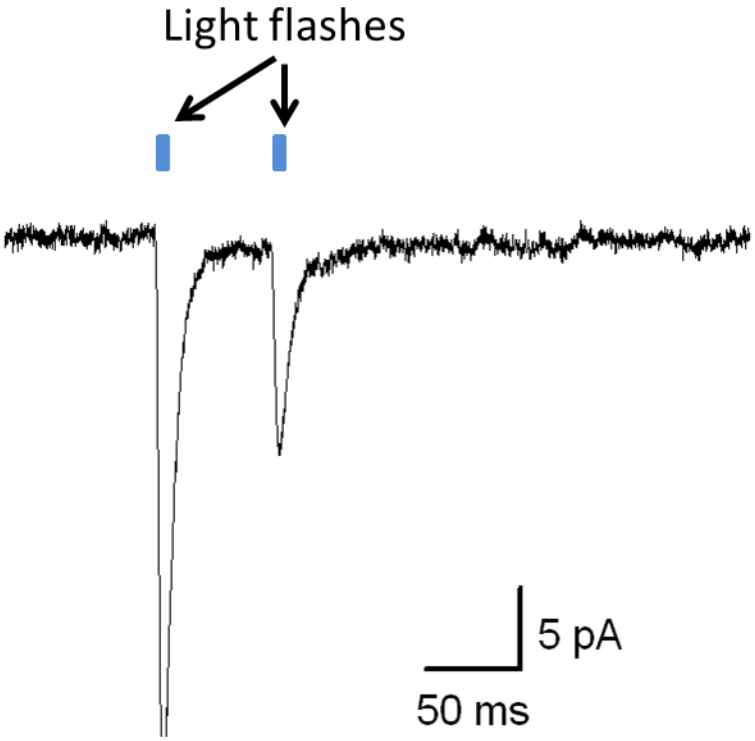

Figure 4.9 Short term synaptic plasticity driven by pre-synaptic ChR2 activation

Dispersed hippocampal cultures were transfected between DIV 12-14 with ChR2-EYFP, and recorded from 48-72 hours later. A non-transfected cell was chosen to patch-clamp This example trace shows two responses from a neurone which is innervated by a pre-synaptic partner. Two blue light flashes applied to the dish produce two responses in the patch-clamped post-synaptic neurone. The second response is smaller than the first, indicative of paired-pulse depression.

4.4.7 Enhanced network activity driven by Channelrhodopsin-2

Dispersed hippocampal cultures are highly variable in their connectivity, even when age-matched. Therefore it is not surprising to see a large amount of variation in activity as well. This is reflected in the two following figures. In both a non-ChR2-expressing neurone was patched, and the culture it was part of was exposed to blue light stimulation. In figure 4.10 (*top*) we recorded for 100 seconds, which included a 30 second blue light flash. Simultaneously to the light stimulation, activity increased in the patched cell. This was highly repeatable. Figure 4.10 (*bottom*) shows a conceptually similar experiment. In this example we stimulated with a train of 10 ms light flashes delivered at 4 Hz. This overlaps with the theta frequency band which is highly physiologically relevant (see (Young C.K., 2011)). This example is also notable for the low levels of activity in the post-synaptic cell when the light is off, compared to when the light train is being delivered.

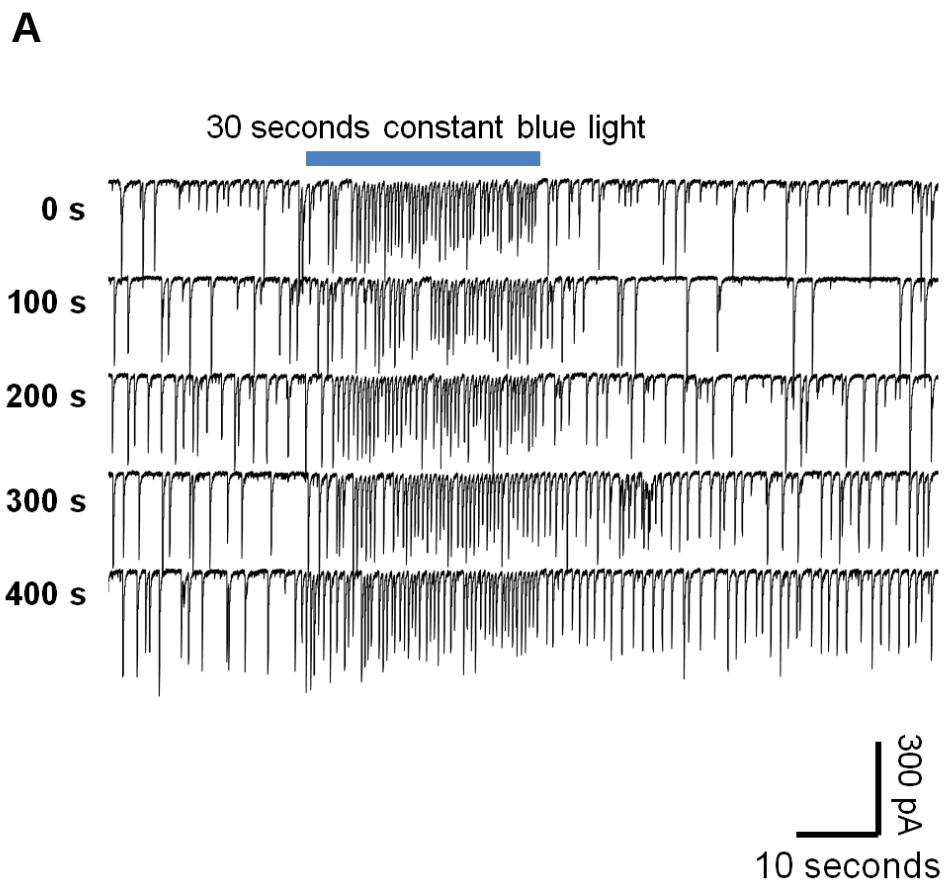

Figure 4.10 Enhanced network activity driven by ChR2 activation

Dispersed hippocampal cultures were transfected between DIV 12-14 with ChR2-EYFP, and recorded from 48-72 hours later. A non-transfected cell was chosen to patch-clamp. In this figure gabazine was added to the ECS at 10 µM.

A - an example of the response in a non-transfected neurone to the culture dish being exposed to 30 seconds of continuous blue light. Activity in the target patch-clamped cell increases during light stimulation. 5 such light flashes are shown, all from the same cell.

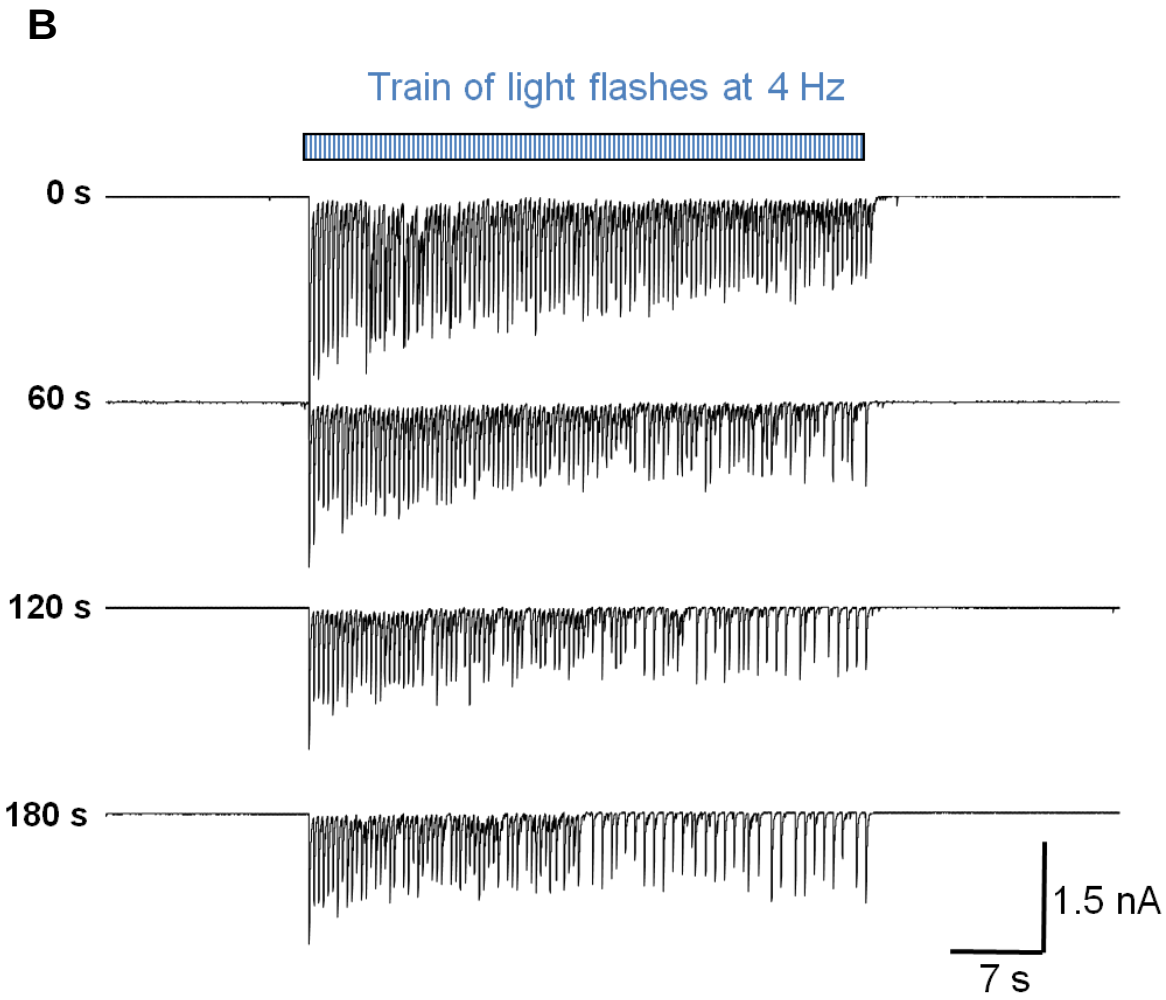

Figure 4.10 continued Enhanced network activity driven by ChR2 activation

Dispersed hippocampal cultures were transfected between DIV 12-14 with ChR2-EYFP, and recorded from 48-72 hours later. A non-transfected cell was chosen to patch-clamp. In this figure gabazine was added to the ECS at 10 µM.

B - an example of the response in a non-transfected cell after the culture dish was exposed to a train of blue light flashes. The light flashes were delivered at 4 Hz. Activity in the patch-clamped cell is near zero when the light is off, but high when the light is on

4.5 Discussion

Studies done by previous labs have shown ChR2 to express well in neuronal cells, without the need for additional co-factors (i.e. retinal) and to be able to modulate neuronal spiking activity, in cultured neurones, slices and *in vivo* (Boyden, Zhang et al. 2005; Zhang, Wang et al. 2006; Aravanis, Wang et al. 2007; Wang, Peca et al. 2007). Neurones tolerate ChR2 well, and basic membrane properties of the cells (resting membrane potential, membrane resistance) are unchanged in cells expressing the transgene (Boyden, Zhang et al. 2005). Additionally illuminating ChR2 with blue light has been shown to allow precise control of action potential generation, down to millisecond time periods, and can drive spike trains of multiple action potentials (Boyden, Zhang et al. 2005; Zhang, Wang et al. 2006; Han, Qian et al. 2009; Chater, Henley et al. 2010). My results are in good agreement with previously published data. I am able to drive action potential generation in neurones using light flashes, with both the rhodopsins and the neurones responses following the light flashes well.

I also saw several novel epiphenomena related to the experimental paradigm of expressing ChR2 in a small subpopulation of neurones in a dispersed hippocampal cell culture. Even though the transfection efficiency is low (between 2 and 5% of neurones end up expressing the rhodopsin), illumination of the culture with blue light, and the subsequent activation of the ChR2-expressing cells can have wide-ranging effects on the whole network. This is most clearly apparent in figure 4.6, where in the presence of a GABA antagonist individual 5 ms flashes cause massive self-perpetuating waves of depolarisation across the network. Hippocampal cultures are hyper-wired, and it is likely that the lack of regulated connectivity in them allows this type of runaway activity. Expression of ChR2 *in vivo* would be unlikely to precipitate this form of activity due to the brains tightly regulated connectivity and synaptic inhibition. However, expression of ChR2 into particular brains regions might be a possible tool to stimulate this epileptiform activity, and to study epilepsy.

Figure 4.10 also shows the potentially large effect of ChR2 activation on non-expressing neurones. As represented in figures 4.5 and 4.7, ChR2-expressing

neurones are not only relatively isolated in my dispersed culture, but may innervate untransfected cells in mono- or poly-synaptic connections. This is apparent in several figures in this chapter. Figure 4.10 shows the increase in activity in post-synaptic non-expressing partners of pre-synaptic ChR2 expressing cells. This data is reassuring as it strongly suggests that blue light flashes delivered to our cultures are driving action potential generation in neurones, and that these cells are releasing neurotransmitter onto their post-synaptic partners. This is also supported by the data shown in figures 4.8 and 4.9.

Interestingly figure 4.10 A and B show different trends in neuronal network activity, with activity increasing upon successive light exposure in 4.10A, and decreasing upon successful 4Hz train exposures in 4.10B. This is difficult to explain simply, but most likely reflects differences between cultures, with more or less cells being transfected in each dish. This is hinted at in the difference between baseline (light off) activity between the two recordings. Increased activity may drive increased recurrent network activity, but also increasing activity should increase receptor desensitisation.

Currently the recovery from desensitisation is not fully understood, and exploring the mechanism underlying this recovery was beyond the scope of this investigation. However, studies utilising time-resolved UV-vis spectrometry to look at photocycle products have identified a stage in ChR2's photocycle (termed P4) that may be responsible for the desensitisation. Upon absorbing a protein the protein passes through 2 intermediates (p1 and p2) followed by a P3 photoproduct that is responsible for both the channel's opening and closing (see (Bamann, C., Kirsch, T. et al., 2008) and (Ernst, O. P., Sanchez Murcia, P. A. et al., 2008)).

Within the wider field of neuroscience and optogenetics the results presented above (and in the previous chapter) indicate a need for careful controls when using ChR2. Whilst temperature is likely to remain stable *in vivo* (and should be controlled in *in vitro* experiments), the voltage dependence of ChR2 kinetics can change throughout an experiment, especially when the cell expressing ChR2 is not being voltage clamped. The issue of desensitisation during repeated stimulation has been already been addressed by the creation of ChR2 mutants, but may still be an issue for labs that are using the original ChR2 protein.

Chapter 5

5.1 Aims

To investigate the role of PKM zeta in glutamate receptor trafficking using patch clamp electrophysiology and the inhibitor of PKMzeta, ZIP.

5.2 Introduction

Since Bliss and Lomo's seminal paper describing long term potentiation (LTP) (Bliss and Lomo 1973), and a few years later the description of long term depression (LTD) (Lynch, Dunwiddie et al. 1977) much research has concentrated on the mechanisms underlying the induction, and maintenance, of LTP and LTD (see (Derkach, Oh et al. 2007; Santos, Carvalho et al. 2009) for review).

LTP can be divided into several different types, depending on location, method of induction, and timescale. Different forms of LTP exist at different synapses, where activation of different receptor complexes and signalling pathways are involved. In the hippocampus, research has identified distinct forms of LTP that can be NMDAR- dependent or independent (Bear and Malenka 1994; Malenka and Bear 2004). An example of the diversity of LTP within the hippocampus is provided by Schaffer collateral LTP (NMDAR-dependent) and the mossy fibre pathway LTP (NMDAR-independent, see (Harris and Cotman 1986) and the previous two citations). There are also age dependent differences in LTP (Yasuda, Barth et al. 2003).

5.2.1 LTP and LTD

LTP can be divided into several phases. First, induction, immediately post-stimulus, then a maintenance phase, where changes initiated in the induction phase are built upon, resulting in altered synaptic transmission that persists for some time. To maintain LTP it has been suggested that one possible mechanism is increased

and persistent phosphorylation of the target proteins involved, via increased and lasting kinase activity (Bliss and Collingridge 1993; Schwartz 1993). Conversely, maintenance of LTD may involve changes in the level of protein phosphorylation in the opposite direction (i.e. dephosphorylation, see (Mulkey and Malenka 1992; Mulkey, Herron et al. 1993)).

5.2.2 PKC and PKM

Protein kinase C is a family of isoenzymes responsible for phosphorylating multiple proteins in the mammalian brain, and may be involved in both the induction and maintenance phase of hippocampal CA1 LTP (Sacktor, Osten et al. 1993).

The family of PKC proteins is divided into three classes, organised by their secondary-messenger activation pathways. These three classes are; conventional, new and atypical (Nishizuka 1995; Nishizuka and Nakamura 1995; Hrabetova and Sacktor 1996). PKC can be changed into a new form, called protein kinase M, by modification of the hinge region of the protein that separates the catalytic and regulatory domains. This modification is brought about via proteolysis (Takai, Kishimoto et al. 1977). These PKM molecules are secondary messenger independent (Takai, Kishimoto et al. 1977). In the mammalian brain, activation of PKCs and PKMs post-LTP-induction are strictly controlled, becoming activated in a reproducible temporal pattern (Hrabetova and Sacktor 1996).

Upon induction of LTP in rat hippocampal brain slices, at the CA1 synapse, the majority of PKC isoforms were found to translocate into the particulate fraction (Sacktor, Osten et al. 1993), but this increase did not continue into the maintenance phase of LTP. An isoenzyme of PKC, PKMzeta is a constitutively active kinase expressed in neurones. PKMzeta was shown to increase in the cytoplasmic fraction of neurones in the maintenance phase of LTP (Sacktor, Osten et al. 1993). This increase in PKMzeta lasts at least 2 hours, and correlates well with a corresponding increase in EPSC magnitude (Osten, Hrabetova et al. 1996), suggesting PKMzeta is somehow stabilising AMPARs at the surface of the cell at synaptic sites. PKMzeta

has a catalytic domain, but lacks the autoinhibitory domain found in PKC isoforms (Hernandez, Blace et al. 2003). This structure means that PKMzeta is constitutively active and can maintain its activity in the absence of LTP-inducing stimuli (for example synaptic activation leading to calcium influx).

Protein kinases, and specifically the family of PKC isoforms, can be reversibly inhibited by a large set of commercially available molecules. However these drugs tend to be non-specific, leading to confusion in the literature regarding the effects. Some inhibitors are capable of reversing LTP, but at the same time affect baseline synaptic transmission. The inhibitor termed H7 (1,(5-isoquinolinesulphonyl)2methylpiperasine dihydrochloride) behaves in this fashion, with reversal of LTP shown by several groups (Malinow, Madison et al. 1988; Colley, Sheu et al. 1990), but also effects upon baseline seen by others (Muller, Buchs et al. 1990; Waxham, Malenka et al. 1993). Other studies on protein kinase blockade have come to similar conclusions (Huber, Mauk et al. 1995).

PKMzeta is necessary and sufficient for LTP maintenance (Ling, Benardo et al. 2002) and introduction of PKMzeta into CA1 cells potentiates AMPAR responses (Ling, Benardo et al. 2006), this was shown through non-stationary fluctuation analysis to be due to an increase in the number of AMPARs. PKMzeta has also been shown to be regulated in a bidirectional fashion in LTP and LTD, with increases seen after LTP induction protocols, and decreases after LTD (Hrabetova and Sacktor 1996).

5.2.3 Zeta Inhibitory Peptide

Another way of decreasing activity of protein kinases is with small inhibitory molecules that bind to and block the catalytic site of the target protein. Zeta inhibitory protein (ZIP) does exactly this (Ling, Benardo et al. 2002; Pastalkova, Serrano et al. 2006). ZIP has been used to reverse spatial learning (Pastalkova, Serrano et al. 2006) and gustatory learning (Shema, Sacktor et al. 2007) *in vivo.* ZIP has also been shown to reverse L-LTP, but have no effect on the induction phase of LTP.

5.3 Materials and Methods

5.3.1 Electrophysiology

Dissociated neuronal cultures were dissected out and plated as described in Chapter 2. After 14-21 DIV, neurones on a coverslip were transferred to a recording chamber and whole cell patch clamped in the presence of TTX (1µM) and gabazine (5µM). TTX was used to prevent any action potential generation in the cultures, leaving only spontaneous vesicle fusion events. Gabazine blocked inhibitory activity. Each cell was recorded for five to ten minutes.

Analysis of mini excitatory post synaptic currents was performed in pCLAMP (Axon laboratories) using a template search.

5.3.2 Imaging

Cells were imaged on an Zeiss confocal (LSM 510 UV META Axiovert 200M, Oberkochen, Germany) laser scanning microscope. Fluorophores were excited with a 488 nm laser light and emission was detected through a 505 long pass filter (also Zeiss).

5.3.3 Immunocytochemistry

Surface staining was achieved by rinsing coverslips in warm Earles buffer, and then adding primary antibody against GluA2, diluted to the appropriate concentration. This was then left on for 20 minutes. After this the coverslips were rinsed three times in Earles buffer and fixed with 3.7% formaldehyde. For full methods see Chapter 2.

5.3.4 Antibody feeding

20µl primary antibody (diluted to the appropriate concentration) was added to all coverslips at 16^{o}C and left for 30 minutes. Coverslips were then rinsed three times in PBS. At this time point some coverslips were fixed as non-internalising controls. Remaining coverslips were treated with drug (ZIP) or DMSO as a control

and left at 37^{o}C for 15 minutes. Finally coverslips were rinsed again 3 times in PBS, and then fixed at room temperature.

5.4 Results

PMKzeta has been shown to be involved in neuronal plasticity, especially LTP. Therefore we attempted to use the PKMzeta inhibitory peptide ZIP to reduce PKMzeta activity in dissociated neuronal cultures, and use imaging and electrophysiology to monitor any resulting effects on AMPARs.

Dissociated hippocampal cells were cultured for 2 to 3 weeks and then treated with 1µM of the PKMzeta inhibitor ZIP, or a scrambled control peptide. Following treatment the proportion of internalized GluA2 was determined via an antibody feeding assay. Figure 5.1 shows the internalised levels of GluA2 in dendrites after 15 minutes treatment with 1µM ZIP, in comparison to the scrambled control peptide. There is a significant increase in the levels of GluA2 internalised in the dendrites after treatment with ZIP.

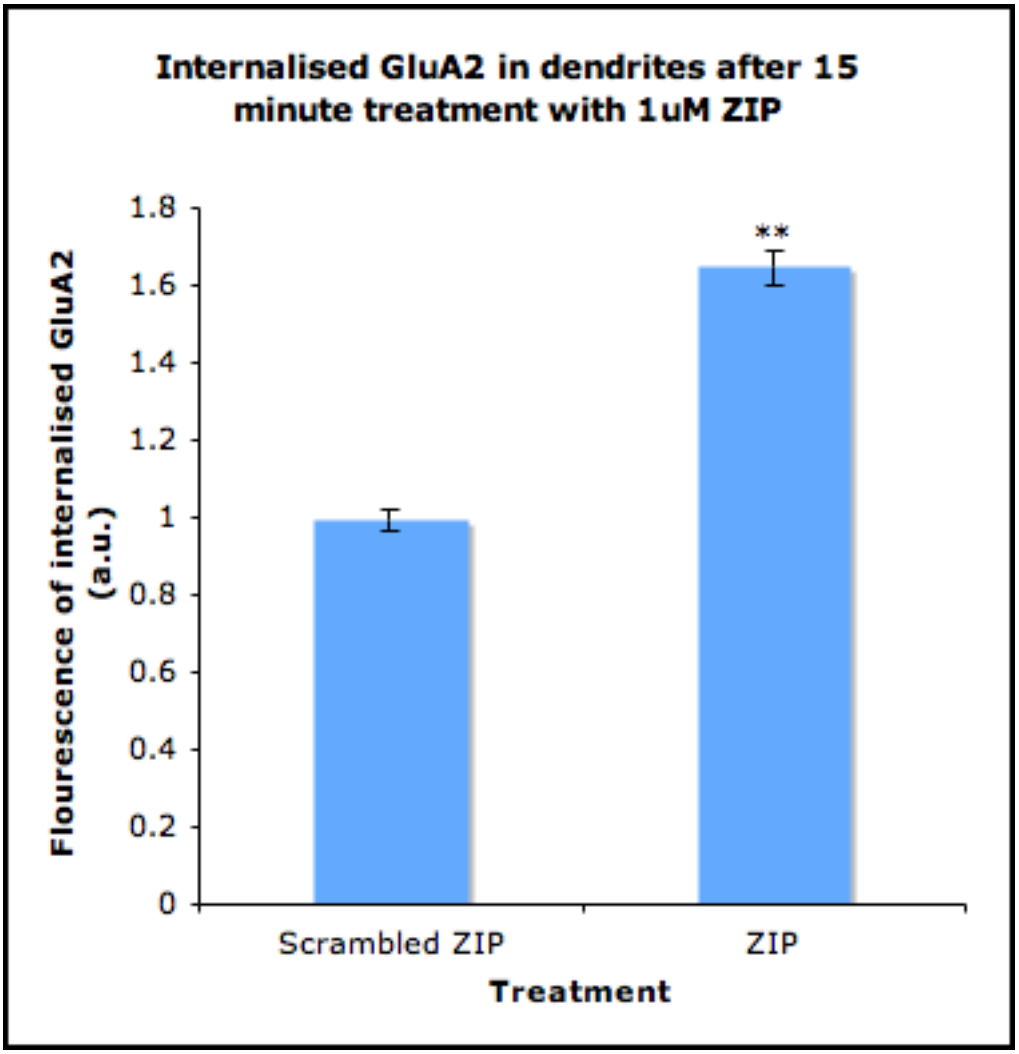

Figure 5.2 shows the proportion of surface GluA2 with respect to total GluA2 in dissociated hippocampal neuronal culture in response to treatment with the PKMzeta inhibitor ZIP. ZIP (1μM) or a scrambled control peptide was added to the neuronal media, and the cells were subsequently fixed after 1, 2 or 4 hours in the presence of ZIP, or 4 hours in the presence of the scrambled peptide. Compared to the control conditions, levels of surface GluA2 fall in a time dependent manner, with the maximum decrease of surface GluA2 relative to internalised GluA2 seen after 4 hours treatment.

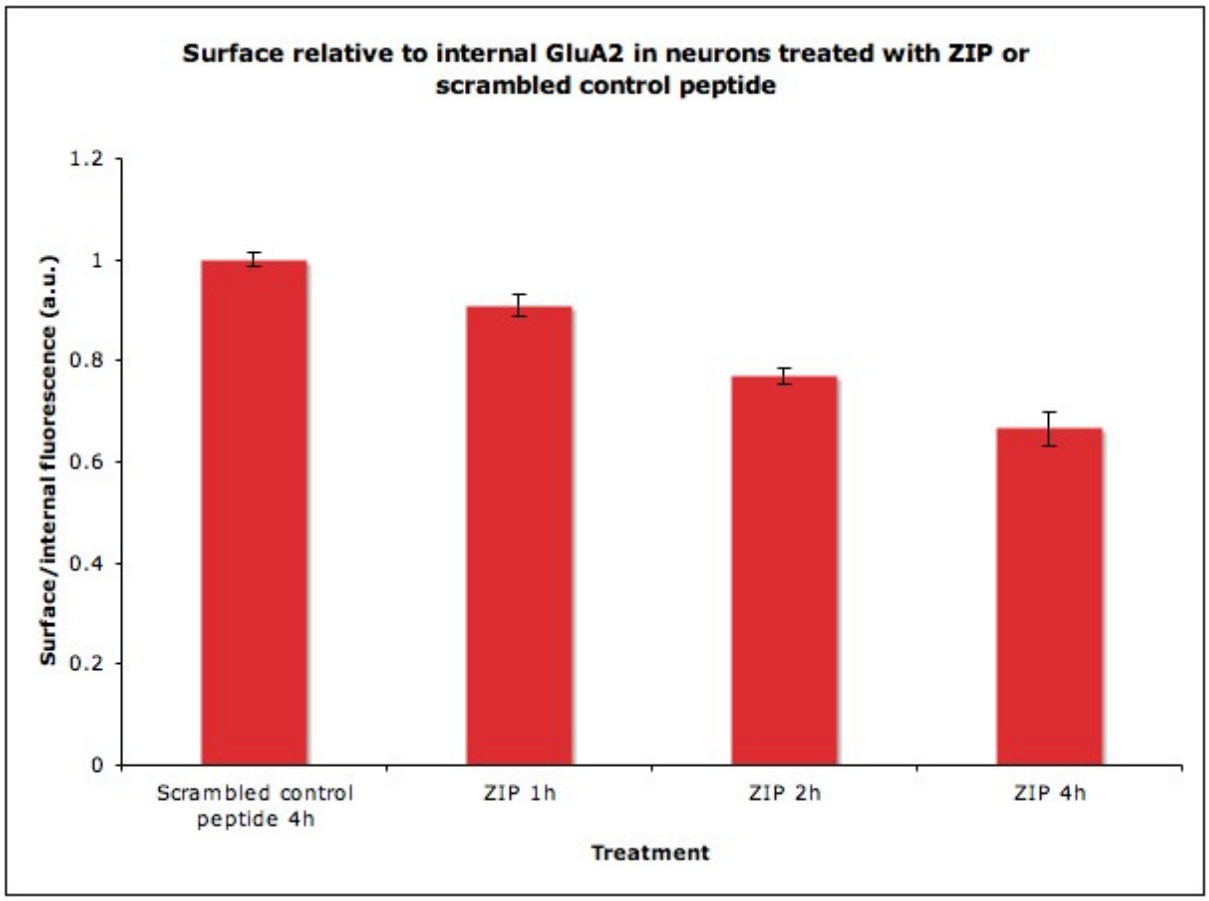

Figure 5.2 – Effect of ZIP on surface relative to internal GluA2
Neurones were used between DIV 14 and 21,
Cells treated with scrambled control peptide for the duration of the experiment. B-D - cells treated with ZIP at time points of 1, 2 and 4 hours

Figure 5.3 shows the response to either no treatment (cells fixed at time point 0, A), treatment with a scrambled control peptide (B), or treatment with ZIP (C) Left to right, surface GluA2, internal GluA2, merge. Again, treatment with ZIP causes an increase of endocytosis of GluA2 with respect to control.

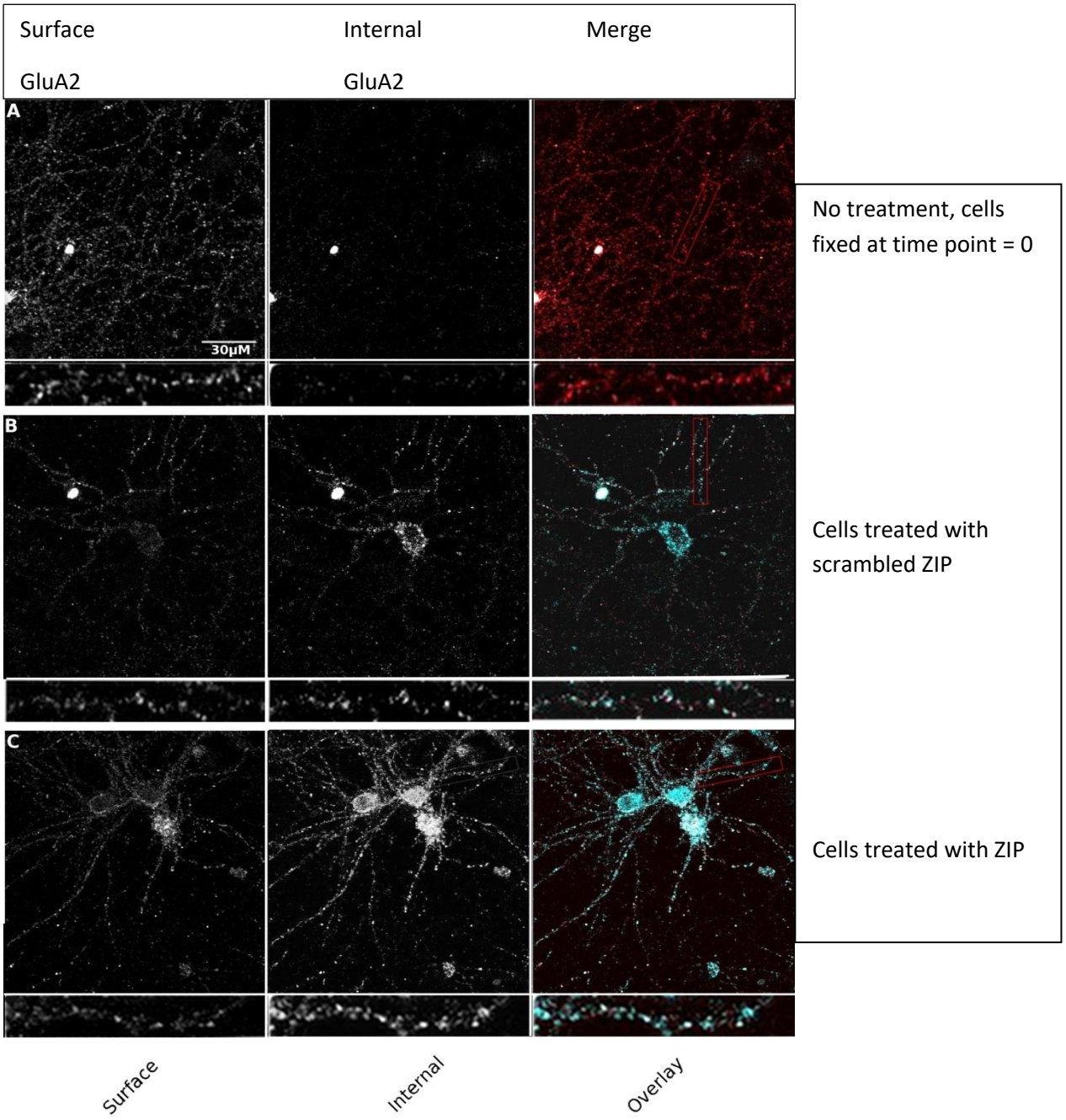

Figure 5.3 - Imaging of surface and internal GluA2

A - Untreated cells fixed at time point 0 with no receptor internalisation.
B - Cells treated with scrambled control peptide.
C - Cells treated with ZIP peptide.

Scale bar 30 μm

Figure 5.4 shows average mEPSC amplitude in cells treated with ZIP or with vehicle. mEPSC amplitude is slighter larger in ZIP-treated cells, but not significantly larger (p=0.12, student t test).

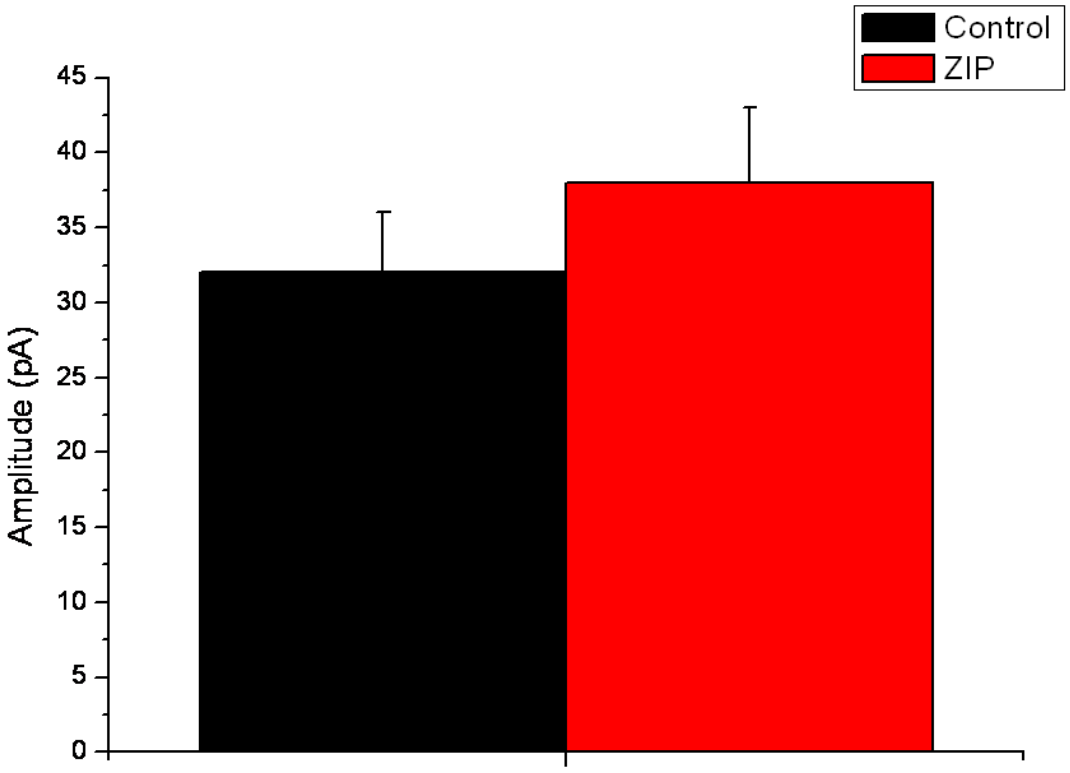

Figure 5.3 – Effect of ZIP on mEPSC amplitude

Neurones were whole cell patch clamped after either being incubated with ZIP (5µM for 1 hour) or scrambled control peptide

(p=0.12, students t-test, n=10)

Figure 5.4 shows the effect of treatment with ZIP on the inter-event –interval (IEI) of mEPSCs. There was a trend towards a larger IEI with ZIP treatment, but this trend was not significant (p=0.18, students t test).

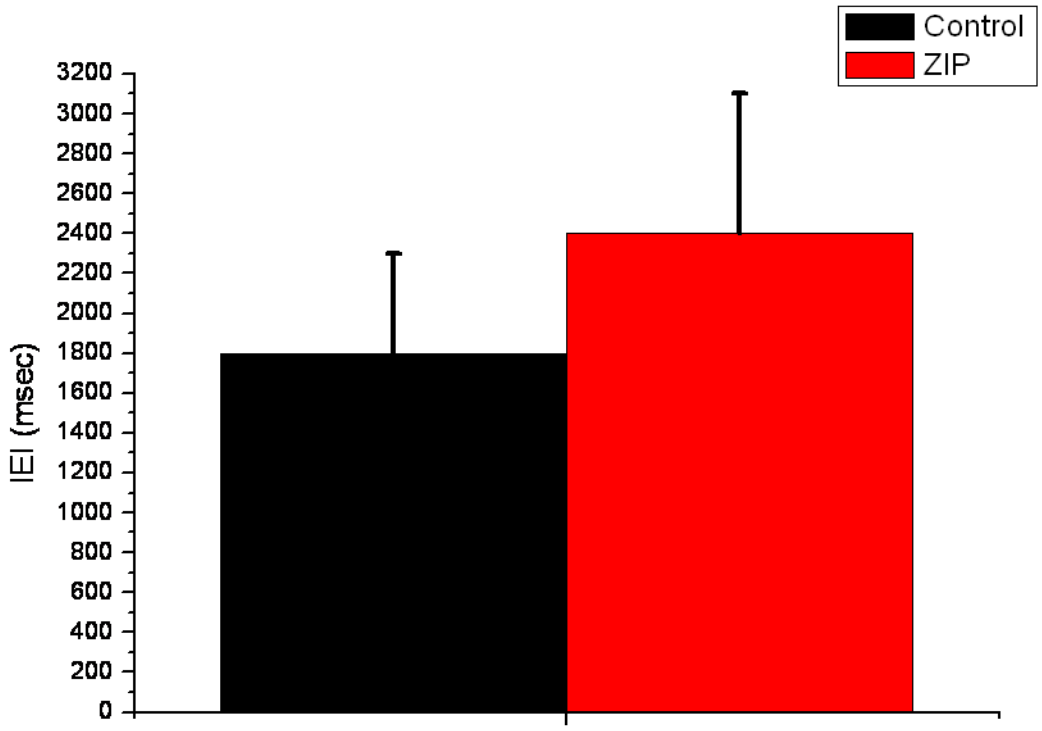

Figure 5.4 – Effect of ZIP on inter-event-interval (IEI)

Neurones were whole cell patch clamped after either being incubated with ZIP (5µM for 1 hour) or scrambled control peptide

(p= 0.18, students t test, n=10)

5.5 Discussion

5.5.1 ZIP has an effect on the surface composition of GluA2 in dissociated hippocampal neurones

Upon treatment with 5 μm ZIP, the composition of surface AMPARs changed. There was an increase in endocytosis of GluA2, with respect to total (figure 5.1). This increase showed a time dependent function, with the largest increase after 4 hours. Levels of endocytosis of GluA2 increase in all biochemical and imaging-based data sets upon treatment with ZIP.

These results are interesting, however this is looking at total surface AMPAR, with no distinction between synaptic, peri-synaptic, and extra-synaptic. I therefore attempted to use electrophysiology to look at synaptic AMPARs

5.5.2 ZIP has no effect on amplitude or frequency of mini EPSCs

Incubating dissociated neurones in 5 μm ZIP and then whole cell patch clamping them revealed no significant differences in either mEPSC amplitudes (figure 5.3) or mEPSC frequency (figure 5.4). These results suggest that synaptic total AMPAR levels are not changing significantly.

5.5.3 Why does ZIP have no effect in an electrophysiological context?

Although it is not clear, the underlying reason behind the discrepancy in these results, and the mass of the published data, is likely due to the plasticity state of the neurones. Cultured neurones exist in a hyper-wired state, with effectively random

inputs to each cell, and correspondingly random activity between cell partners. Correlates of LTP and LTD in cultured neurones differ from brain slice versions of the LTP and LTD, and many studies that use plasticity protocols in culture tend to utilise chemical induction of plasticity (for example, DHPG for LTD, and tetraethylammonium chloride (TEA) for LTP, see (Huber, Mauk et al. 1995)). One possible reason for the lack of effect of ZIP in these cultured cells is that they are not potentiated to begin with. Consistent with the main hypothesis of the method of action of PKMzeta, ZIP should not affect baseline transmission, only potentiated transmission.

5.5.4 Future directions

Repeating the imaging experiments with markers for synaptic sites (for example PSD-95 for the post-synaptic region) may allow the determination of whether or not the increases seen in GluA2 levels after ZIP treatment are synaptic or extrasynaptic. The electrophysiological data seems to suggest they are non-synaptic changes, but if this is the case, where are the additional GluA1 subunits being inserted? They could be adding to the somatic, dendritic, or axonal compartments or some combination of them. Alternatively, they could be being inserted in or near the spine head, but not being incorporated into the synapse itself.

Chapter 6

Investigating the effects of hypoxia and small metal particles on a placental model coupled to neuronal and fibroblast culture

.

6.1 Aims

1- To add cobalt chromium nano- and microparticles to cultured BeWo cell barriers, and investigate the effects on co-cultured neurones and fibroblasts

2 - To expose BeWo cell barriers to hypoxic conditions, and monitor the downstream effects on co-cultured fibroblasts or neurones

6.2 Introduction

6.2.1 Small metal particles

The field of nanotechnology has expanded hugely over the last few years. Small particles (of usually metal) are finding their way into a huge range of engineering, scientific, and medical roles (Tiede, Boxall et al. 2008). Small metal particles are defined by their size; microparticles are defined as having a size between 100-500 nm and nanoparticles are defined as having a size between 1-100 nm. Because of their small size, the properties of nanoparticles cover a range between molecules and macroscopic objects. This feature affects their behaviour, and allows nanoparticles to act in ways that are not necessarily predictable from the

macroscopic behaviour of the same material. Nanoparticles are increasingly being used in medical situations for a wide variety of tasks, including helping target drugs to specific tissues, and also in imaging (Faraji and Wipf 2009; Sajja, East et al. 2009). Nanoparticles are likely to interact with biological tissues in specific ways that are not yet well understood, and may well be toxic (Nel, Xia et al. 2006).

The other side of nanoparticles wide usage is exposure to humans is becoming unavoidable. This includes most medical situations. Exposure to nanoparticles may be deliberate (for example titanium dioxide particles in sunscreen, see (Nohynek, Lademann et al. 2007; Nohynek, Dufour et al. 2008)), environmental (e.g. air pollution, (Stone, Johnston et al. 2007)) or a side effect of another medical (or engineering) intervention. This final category of exposure is illustrated by cobalt-chromium (CoCr) nanoparticles produced by hip replacements. In neuroscience specifically, quantum dots (QDs) have been widely used as probes to tag molecules and follow their movements (Giepmans, Adams et al. 2006). However QDs are not yet widely used in medical applications (at least in human patients) and this particular implementation of nanoscale particles is thus far purely an experimental tool.

6.2.2 Hip replacements

Total hip replacements (THR) and resurfacing athroplasty have become relatively commonplace in human society, especially in the West. As the field has evolved, several different materials have been employed in the construction of both the ball (head of femur) and the socket (implanted into pelvis) including ivory, titanium, cobalt-chrome allows, Teflon, stainless steel, polyethylene (PE) and PMMA bone cement (Learmonth and Spirakis 1989), (Jazrawi, Kummer et al. 1998; Sharkey and Parvizi 2006). Hip replacements are some of the most successful modern surgical interventions, with patients often able to walk within days of the operation, and hip replacements improve the mobility and thus the quality of life of patients.

Until recent years hip replacements generally consisted of a metal ball (head of femur) and a plastic sockets (in the pelvis). Through wear and tear these produced small particles of metal that were then free to move about the body, either in tissues near the site of the implant, or systemically through the blood/lymph system. More

modern hip replacements have replaced the plastic socket with a metal variant. These have several advantages, the primary one being their durability. Metal-on-metal hip replacements last much longer than metal on-plastic, and therefore lessen the frequency of surgery. Figure 6.1 depicts an example of a typical; metal-on-metal implant.

Figure 6.1

An example image of a metal-on-metal hip replacement before implantation.

6.2.3 Wear and tear in total hip replacements

As the two parts of a hip replacement move against one another, debris is produced by mechanical wear, and also surface corrosion of the metal. Particles produced from these erosive actions can be a variety of sizes, and can also be soluble or insoluble in bodily fluids. One study has estimated that a metal-on-polyethylene articulation may produce 5 x 10^{11} particles per annum, whilst metal-on-metal articulations can produce 6.7 x 10^{12} to 2.5 x 10^{14} particles per annum, which is about 13,500 times more. (Doorn, Campbell et al. 1998) Contrary to this, the actual amount of wear seen by a metal-on-metal articulation is less, due the harder nature

of the material. The increase in particle number reflects the fact that these metal particles are small, in the micro- or nanoparticle range. Metal particles are typically smaller than 50 nm, whilst PE particles are not usually less than 100 nm. The surface of the metal joint articulation can either simply corrode, or produce a protective passive layer. Practically all metals used in prostheses and implants have been shown to corrode and produce either oxides or hydroxide products.

The majority of particles are found near to the site of the implant itself, primarily in the synovial fluid, the synovial capsule, and peri-prosthetic tissues. However, the small size of nanoparticles makes it more likely that these foreign bodies may gain access to more privileged sites in the body, first by entering the circulatory systems (blood, lymph), and then from them other sites, such as organs far removed from the site of the implant itself. The extent of the transport and dissemination of metal particles around the body is not well understood at present.

6.2.4 Patients of child bearing age

Due to the wider prevalence of hip replacements (and other similar procedures), the absolute number of patients undergoing these surgeries is increasing, and some of these patients are women of child bearing age. The maximum age for the mother at the time of conception has risen over the last few decades as medical technology has improved, with treatments such as in vitro fertilization (IVF) allowing older and older women to conceive. There is now a situation where women who have already had a hip replacement might conceive, and there is a concern that nano- or microparticles produced by hip replacements might be able to cross the placenta and affect the unborn child (Bosman, Nieto et al. 2005). This could be in a number of ways, but in this particular case I was interested in the possible effects on the developing nervous system of the foetus.

A recently study has shown that nanoparticles can cross the placenta and build up in foetal mice.(Kohei Yamashita, Masatoshi Nozaki et al. 2011). This particular study did not use CoCr nanoparticles, instead using silica nanoparticles of

differing sizes. The majority of these accumulated in the liver of the mother, but nanoparticles were still detectable in foetal tissue, including the brain. Previous work has already shown that the take-up of particles through the placenta has a size-determined effect, with particles larger than around 80nm being excluded. In the silica nanoparticles paradigm, 2 days of exposure to the particles was enough to significantly affect placental function, with growth abnormalities seen in both structure and blood flow, and sometimes foetal death was also observed (Kohei Yamashita, Masatoshi Nozaki et al. 2011).

6.2.5 BeWo *in vitro* model

BeWo cells are a human trophoblast choriocarcinoma derived cell line. These all widely used and well characterised by other groups, and are a standard *in vitro* model for a barrier such as the placenta (Orendi, Kivity et al. 2011). Previous studies have used BeWo barriers to explore the transport across the placenta of several different substances, such as amino acids, immunoglobins, fatty acids, transferrin, and viruses (Bhabra, Sood et al. 2009). In this study I looked at the indirect effect of metal particles on neurones, via the BeWo cells. BeWo cells were cultured and then placed above cultured neurones or fibroblasts. This is depicted in figure 6.2.

BeWo barriers are grown on transwell inserts (see methods for greater detail) and can either be used as a monolayer, or bilayers. In these experiments I used both configurations. The cells are plated and grown on a mesh, and as the cells reach confluence they form tight barriers in-between one another. However it is still possible that nano- and/or microparticles could pass through these gaps. Therefore I utilised bilayers to ensure that any small gaps were covered by the second layer of cells. The confluency and the arrangement of the barriers can be checked post-experiment by histology.

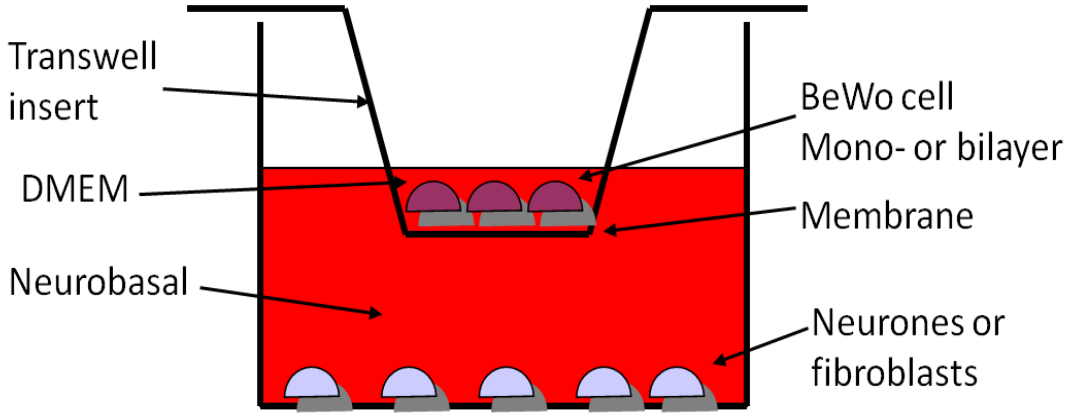

Figure 6.2

A schematic of the co-culture experimental paradigm. Neurones or fibroblasts are cultured onto glass coverslip (bottom). Transwell inserts with cultured BeWo barriers are placed into the wells. Metal particles can then be added to the media above the BeWo cells. There is no direct path to the neurones/fibroblasts for the metal particles

Previous studies have shown definite toxic effects of CoCr particles upon human tissue in culture. CoCr particles have been shown to have both damaging effects at both the cellular level (cytotoxic) and the genome level (genotoxic) (Papageorgiou, Brown et al. 2007). If applied to tissue above a certain concentration, DNA damage and aberrations in chromosome structure lead to cell death. However not only do these concentrations vastly exceed the levels likely to be found *in vivo*, they do not explore the effects of CoCr particles applied to a tissue indirectly, as proposed in this particular experimental paradigm, where the metal does not directly interact with the cultured neurones or fibroblasts.

6.2.6 Monolayers and bilayers

Throughout normal embryological development the human placenta moves from a bilayer (100% at 3 months) to a partial monolayer (by 9 months approximately 15% of the placental barrier is a monolayer). We can model this in vitro by growing our BeWo barriers for a longer time. After 3-4 days of growth a monolayer has

developed on the transwell insert membranes. After 7 days growth, a bilayer has developed. This can be checked by various assays, including confocal Z-stack microscopy and histology, and has previously been characterised within this lab.

6.2.7 Hypoxia

We also examined the effects of hypoxic condition on our barrier model. *In vivo* in the mammalian placenta the partial pressure of oxygen is much lower than in the circulation. It has been proposed that this low partial pressure helps protect the developing embryo from toxic oxidative stress effects (Dunwoodie 2009). BeWo cells can be grown at both normal oxygen partial pressures and hypoxic partial pressures. To explore the effects of oxygen levels, we grew BeWo barriers at standard atmospheric levels, and also at lower hypoxic levels. We then exposed the hypoxic barriers to normal atmospheric levels. This is an attempt to model the effects of an *in vivo* placental bleed, where highly oxygenated blood comes into contact with placental tissue sitting at a much lower partial pressure of oxygen. After these two conditions we then place our BeWo barriers above standard HEPES media. Factors released by the barriers diffuse into the HEPES. We term this ‘conditioned HEPES’. This conditioned HEPES is then snap-frozen with liquid nitrogen, and stored for use. When needed the conditioned HEPES is defrosted and perfused onto our cells (either neurones or fibroblasts) in the calcium imaging experiments.

6.2.8 Techniques

To explore the possible effects of nano- and microparticles on cultured cells, we decided to use a variety of techniques. Some of these techniques reflect previous work done in this field by my collaborators, and have already been shown to be a workable readout for certain aspects of the experiment. This is true of comet analysis (Singh, McCoy et al. 1988; McKelvey-Martin, Green et al. 1993). Comet analysis looks at the amount of DNA damage sustained by a cell. Damage to the cell’s DNA (stored in the nucleus) can lead to breaks in the DNA helix. These breaks can either be single-stranded, or double stranded. As breaks build up in the genetic material in the nucleus, the cells repair mechanisms cannot cope, and fail to quickly repair these breaks. If the nucleus is placed in an electric field, as it migrates through the field

fragments of DNA (caused by multiple breaks) can actually leave the nucleus, and are seen under the microscope as a ‘tail’ following the nucleus. From the absolute size and intensity of the tail, a ‘tail moment’ can be constructed. This figure gives an indication of the level of DNA damage present in the cells. Although not presented in this work, as referenced above this has shown a clear increase in DNA upon exposure to CrCo nanoparticles (Singh, McCoy et al. 1988; McKelvey-Martin, Green et al. 1993).

We also attempted to look at cell morphology. We hoped to see an effect on neurite outgrowth with the addition of nanoparticles Our approach was to either infect young neuronal cells with a virus expressing a fluorescent protein. This was intended to be used simply as a morphological marker, filling the cell with a red or green fluorescent protein, which would then allow accurate imaging of the cell body along with all the processes (neurites, both axonal and dendritic). Another, similar approach was to utilise immunocytochemistry to label axons and dendrites separately. For this we chose to use MAP2 and NF as our markers. MAP2 is microtubule associated protein 2, and localises to all neurites except the axon. Neurofilament (NF) localises to all neurites (Wu, Fang et al. 1998). Therefore with the combination of the two stains, we should be able to identify dendrites (stained for MAP2 and NF) and axons (stained just for NF).

We also decided to use calcium imaging, utilizing the calcium sensitive dye FURA-2. Fibroblasts and neurones can be plated on glass coverslip, loaded with a calcium-sensitive dye, and then imaged to look at the levels of internal calcium. By controlling the extracellular environment by washing on different solutions (e.g. plus/minus nanoparticles) we were able to explore the effects of different substances on calcium signalling in our cells (see (Hockberger, Tseng et al. 1989) for examples).

For example, we could compare the difference between media that had been exposed to barriers, that themselves had been exposed to metal particles, and normal unconditioned media, and to direct metal particles.

6.3 Materials and Methods

6.3.1 Cell culture

BeWos were cultured in Dulbeccos Modified Eagles Medium (DMEM), supplemented with 1% l-glutamine, penicillin and streptomycin, 1% aphotericin B solution (AmpB) and 10% foetal bovine serum (FCS) at 37^0C and 5% CO_2. BeWo cells were seeded at 100,000 cell per centimetre squared onto polyester membranes (pore size 0.4µm) placed in a Transwell plate and grown with regular media changes for 7 days. After 7 days the barriers were considered confluent.

Fibroblasts were purchased from Invitrogen and were grown in minimal essential media (Sigma) supplemented with the following; 10% foetal bovine serum (FBS), 1% penicillin/streptomycin solution (Sigma) 2% HEPES buffer (Sigma), 1% l-glutamine (Sigma), and 1% sodium pyruvate solution (Sigma). Fibroblasts were also plated onto coverslips for calcium imaging using Poly-L-lycine as a adhering factor (preparation is the same as in the main methods chapter).

6.3.2 Preparation of metal particles

Generation of CoCr nanoparticles was via a flat pin-on-plate tribometer. This apparatus physically scrapes nanoparticles off the surface of the, when they diffuse into the water surrounding the pin/plate mechanism. Recovery of nanoparticles was via filtration onto 25mm polycarbonate filters (pore size 100 nm) and the total mass was determined gravimetrically. Filters were then placed in sterile water and sonicated to resuspend the nanoparticles. Solutions containing nanoparticles were also sonicated immediately prior to adding them to cells/solutions.

Microparticles were purchased directly from Osprey metals Ltd (Neath, UK). The metal composition of the cobalt chrome alloy was (in increasing order) 0.53% Fe, 0.057% C, 0.59% Mn, 0.71% Ni, 0.87% Si, 6.3% Mo, 28.7% Cr and 62.2% Co. The composition of these microparticles is similar to the composition of the metal used in metal-on-metal hip replacements. As described for the nanoparticles these were also

suspended in water, and then collected onto filters. Figure 6.3 shows example images of both microparticles and nanoparticles after preparation.

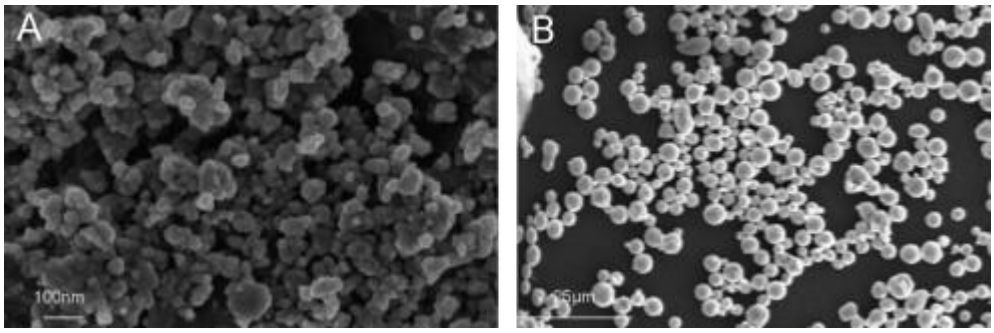

Figure 6.3

Example images showing microparticles (left) and nanoparticles (right). Reproduced from (Papageorgiou, Brown et al. 2007) Scale bar is 100nm (left) and 25 µm (right)

6.3.3 Calcium Imaging

Cells were labelled with FURA-2 (25 µl pluronic acid, 25 µl DMSO added to the FURA-2, then vortexed, then the entirety of the solution added to 25ml of standard ECS) Cells had their media (DMEM or Neurobasal plus supplements) replaced with FURA-2 dosed ECS, and were left for 30-45 minutes in order to allow the FURA-2 levels to build inside the cells. Loaded cells were then imaged on an inverted microscope at 2 wavelengths of light (340nm and 380nm). As FURA-2 is a ratiometric dye, it is possible to monitor both the bound and unbound forms of FURA-2.

6.3.4 Immunocytochemistry

Cortex and hippocampus were dissected out of E18 embryos as described in Chapter 2 (materials and methods). Cells were plated onto PLL-coated glass coverslips, and then fixed and stained at DIV 1-7.

6.4 Results

6.4.1 Fixed Cell Imaging

To attempt to measure neuronal morphology (neurite outgrowth, extent of dendritic arbour, spine development) we utilised two different fixed cell imaging protocols.

Figure 6.5 shows examples of hippocampal neurones cultured for 3 DIV then infected with SindBis-GFP, and subsequently fixed. Unfortunately all the samples examined using this protocol had disrupted cellular morphology (control and treatment groups). For completeness I have included this data as an example of trying different directions in order to determine the optimal experimental paradigm.

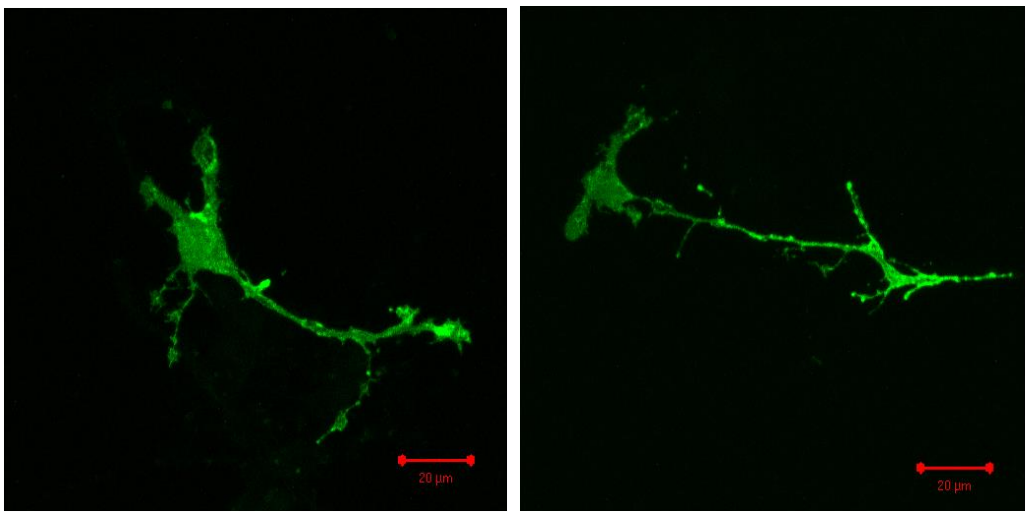

Figure 6.5 - Neurones infected with GFP-Sindbis

Dispersed hippocampal neurones were grown for 3 DIV on glass coverslips, and then infected with a virus encoding GFP. 8-12 hours later cells were fixed and mounted and imaged on a confocal microscope. Note wide aberrant neurites and soma.

Scale bar is 20 µm throughout

Figures 6.6 and 6.7 shows examples of cultured hippocampal neurones cultured for 3 DIV then fixed and stained for MAP2 and NF.

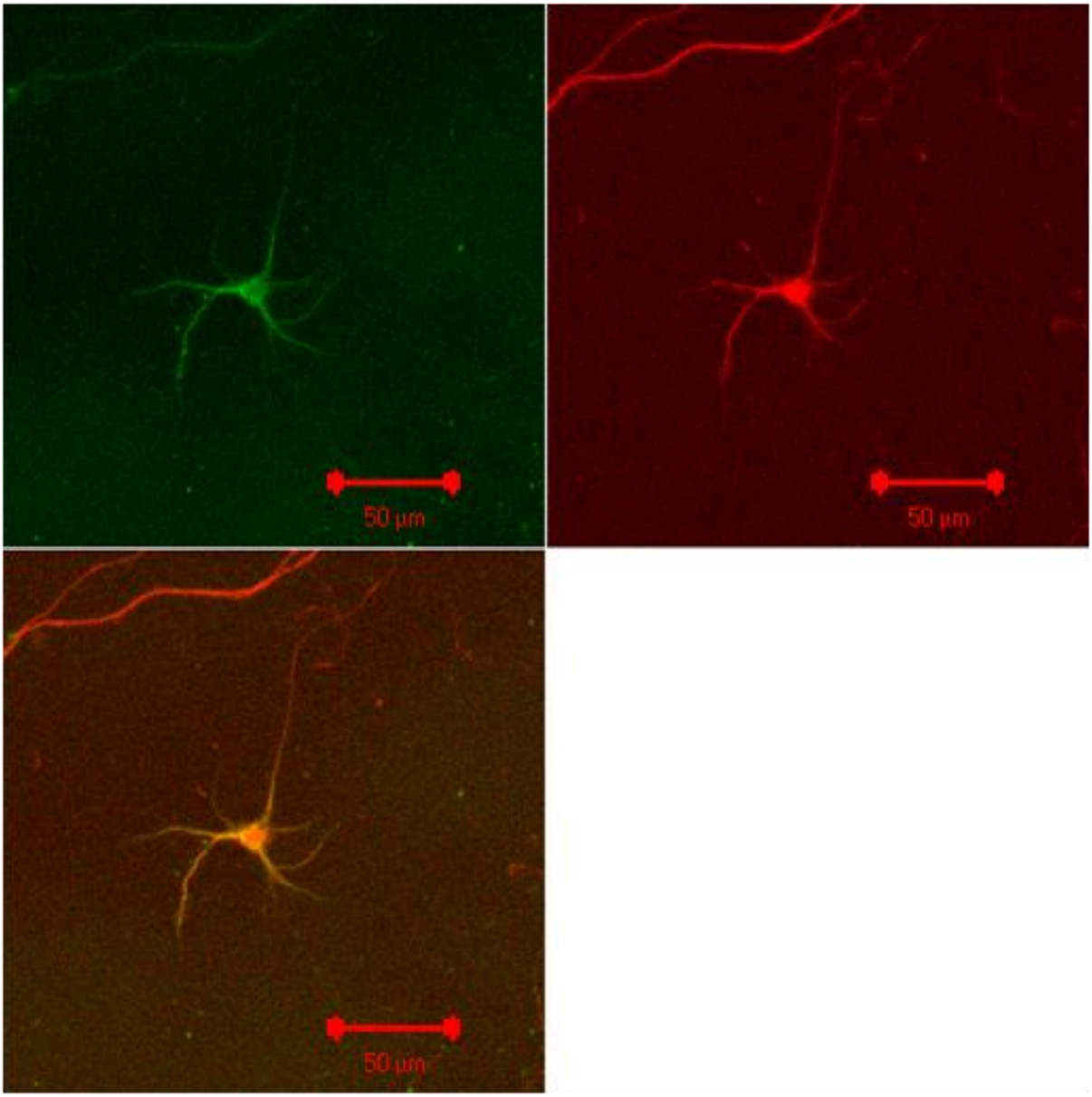

Figure 6.6 – Neurones co-stained for MAP2 and NF

Dispersed hippocampal cultures were grown in culture for 3 days, then fixed and stained for MAP2 (green, top left panel) and NF (red, bottom left panel), then imaged on a confocal microscope. MAP2 is restricted to the soma and the dendrites, whilst NF staining is detected throughout the neurone including in the axon.

Scale bar is 50 µm throughout

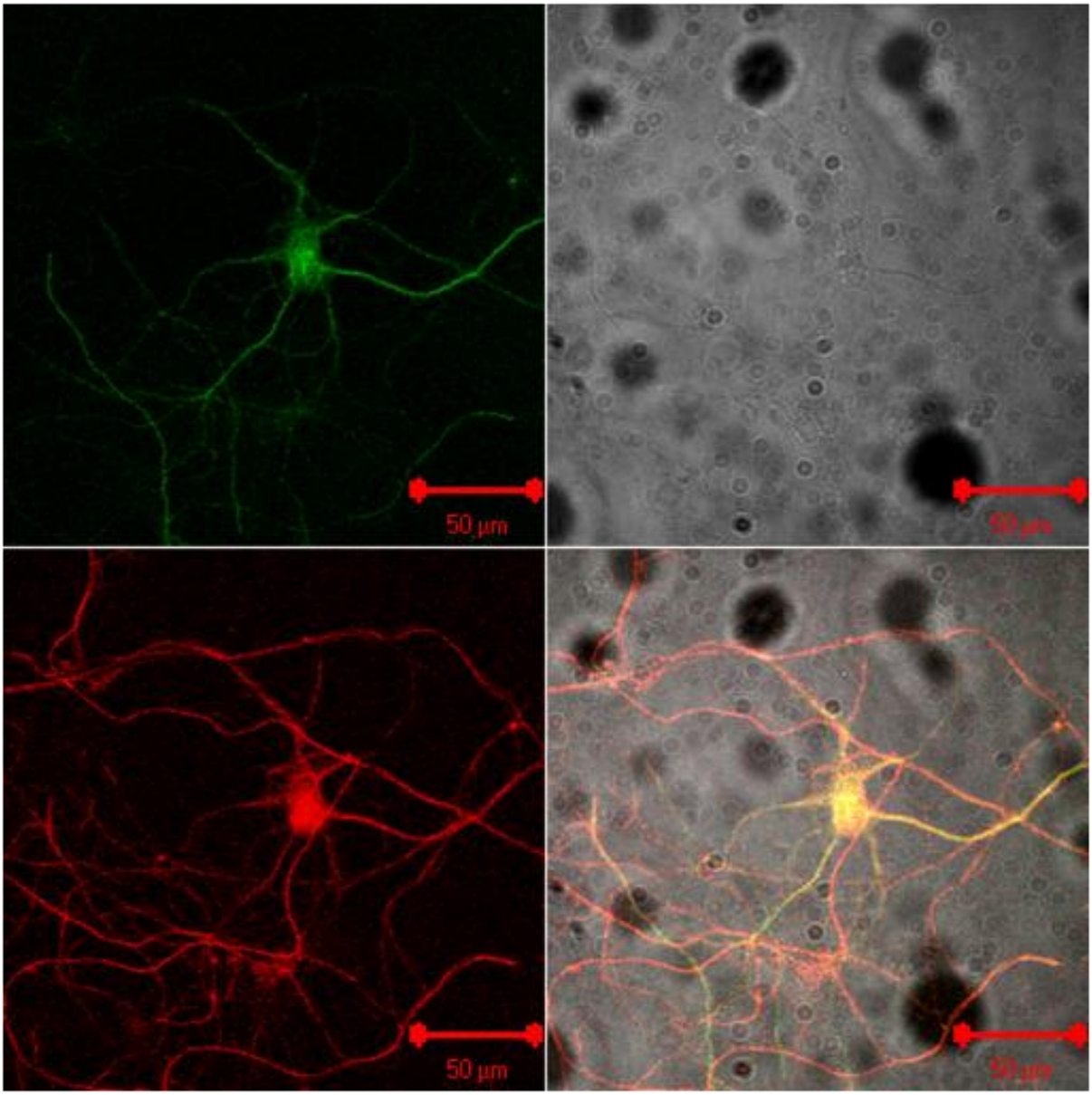

Figure 6.7 - Neurones co-stained for MAP2 and NF

Dispersed hippocampal cultures were grown in culture for 3 days, then fixed and stained for MAP2 (green, top left panel) and NF (red, bottom left panel), then imaged on a confocal microscope. MAP2 is restricted to the soma and the dendrites, whilst NF staining is detected throughout the neurone including in the axon.

Scale bar is 50 µm throughout

6.4.3 Calcium imaging

Dispersed hippocampal neuronal cultures (DIV 7) were grown on glass coverslips and then loaded with FURA-2. Neurones were then imaged and exposed to conditioned media from BeWo mono- or bilayer barriers either previously exposed to hypoxic or atmospheric conditions. Figures 6.8 through to 6.14 shows that exposure of cells to media that has previously been in contact with a BeWo barrier, whichever condition, elicits calcium rises in the cells. This is not true for media that has not been in contact with a barrier (see figure 6.12, HEPES does not induce a rise in the levels of calcium). Table 6.1 summarises the figures that follow.

Figure number	Cell type	Source of experimental media	Nanoparticles directly added? (yes/no)	Microparticles directly added? (yes/no)
6.8	Neurones	Hypoxic monolayer	No	No
6.9	Neurones	Atmospheric monolayer	No	No
6.10	Neurones	Hypoxic bilayer	No	No
6.11	Neurones	Atmospheric bilayer	No	No
6.12	Neurones	Hypoxic bilayer	No	No
6.13	Neurones	Atmospheric monolayer	No	No
6.14	Fibroblasts	n/a	Yes	No
6.15	Fibroblasts	n/a	Yes	No
6.16	Fibroblast	n/a	No	Yes

Table 6.1 – Experimental conditions used for calcium imaging

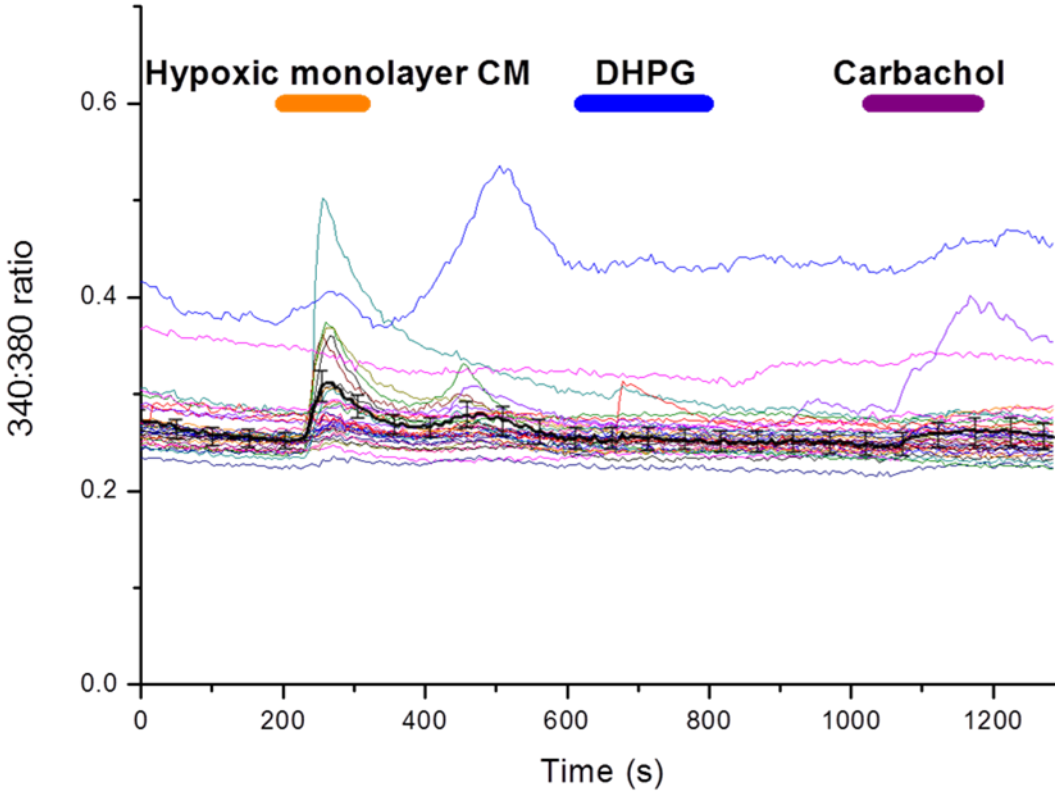

Figure 6.8 - Effect of conditioned media from hypoxic monolayer on neurones

Dispersed hippocampal neurones (DIV 7) were loaded with FURA-2 and then imaged. Perfusate collected from BeWo monolayers that had previously been exposed to hypoxic conditions elicited calcium rises in the neurones. Black trace shows average, error bars SEM

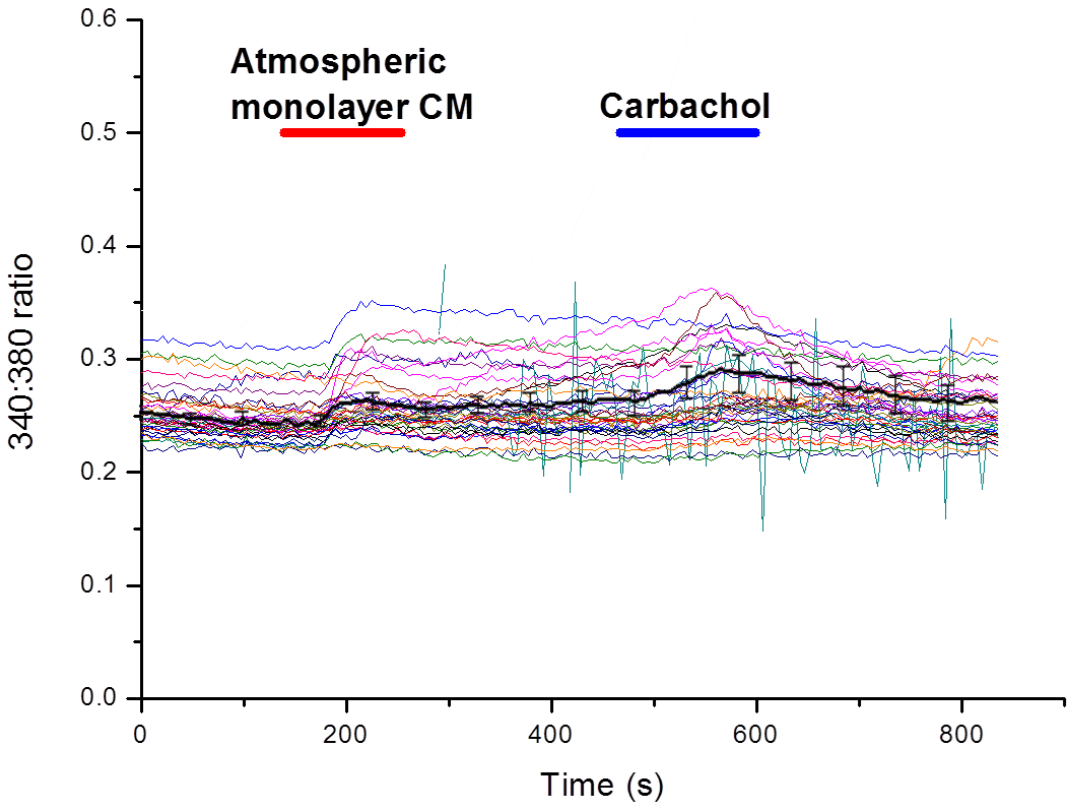

Figure 6.9 - Effect of conditioned media from atmospheric monolayer on neurones

Dispersed hippocampal cultures (DIV 7) were grown on glass coverslips and then loaded with FURA-2, and then exposed to conditioned perfusate from BeWo barriers exposed to standard atmospheric conditions. Presented here are ROIs from 38 cell bodies. Black trace shows average, error bars SEM

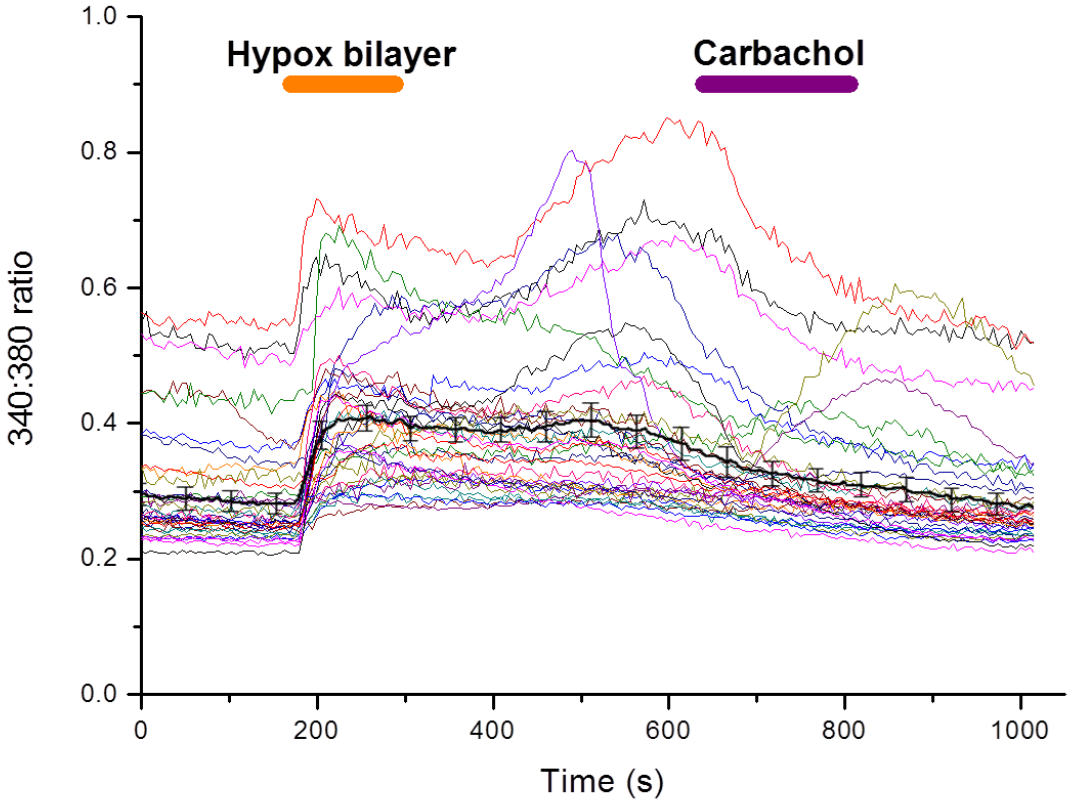

Figure 6.10 - Effect of conditioned media from hypoxic bilayer on neurones

Dispersed hippocampal cultures (DIV 7) were grown on glass coverslips and then loaded with FURA-2, and then exposed to conditioned perfusate from BeWo bilayer barriers exposed to hypoxic conditions. This graph shows 35 traces recorded from ROIs corresponding to neuronal cell bodies. Black trace shows average, error bars SEM

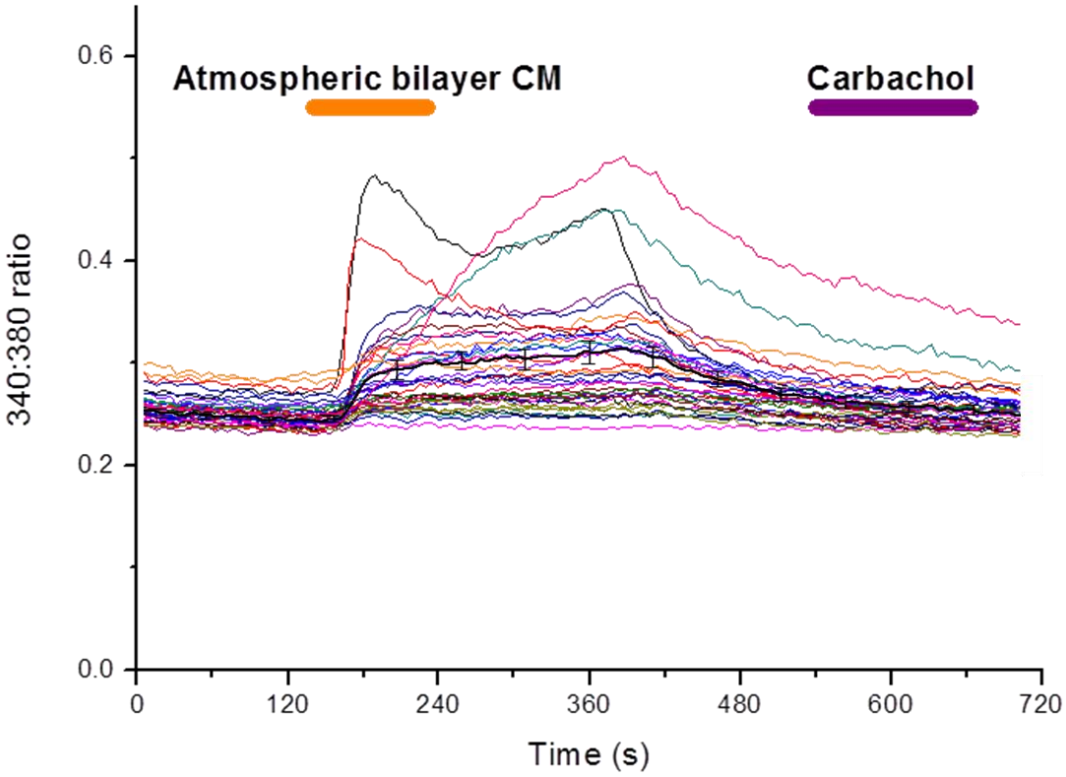

Figure 6.11 - Effect of conditioned media from atmospheric bilayer on neurones

Dispersed hippocampal cultures (DIV 7) were grown on glass coverslips and then loaded with FURA-2, and then exposed to conditioned perfusate from BeWo bilayer barriers exposed atmospheric conditions. Traces from 35 ROIs corresponding to neuronal cell bodies are shown. Black trace shows average, error bars SEM

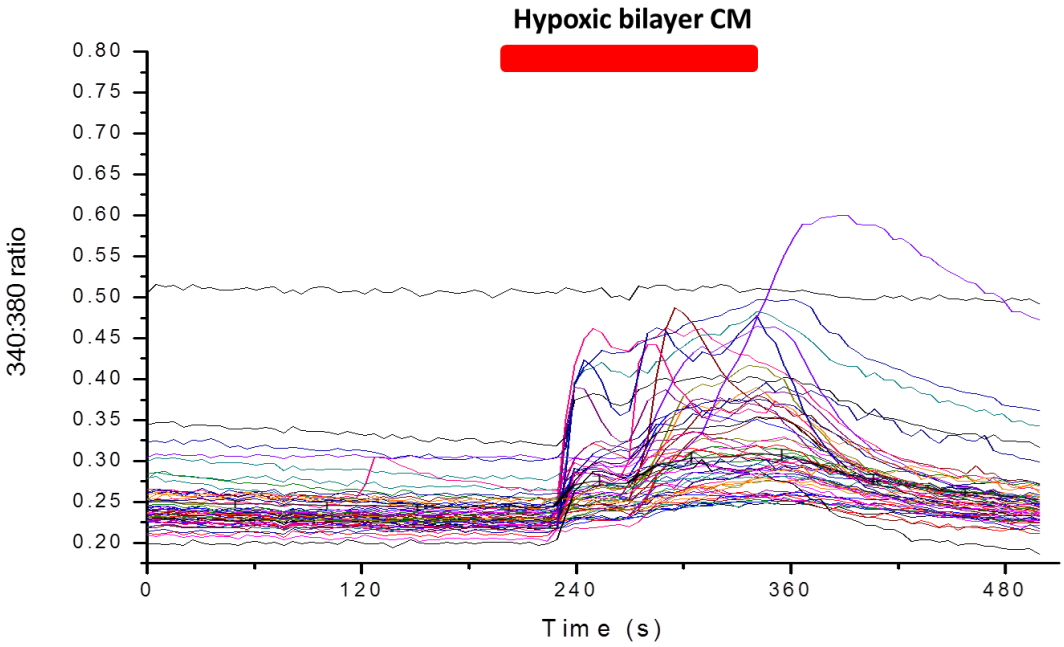

Figure 6.12 - Effect of conditioned media from hypoxic bilayer on neurones

Dispersed hippocampal cultures (DIV 7) were grown on glass coverslips and then loaded with FURA-2, and then exposed to conditioned perfusate from BeWo bilayer barriers exposed hypoxic conditions. Traces from 56 ROIs corresponding to neuronal cell bodies are shown. Black trace shows average, error bars SEM

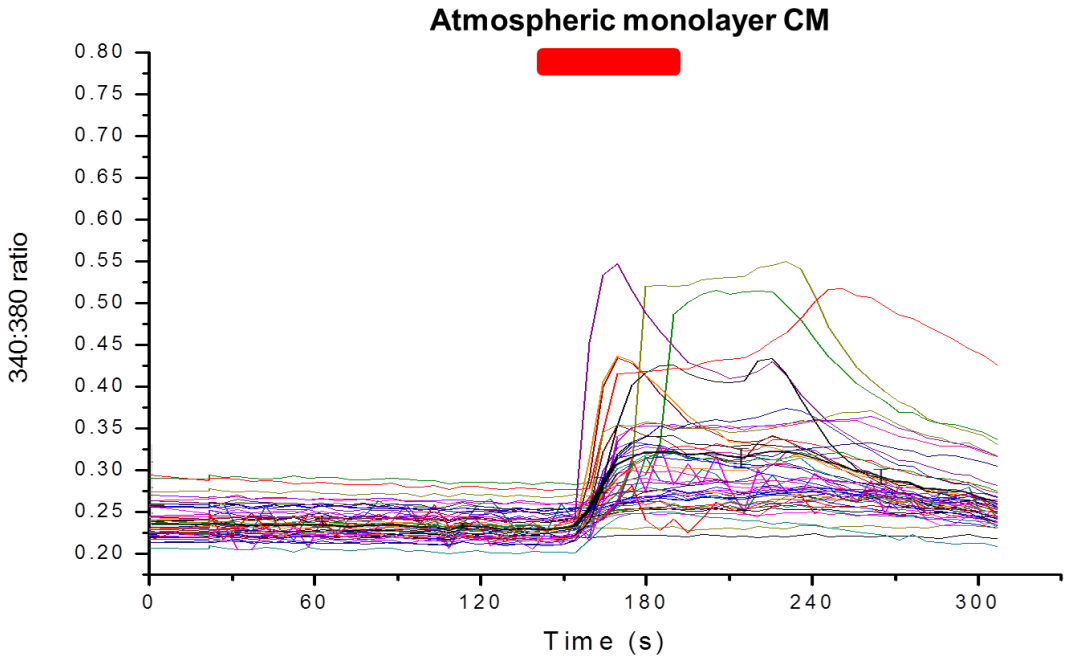

Figure 6.13 - Effect of conditioned media from atmospheric monolayer on neurones

Dispersed hippocampal cultures (DIV 7) were grown on glass coverslips and then loaded with FURA-2, and then exposed to conditioned perfusate from BeWo monolayer barriers exposed atmospheric conditions. Traces from 47 ROIs corresponding to neuronal cell bodies are shown. Black trace shows average, error bars SEM

Figures 6.15 to 6.17 show the effect on intracellular calcium levels after perfusion on of small metal particles, either CoCr nanoparticles (6.15 and 6.16) or CoCr microparticles (6.17). Adding metal particles to the fibroblasts tends to also cause a rise in intracellular calcium, with an initial rise followed by some sharp calcium peaks in some, but not all, of the cells.

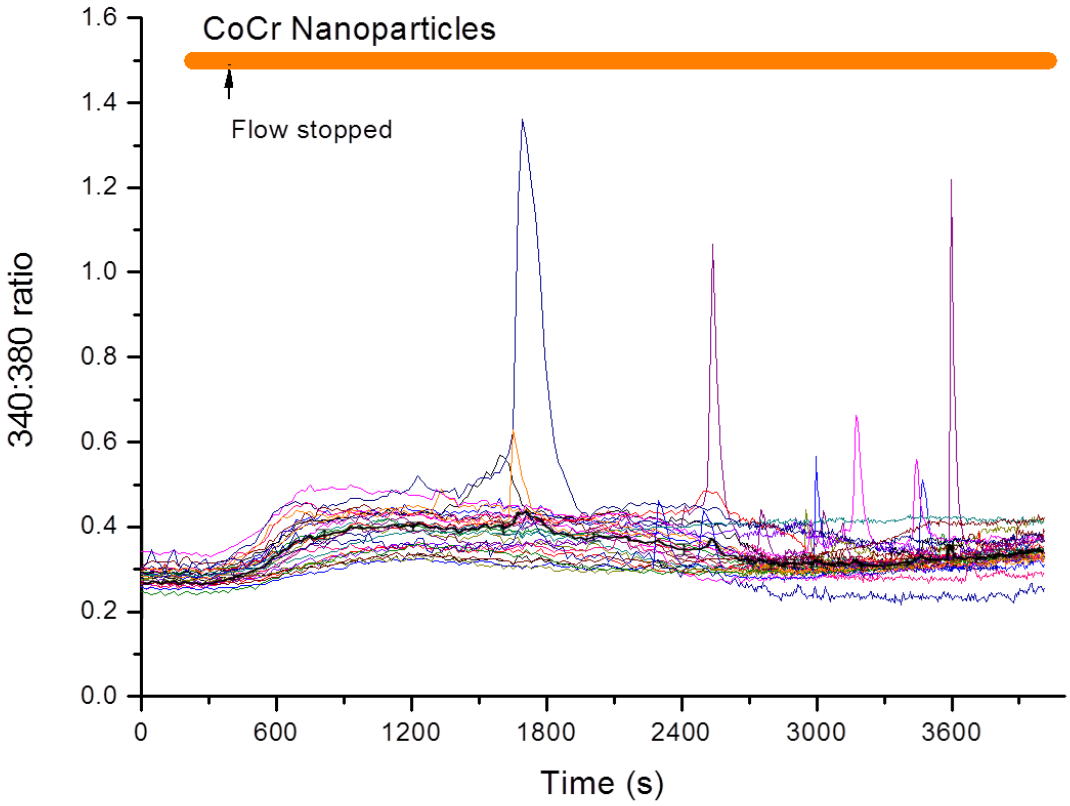

Figure 6.14- the effect of CoCr nanoparticles on cultured fibroblasts

Fibroblasts were grown in culture for 2 days on glass coverslips. They were the loaded with FURA-2 and imaged. CoCr nanoparticles were perfused on (3 mL) and then the flow was stopped. The experiment was performed this way to conserve nanoparticles. This figure shows traces from 26 ROIs. Black trace shows average, error bars SEM

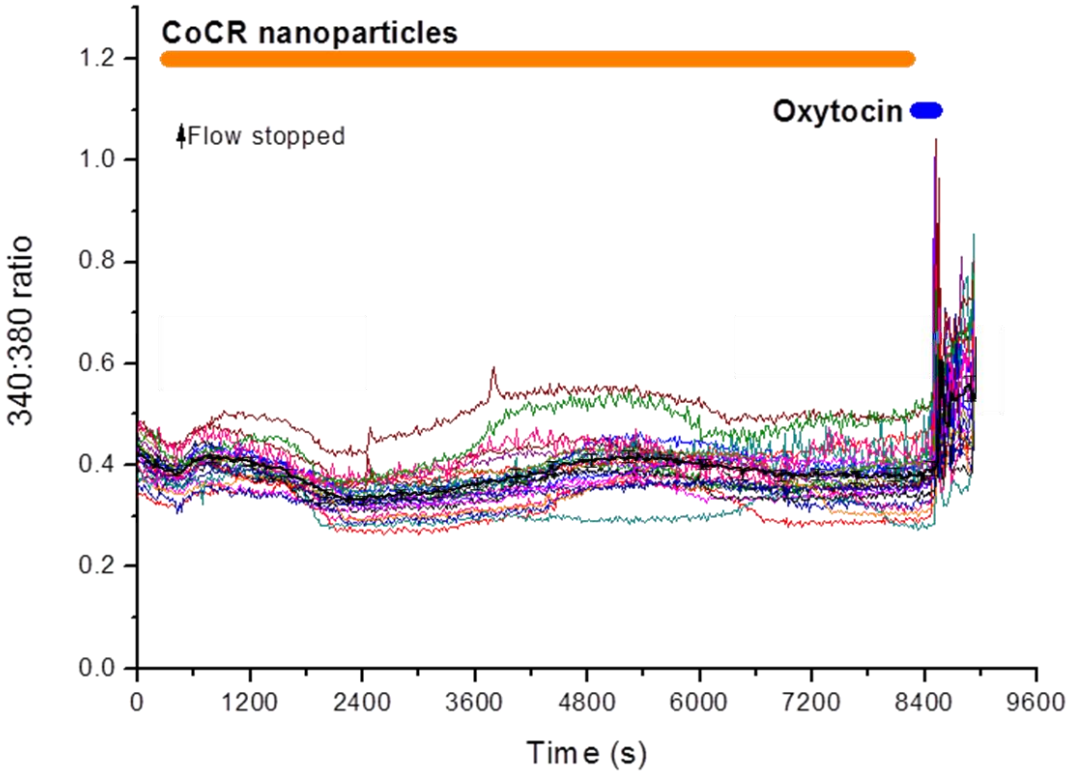

Figure 6.15 - the effect of CoCr nanoparticles on cultured fibroblasts

Fibroblasts were grown in culture for 2 days on glass coverslips. They were the loaded with FURA-2 and imaged. CoCr nanoparticles were perfused on (3 mL) and then the flow was stopped. The experiment was performed this way to conserve nanoparticles. Oxytocin was perfused on at end as a positive control

This figure shows 24 separate ROIs. Black trace shows average, error bars SEM

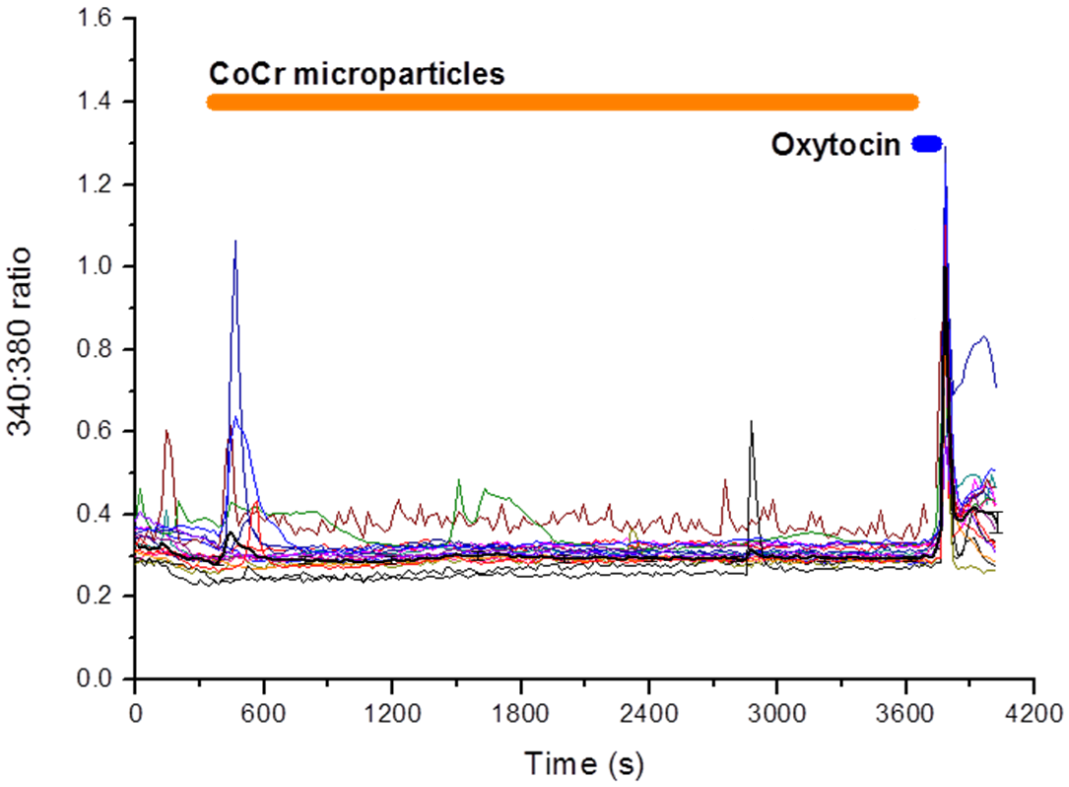

Figure 6.16 - the effect of CoCr microparticles on cultured fibroblasts

Fibroblasts were grown in culture for 2 days on glass coverslips. They were the loaded with FURA-2 and imaged. CoCr microparticles were perfused on (3 mL) and then the flow was stopped. The experiment was performed this way to conserve microparticles. Oxytocin was perfused on at end as a positive control

This figure shows traces from 17 ROIs. Black trace shows average, error bars SEM

6.5 Discussion

In this study I have shown that exposure to several different types of stimuli causes change in cell lines and cultured neurones. This includes indirect effects, via human trophoblast choriocarcinoma cultured barriers, and direct effects, such as adding media containing metal particles directly to cultured cells.

6.5.1 How do nanoparticles affect cells?

Previous studies have shown that when a media containing metal particles is added to a cell preparation, the metal particles sink out of solution and attach to the surface of the cells. They then can either form aggregates at, or near, the cells surface, or may be endocytosed into intracellular compartments. In work previously performed by this group, the addition of nanoparticles caused no actual cell death (Bhabra, Sood et al. 2009). 95% of the CoCr nanoparticles become embedded in the superficial (top) layer of the BeWo cells.

Introduction of nanoparticles can change a cells physiology by several mechanisms. Blocking channels and preventing normal ionic flow is one. Intracellularly, aggregation of nanoparticles could disrupt normal cellular function in these locations. A preference for a particular type of protein might mean that nanoparticles affect certain pathways more than others.

6.5.2 Signalling across barriers

There are some purely physical restrictions to consider when attempting determining the effect of signalling across barriers. Firstly, the composition of the barrier can have an effect on signalling. As stated in the introduction, barriers can be mono- (a single cell layer) or bilayers (a double cell layer). In a physiological context this is more complicated than our in vitro model, with different cell types being involved in the structure of the barriers, as opposed to our BeWo paradigm.

6.5.3 Monolayer signalling

. Signalling across a monolayer is likely to be restricted in vivo to a small percentage of a placenta, with the current estimate being up to 15% of the total barrier by the end of pregnancy. A monolayer structure mean that the cells that receive the external signal (nanoparticle exposure, conditioned media) can directly release or traffic signalling factors into the media on the other side of the barrier. Figure 6.18 illustrates the signalling possibilities in this system. Whilst crosstalk between BeWo cells is possible (mediated by gap junction or perhaps cell adhesion molecules) it is not absolutely necessary to transmit a signal across the entire barrier.

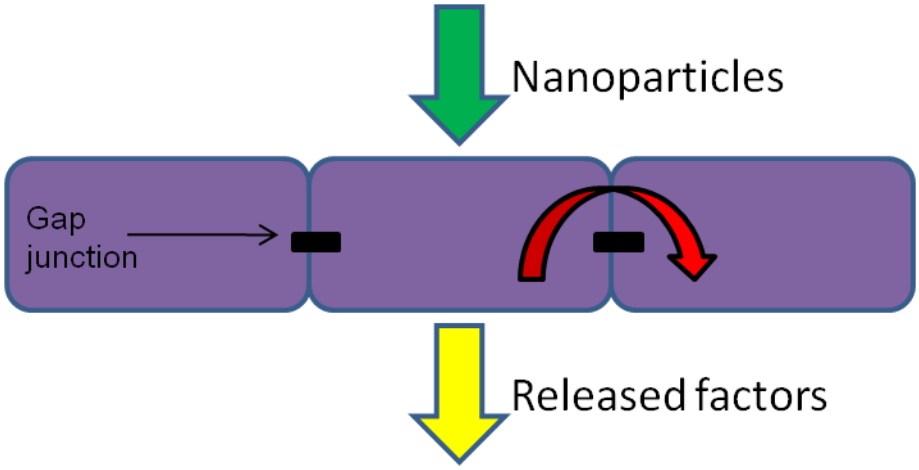

Figure 6.18

Schematic illustrating signalling possibilities with a BeWo monolayer barrier.

BeWo cells form a monolayer on the Transwell insert membrane (purple oblongs). This separates the media above and below the barrier into two distinct compartments. Nanoparticles added to the top media settle out onto the BeWo cells (green arrow). The BeWo cells then release factors into the bottom media compartment (yellow arrow). There is also potential for communication between BeWo cells horizontally via proteins such as gap junctions (e.g. connexins), represented here by the curved red arrow

The basic mechanism is this – cells exposed to metal particles' send messengers to neighbouring (un-exposed) cells, either through physical connections (for example gap junction, from the top layer of the barrier to cells in the bottom layer of the barrier) or secreted effects (for example from the cells forming the barrier to the neurones/fibroblasts), or indeed a combination of the two.

6.5.4 Bilayer signalling

Signalling across a bilayer is potentially more complex than across a monolayer. Tight junction between neighbouring BeWo cells prevent cells exposed to the top compartment of media being able to directly access the bottom compartment, and thus any signalling molecules have to pass through an additional layer of barrier cells. This is illustrated in figure 6.19 below. In this case, signalling across the barrier can be divided into two broad categories; signals that leave one cell layer, and diffuse across to the second cell layer, and signals that move directly between the two layers via gap junctions.

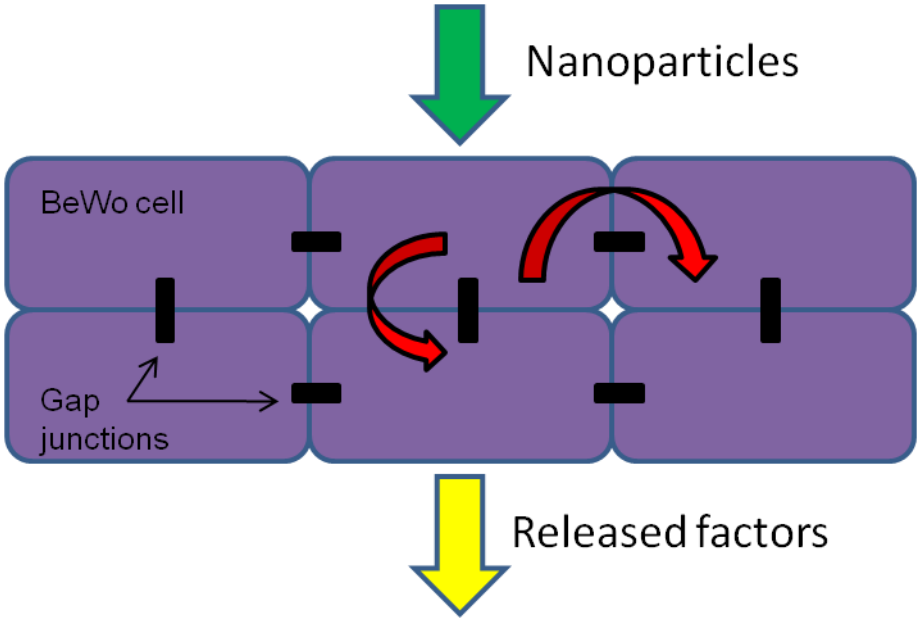

Figure 6.19 - Schematic of signalling in and through a BeWo bilayer barrier.

Similar to figure 5.29 the media is divided into two compartments by the BeWo barrier. However in this case any signal released by the top layer of BeWo cells must pass through another layer of BeWo cells before it can enter the lower media compartment.

6.5.5 The issues with imaging

Initially we attempted to quantify neuronal morphology by the use of either viral infection or immunocytochemistry. E18 neuronal cells cultures are still developing, and exposure to insults at this stage may affect neurite outgrow, spine development, and synapse formation, amongst other things. By expressing a pan-neuronal fluorescent marker (in this case mCherry or GFP) which fills the cell, it is possible to monitor the extent of the soma, axon, and dendritic arbour, including the morphology of dendritic spines. It is feasible that early insults to cultured neurones (i.e. either conditioned hypoxic media or small metal particle exposure) could affect the normal developmental progress. However, early stage neurones are especially vulnerable to viral infection and fixation. Both the mCherry and the GFP viral vectors seemed to hamper, rather than enhance, the possibility of gathering usable consistent data for morphological analysis. Young cultured neurones (DIV1-6) tended to be damaged by the fixation and/or viral infection. This was seen in both the controls and the treated samples. We therefore decide to discontinue this line of inquiry, and concentrate on live imaging of neurones without infection or fixation.

In the calcium imaging experiments several cells failed to respond to control drugs (for example carbachol). This is likely due to the young age (DIV 7) of the preparation. It would be useful to repeat these experiments on a wider age range of cultures, ideally up to DIV 21 when cells are considered mature.

6.5.6 Future work

This is an ongoing collaborative project involving several labs. One possible future avenue that is being explored is the use of human placental explants, however this work is not developed enough yet to feature in this work. This is an exciting possibility as this is near to real human physiology as we can get in this field. If metal particles and hypoxia can be tested on human placental explants.

Chapter 7

Culturing dissociated neurones in novel hSAF gels

7.1 Aims

To grow dissociated cortical and hippocampal neurones in a novel gel, and evaluate whether normal neuronal development takes place

7.2 Introduction

There has been an increasing demand in the field of medicine for implantable tissue scaffolds to replace or augment damaged areas of tissue. This demand is across many regions of the body, including (but not limited to) –

- Repairing spinal transections (Cadotte and Fehlings 2011)
- Hip implant (and other prostheses) (Learmonth and Spirakis 1989)
- Regrowing and attaching skin grafts (Hansbrough, Morgan et al. 1993)
- Replacing damaged areas of brain
- Full organ replacement (Macchiarini, Jungebluth et al. 2008)

With this requirement in mind, many groups have been attempting to develop artificial tissue scaffolds that can be created in the laboratory, and then implanted into live organisms to replace or support tissue.

7.2.1 Types of biomaterial

Several different potential scaffolding materials have been developed. Cell culture at its simplest uses materials such as poly-L-lysine and collagen to adhere cell lines and cell types to Petri dishes/coverslips. These preparations are effectively 2-D in shape, flattened out across the surface of the coverslip. This does not reflect the real structure of organs and body tissues. Organs typically have a precisely defined shape dependent on function. Some organs are hollow bodies (for example the bladder), some have more complex multi-region structures (the heart) and others have highly complex divergent structures (for example the cytoarchitecture of the brain). Thus there is a need for 3-dimensional biodegradable biomaterials that can be used in surgical interventions.

7.2.2 Requirements for implant material

Material designed to be implanted into the human body need to meet a number of criteria. They need to be non-toxic, as so not to damage surrounding tissue, and also support any implanted tissue. Areas requiring implants may already be damaged by insults or injury, and may be especially vulnerable to any toxic products of the implant material.

Following on from this, implanted biomaterials must not provoke an immune response, and cause inflammation.

Implanted biomaterials need to integrate with pre-existing bodily material (muscle, bone, tendons etc), but also need to biodegrade when necessary. For example, stem cells may be implanted to repair a damaged site. Once the cells have divided, differentiated, and formed a new structure, the biomaterial supporting them needs to be able to be degraded away by endogenous systems such as metalloproteases. The implanted materials need a certain level of physical strength, but at the same time need to be somewhat flexible to allow for movement of body parts and cell migration within them.

7.2.3 Poly-peptide based biomaterials

A wide variety of peptide based materials have already been developed for use as implants and /or tissue scaffolds (see (Zhang, Holmes et al. 1993; Woolfson and Ryadnov 2006)). The majority of pre-existing peptide based biomaterials fold to form beta-sheets, however recently it has been possible to engineer coiled-coil alpha helical peptide structures.

7.2.4 Hydrogels

Hydrogels have many advantages as a potential implant material. The structure of the scaffold can be chemically defined, and therefore controlled, in both a composition and compliance sense (Banwell, Abelardo et al. 2009) . Hydrogels have consistent internal structure, are transparent, and show little swelling or contracture. They are also relatively cheap (an important point if mass-produced) and are easy to handle and use at both room temperature and physiological temperatures (37^{o}C). In this work I utilised hydrogelating self-assembling fibres (hSAFs). hSAFs are composed of two peptides, and gel when mixed. They have an alpha-helical structure, and have previously been shown capable of supporting cell growth (Banwell, Abelardo et al. 2009). As these peptides are created in the laboratory, the exact composition of the peptides can be altered. In this study I used two different peptide sequences, shown in table 8.1 below.

Name	Sequence
hSAF AAA peptide 1	KIAALKAKIAALKAEIAALEAENAALEA
hSAF AAA peptide 2	KIAALKAKNAALKAEIAALEAEIAALEA
hSAF AAAw peptide 1	KIAALKAKIAALKAEIAALEWENAALEA
hSAF AAAw peptide 2	KIAALKAKNAALKAEIAALEWEIAALEA

Table 7.1 Sequence of peptide comprising hSAF. Changes to W denoted in red

7.2.5 Neuronal culture in 3-D

As discussed in the general introduction, dissociated neuronal cultures are a reductionist paradigm that allows ease of access and experimental convenience, whilst losing much of the connectivity and layout of the intact brain. Here I had an opportunity to grow neuronal cultures in an environment that would permit three-dimensional growth. The most important aspect of an artificial biomaterial is that is supports the cells grown in it, and is not cytotoxic. Neurones are highly vulnerable to insult, both metabolic and mechanical, and provide an ideal test for any biomaterial. Previously hSAF-based gels had been tested on PC12 cells, but not fully differentiated neurones.

7.2.6 Artificial nerve fibre conduits

There has been a significant body of work on attempting to create conduits for nerve regrowth. Fibronectin mats (Whitworth, Dore et al. 1995), with first the addition of neurotrophin-3 (NT3, (Sterne, Brown et al. 1997; Sterne, Coulton et al. 1997), and then with the addition of nerve growth factor (NGF, (Ahmed, Brown et al. 1999) have been trialed in both rats and primates. Collagen-based nerve conduits have also been used. (Kitahara, Suzuki et al. 1999) used collagen mats in an attempt to repair facial nerves in a feline model. Another approach has been to utilise collagen with cross linked brain derived neurotrophic factor (BDNF) in a rat model (Utley, Lewin et al. 1996).Three-dimensional gels constructed from synthetic and naturally derived biodegradable polymers have been widely used in the field of tissue engineering. Various polymers (PGA - polyglycolic acid, PLA – polylactic acid, PGLA - Poly(lactic-co-glycolic acid)) have been made into tubes and filled with collagen as a conduit for nerve regrowth. See (Chen G 2002) for review. More recently PHB (poly-3-hydroxybutyrate) mats filled with Schwann cells have also been trialed (Mosahebi, Wiberg et al. 2003). Before attempting *in vivo* studies with hSAFs (as above) it is useful to trial the novel peptides in *in vitro* conditions with cell lines and neuronal culture.

7.3 Materials and Methods

7.3.1 Gel construction

Peptides were synthesized on a CEM `Liberty' peptide synthesizer using standard solid-phase 9-fluorenyl-methoxycarbonyl chemistry. Amino acids were purchased from Novabiochem Peptides were cleaved using 95% trifluoroacetic acid (Sigma), 2.5% triisopropylsilane (Sigma) and 2.5% 18:2Mohm ultrapure water, purified by reverse-phase high pressure lipid chromatography using acetonitrile (Fisher) water gradients with 0.1% trifluoroacetic acid. Pure peptides were freeze dried from acetic acid, weighed and dissolved in ultrapure water to give 3mM (9 mg ml^{-1}) stocks.

7.3.2 Fluorescence imaging

Neurones were infected with SindBis-GFP, left for 8-24 hours, and then imaged on a confocal microscope, as described in Chapter 2. GFP was excited with a 488nm laser line.

7.3.3 Scanning electron microscopy

Samples were mounted on brass rivets, then flash frozen with liquid nitrogen. Samples were then mounted on a cooled holder, and fractured using a cooled scalpel tip. Finally samples were coated with 2nm Pt/Pd and imaged on a JEOL6301 microscope.

7.3.4 Neuronal culture

Dissections were performed as described in Chapter 2. Neurones were seeded into hSAF gels by simply pipetting the required amount of cells into the media above the centre of the gels. Cells then sank and embedded themselves into the gel. Experiments were then performed 4-14 days later.

7.3.5 Electrophysiology

Patch clamp recording were made from neurones as described in Chapter 2. Briefly, neurones grown in hSAF gel were transferred from an incubator to a recording chamber and whole cell patched clamped.

7.4 Results

7.4.1 Electron microscopy of gels

High magnification scanning electron microscopy images of gels were taken to examine the ultrastructure. Gels were shown to form elaborate crosslinking meshes, with strands separated by pores. Pore size (between 10 µm and 500 µm) are within the size range to permit neuronal cells bodies and processes.

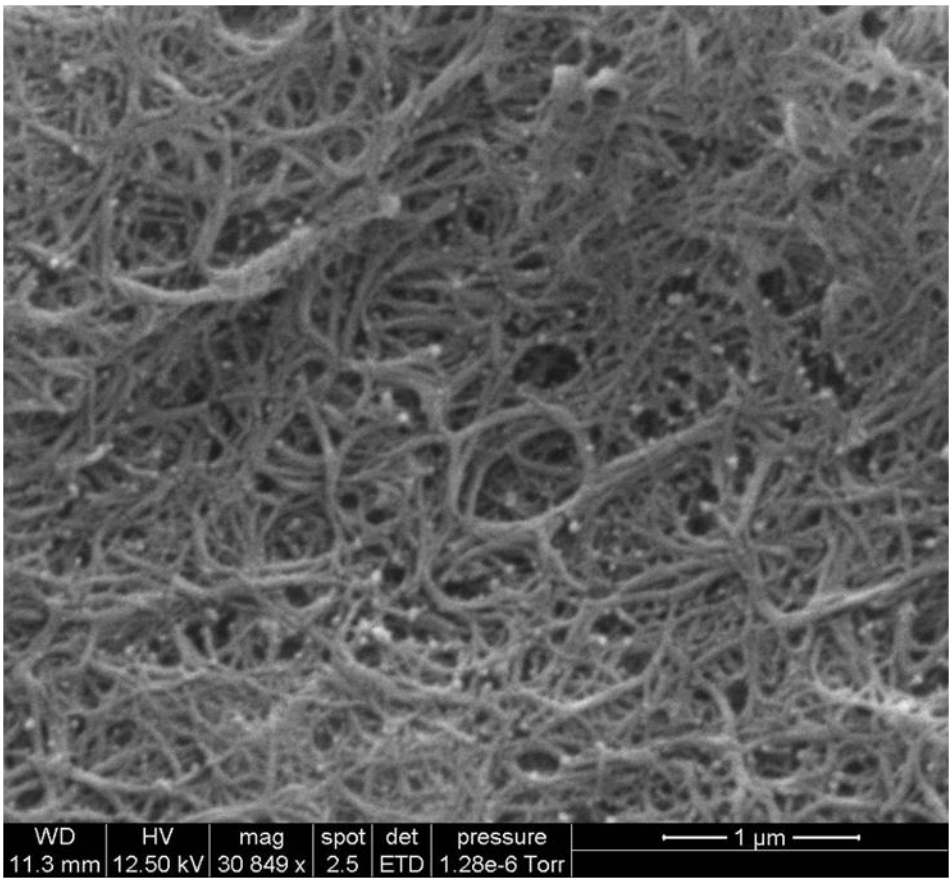

Figure 7.1 - SEM image of the ultrastructure of AAAw hSAF gel. Notice pore formation between strands

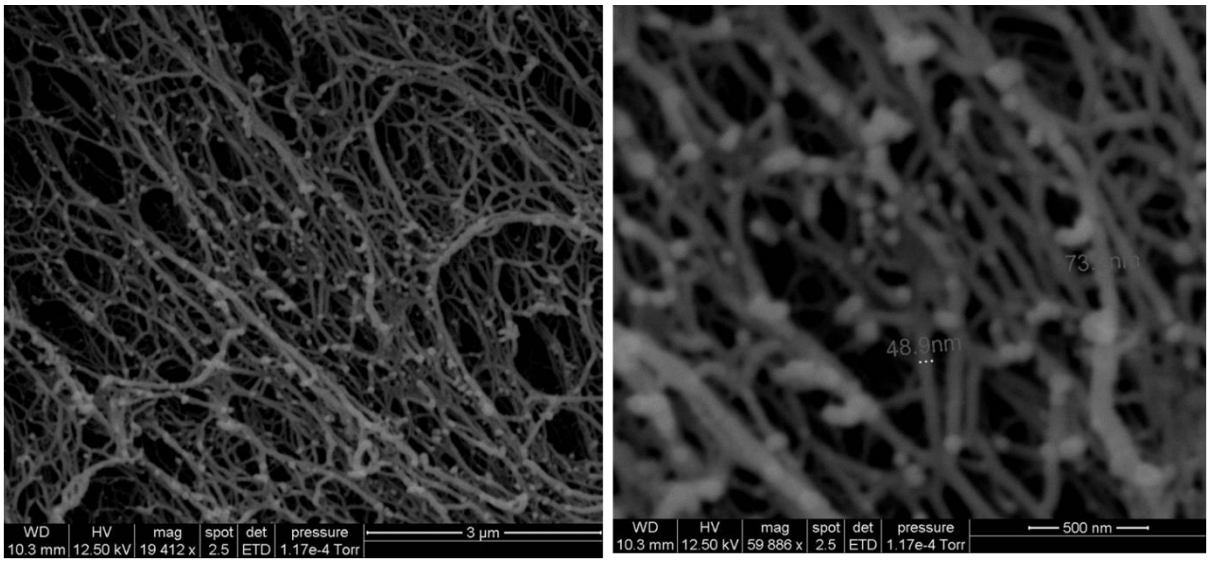

Figure 7.2 - SEM image of the ultrastructure of AAA hSAF gel. Notice pore formation between strands

Both hSAF AAA and hSAF AAAw form a meshwork at the ultrastructural level, with clear strands and pore being visible (figures 7.1 and 7.2). This structure appears suitable for cellular growth, with both support being provided by the mesh like network of strands, and space for growth being provided by the pores formed in-between peptide strands.

7.4.2 Images of outgrowth

Cultured cortical neurones were dissected out and prepared as described in Chapter 2. They were then pipetted into the media above pre-prepared wells with hSAF gel and media. Cells were left to grow and then imaged after 7 DIV. Figures 7.3 and 7.4 show images of cultured neurones growing in hSAF gel.

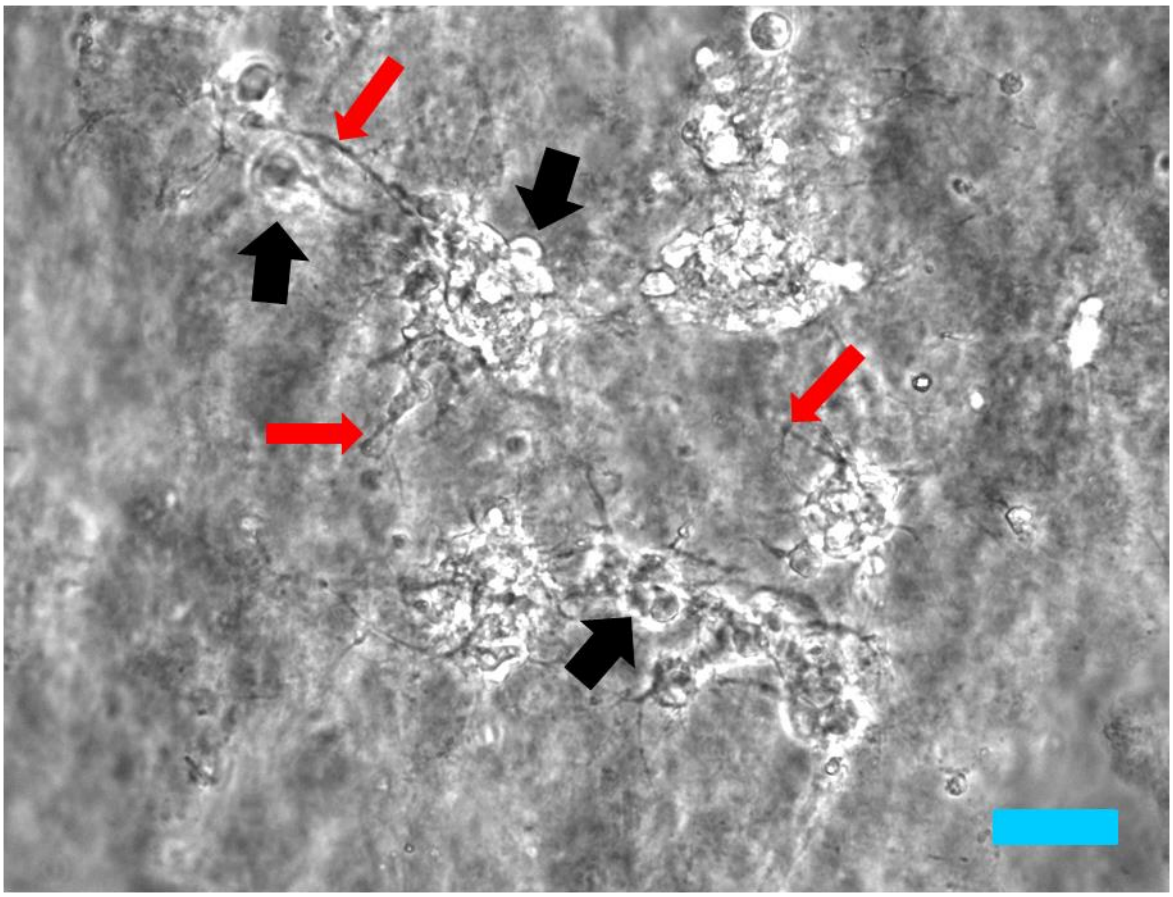

Figure 7.3 - DIC image of cultured hippocampal neurones growing and embedded in AAAw hSAF. Labeled are cell bodies (black arrows) and neurites (red arrows)

Scale bar is 200 µm

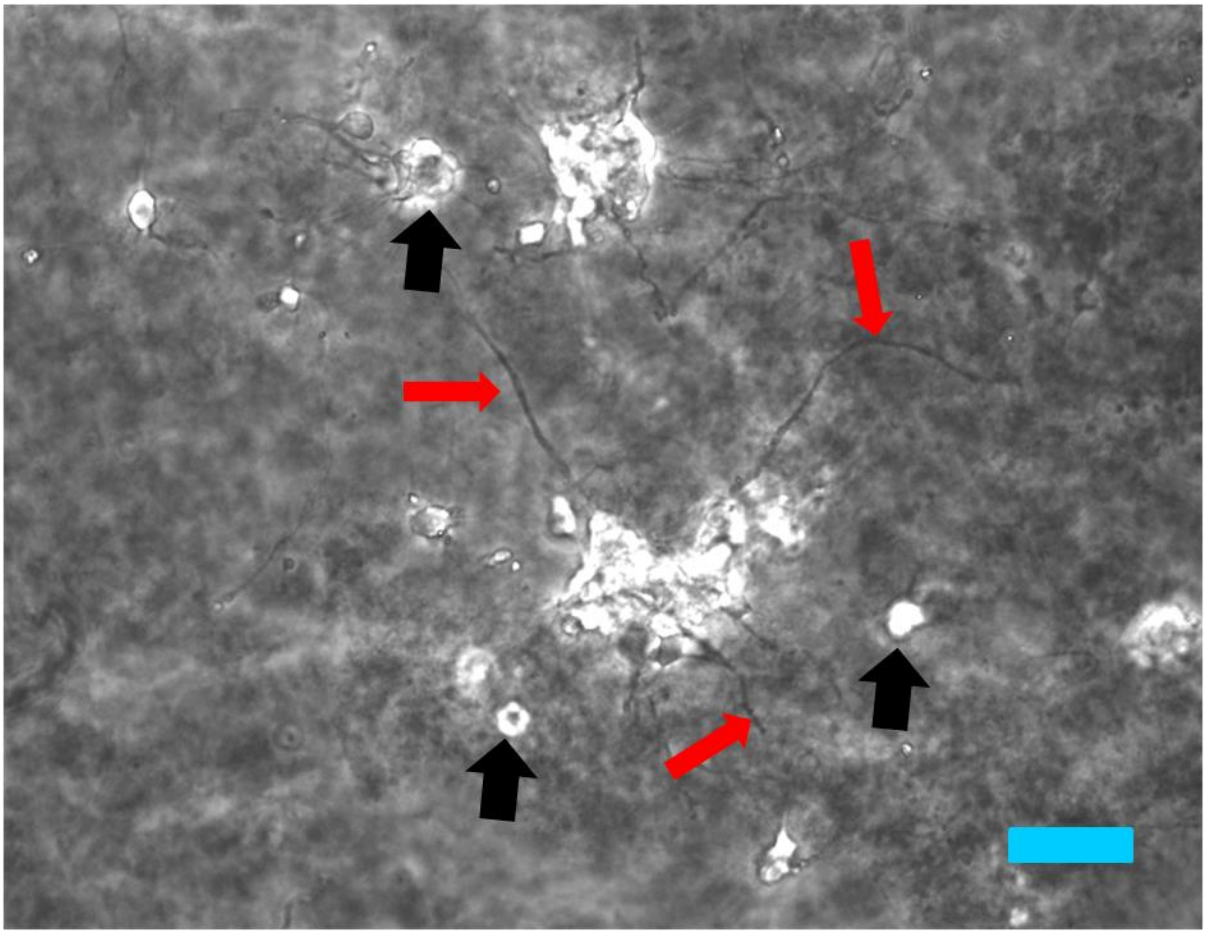

Figure 7.4 - DIC image of cultured hippocampal neurones growing and embedded in AAAw hSAF. Labeled are cell bodies (black arrows) and neurites (red arrows)

Scale bar is 200 µm

7.4.3 Fluorescent microscopy

Neurones were dissected out and dissociated as described previously. They were then added to pre-prepared well containing hSAF gels and media. After 7 DIV, 2 µl of SindBis-GFL virus was added to the media, and the dishes were returned to the incubator. 12-24 hours later, neurones were imaged.

Figure 7.5 shows a confocal image taken from a well of Matrigel with virally-infected neurones expressing GFP. The projection image of the entire Z-stack is shown. Notice neuronal cell bodies and neurites are clearly visible

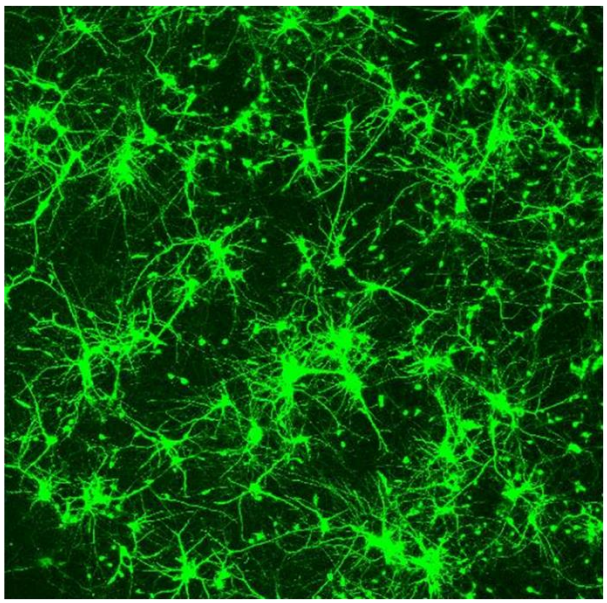

Figure 7.5 – Cultured neurones growing in Matrigel

Confocal fluorescent microscopy image of hippocampal neurones growing embedded in Matrigel. Neurones were dissected out, dissociated, and then pipetted into media above gel. After 7 DIV, neurones were infected with SindBis GFP and imaged 12-24 hours later. Image is projection of Z-stack

Entire field of view is 1500µm

Figure 7.6 (below) shows confocal microscopy images taken from neurones growing in AAA (undecorated) hSAF that are expressing GFP. Neuronal cell bodies and neurites are visible, but neurites are less apparent than from cells grown in Matrigel.

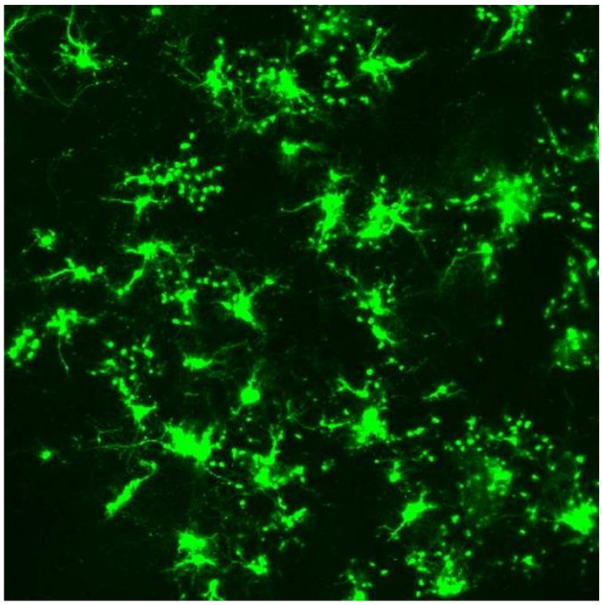

Figure 7.6 - Cultured neurones growing in hSAF AAA

Confocal fluorescent microscopy image of hippocampal neurones growing embedded in undecorated AAA hSAF. Neurones were dissected out, dissociated, and then pipetted into media above gel. After 7 DIV, neurones were infected with SindBis GFP and imaged 12-24 hours later. Image is projection of Z-stack

Entire field of view is 1500µm

Figure 7.7 shows a similar confocal image to above. In this case neurones are grown in AAAw hSAF. Again neuronal cell bodies are visible, but neurite outgrowth appears to be enhanced compared to figure 8.6

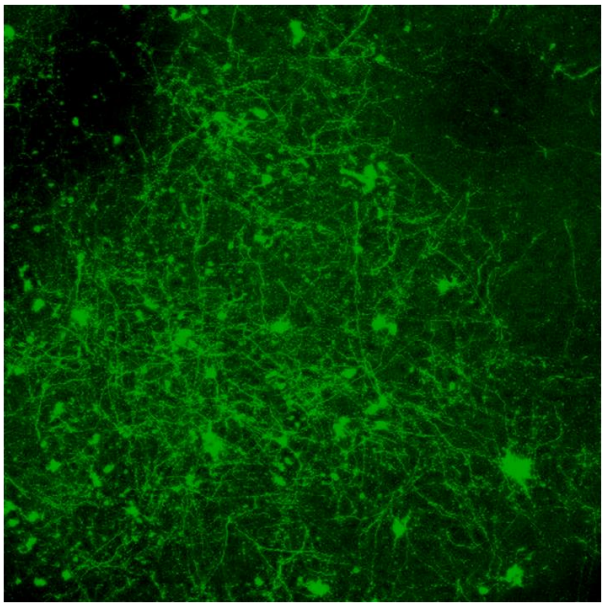

Figure 7.7 Cultured neurones growing in hSAF AAAw

Confocal fluorescent microscopy image of hippocampal neurones growing embedded in AAAw hSAF. Neurones were dissected out, dissociated, and then pipetted into media above gel. After 7 DIV, neurones were infected with SindBis GFP and imaged 12-24 hours later. Image is projection of Z-stack

Entire field of view is 1500µm

7.4.4 Electrophysiology

Neurones were grown as described above in hSAF gel cultures. After 7-14 days, fragments of gel were transferred to a recording chamber on a electrophysiological patch rig, and whole cell patch clamped. Figure 7.8 shows an example image of an individual cultured neurones being patched.

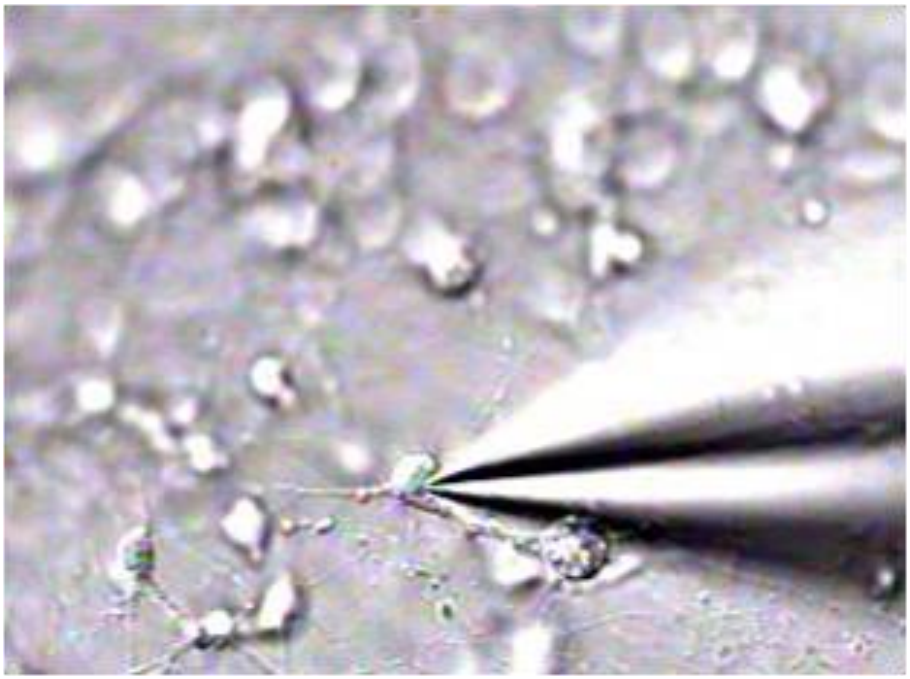

Figure 7.8 DIC image of a patch pipette (right hand side) being placed on a hippocampal neurone

Figure 7.9 shows example traces from neurones obtained from different sources. *Left*, neurones from acute hippocampal slice fire several action potentials in response to a depolarising stimulus. *Middle*, neurones from a two-dimensional dissociated hippocampal culture still fire action potentials, but less than the acute slice preparation. Finally, *right,* neurones grown in hSAF-AAA failed to fire any action potentials.

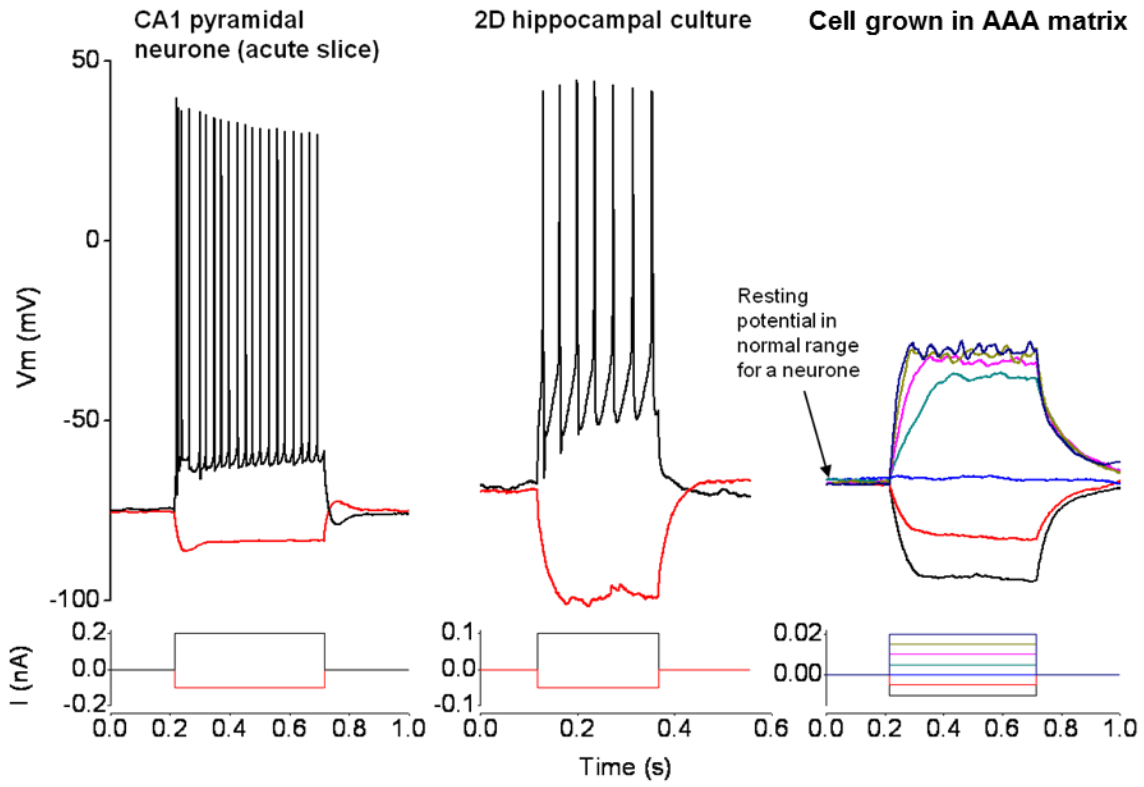

Figure 7.9 – A comparison of neuronal action potential firing in response to depolarising stimuli

Left to right, CA1 pyramidal neurone, 2-D cultured neurone, and neurone grown in hSAF AAA

Figure 7.10 shows responses from three neurones grown in hSAF-AAAw. All three cells fired action potentials, unlike neurones grown in hSAF-AAA. Arrow at left indicates neurones resting membrane potential is within normal values.

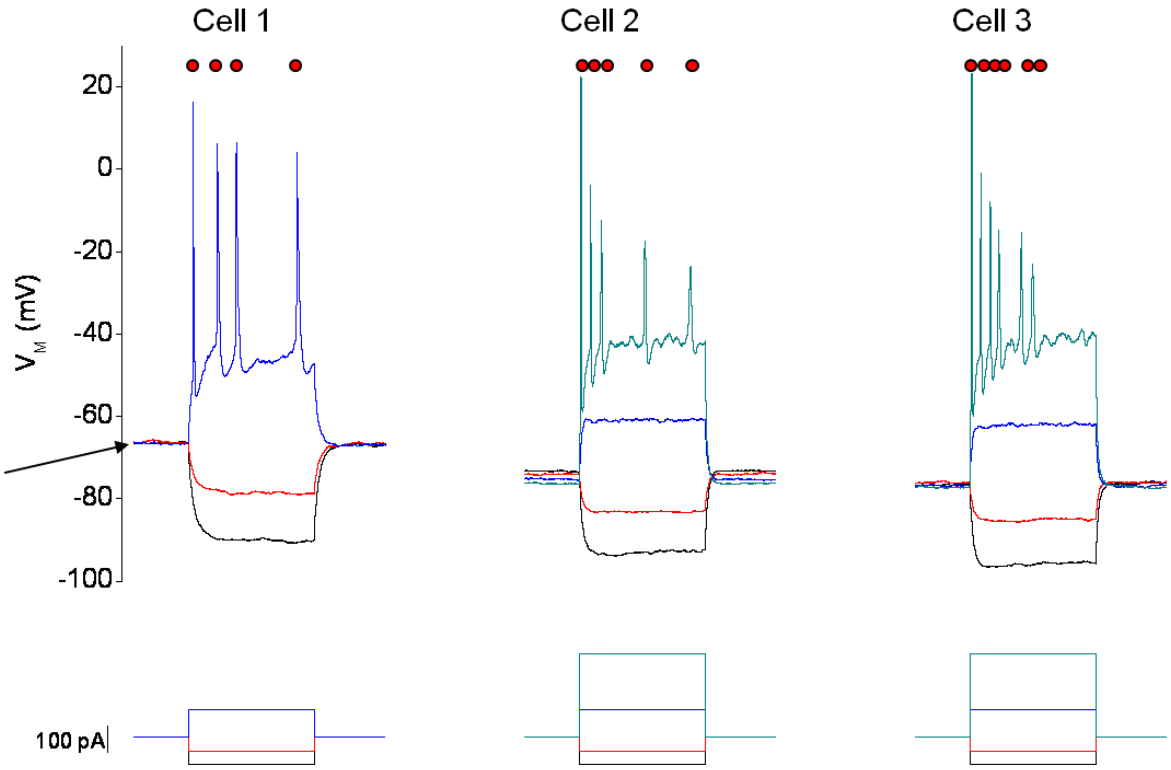

Figure 7.10 - A comparison of neuronal action potential firing in response to depolarising stimuli

All neurones are from hSAF-AAAw, and all fire action potentials in this example

Figure 7.11 (below) shows recording from neurones cultured in hSAF-AAA. These neurones had normal potassium currents, but small sodium and calcium currents.

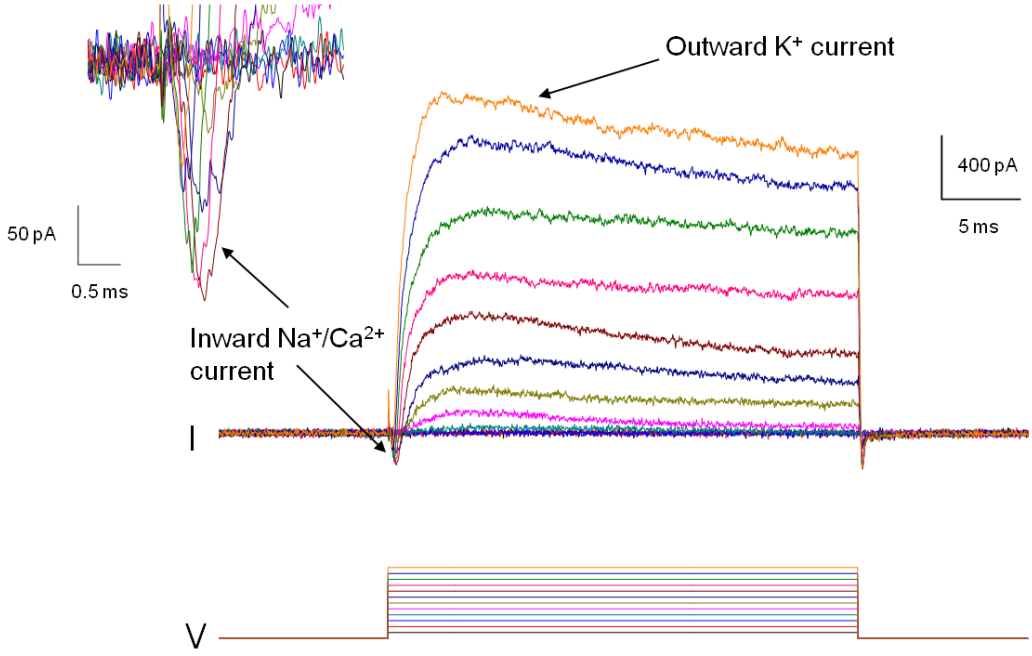

Figure 7.11 – electrophysiological recordings from cultured neurones grown in hSAF-AAA.

A voltage step protocol (bottom) allowed measurement of currents. Large outward potassium currents were observed, but only small inward sodium and calcium currents.

Figure 7.12 shows the same experiment as in figure 7.11 (above), but now in neurones cultured in hSAF-AAAw. Again, neurones display large outward potassium currents, but neurones cultured in this gel-type also displayed inward sodium and calcium currents of more typical magnitude.

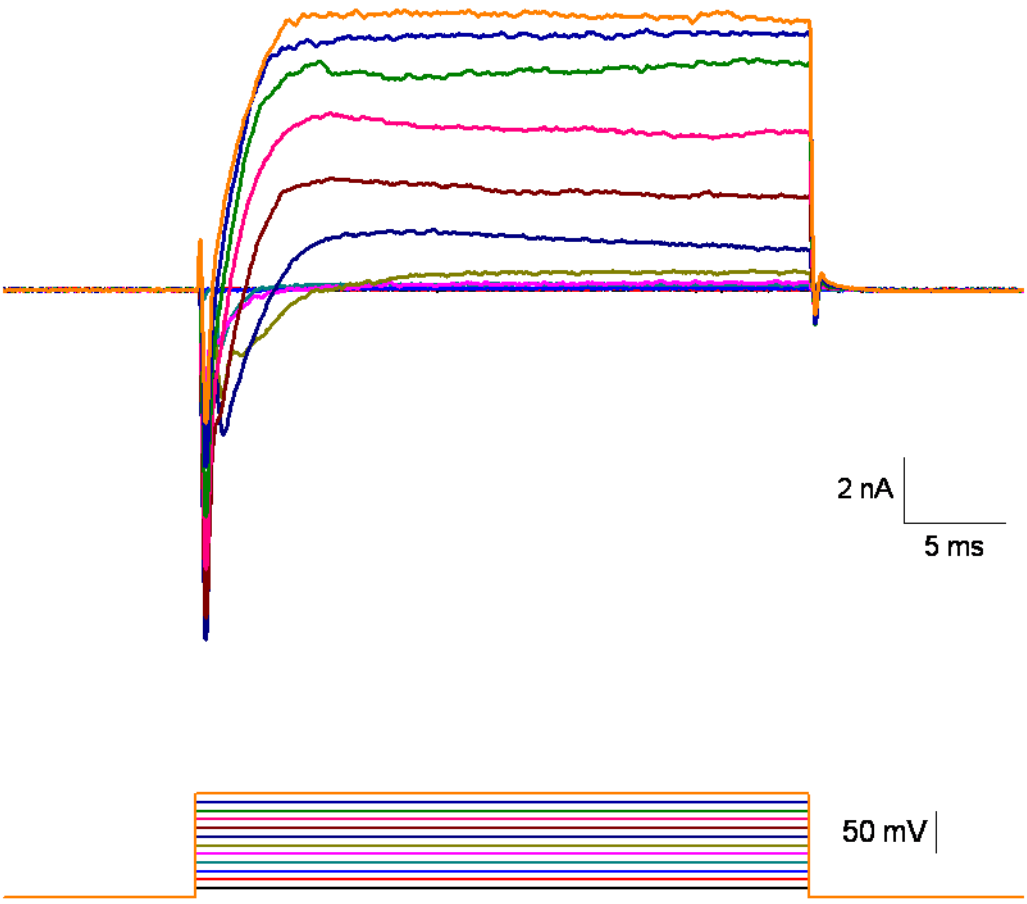

Figure 7.12 – electrophysiological recordings from cultured neurones grown in hSAF-AAAw.

A voltage step protocol (bottom) allowed measurement of currents. Large outward potassium currents and inward sodium and calcium currents. were observed .

Unfortunately performing electrophysiological experiments on neurones grown in gels was challenging, due to the constraints on moving the gel (containing living neurones) between the culture chamber and the recording chamber, and the high

cost of the gel production, so these experiments were not able to be repeated. However this preliminary investigation is still useful as it shows that neurones grown under these conditions do display normal neuronal electrical behaviour.

7.5 Discussion

In this appendix I have attempted to study the compatibility of a novel biomaterial (hSAF gel) with dissociated neuronal cultures. Previously hSAFgel s had been shown capable of sustaining cellular cultures, including PC12 cells, Hep2s, and HUVECS, but not true differentiated neurones.

Both cortical and hippocampal neurones can survive in hSAF gels and are still viable after 7 DIV and viral infection. Neurite outgrowth still occurs in the gels, and the resulting cultures are three-dimensional within the gel (see figures 7.5-7). Comparison between different gel types, and a commercially available cell substrate (Matrigel) shows that neurite outgrowth is indeed different between gel types.

Electrophysiological recordings from neurones cultured in hSAF gels were somewhat inconsistent. Neurones grown in AAA gel failed to fire action potentials, unlike cells from actual brain slices, and age-matched neurons from traditional cultures (grown on coverslips coated with poly-L-lysine). However, neurones grown in the AAAw gel variant did fire action potentials.

Neurones grown in gel had relatively high input resistance (4 GΩ) and had normal outward potassium currents in response to voltage ramps, similar to neurones from brain slices and traditional cultures (figure 7.11). However both Ca^{2+} and K^{+} currents in neurones grown in the AAA gel were small. Again, this was different in the AAAw gel, where larger, more typical Ca^{2+} and K^{+} currents were observed (figure 7.12).

This variability appears to be due to gel composition, with the AAAw gel producing neurones with a more typical phenotype, at least electrophysiologically, and this is an exciting direction to explore in future.

7.5.1 Difficulties of using a 3-D culture

Whilst it is an attractive proposition to be able to grow neurones in a 3-D environment that can be modified (e.g. hSAF-AAA to hSAF-AAAw), there are also some technical drawbacks. Recording from neurones embedded in the gel was difficult, as the gel tended to break up after time in the media, and move around. It was also difficult to image some of the cells, as due to current expense of the gels, only small volumes were available for use. This necessitated the use of small wells, leading to access issue for microscopy.

7.5.2 Future work

The ability to modify gels allows interesting possibilities for future experiments. Currently this venture is a multi-collaborative project, involving several geographically separated laboratories, all with their particular field (and therefore cell type) of interest. We intend to identity the effect of gel modification on the cell types of interest using the ‘half-moon’ experiment.

In this procedure, a gel is placed into a well separated into 2 halves. Neurones (or other cell types) are then seeded into the media above the gel, and left to settle. By changing the gel composition for either half of the gel, it will help understand what factors within the gel itself promote neurite outgrowth. The outgrowth will be directly comparable, as all cells will have come from the same dissection, will be in the same macroenvironment, and the only difference should be small, experimentally-directed change in hSAF composition (see figure 7.13 for schematic). The most exciting possibility in the half-moon experiment is that neurones seeded directly onto the border between gels (down the centreline of the well) will have neurites projecting from the same some into the two different regions of gel. It would be possible in theory to compare neurites from the same gel and the effect of gel composition.

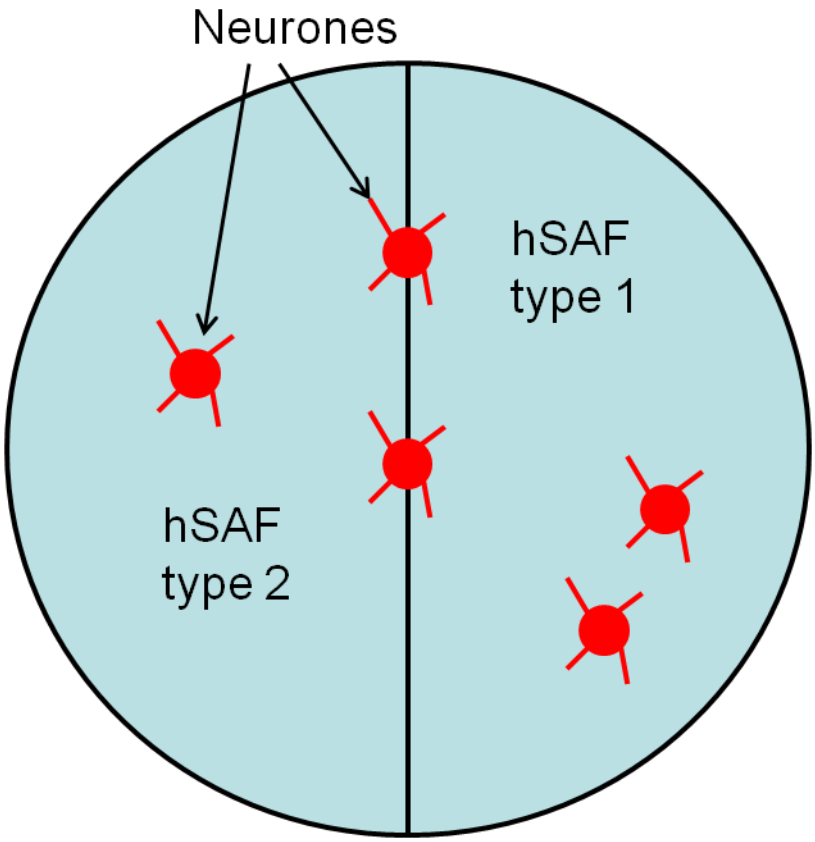

Figure 7.13 – Half-moon experimental design

Top down view of well in dish. One side of well is filled with hSAF variant 1. This is allowed to set, and then the other side is filled with a second variant. Media is added and then neurones (or other cell types) are seeded into the well. Cells grow in both gels, and some cells will settle onto the midline between the two gels

Chapter 8

General discussion and final conclusions

8.1 Channelrhodopsin-2

Previously, other studies have investigated the biophysical properties of channelrhodopsin-2 in several model systems (see (Nagel, Szellas et al. 2003; Zimmermann, Terpitz et al. 2006) collecting much useful data about the channel opening properties, recovery, and inactivation. However, these studies were done at room temperature, and in some model organisms that are not closely related to mammalian systems (for example xenopus oocytes). My work has added to this field by over-expressing a fluorescently tagged ChR2 construct in HEK293 cells and dissociated neurones, and monitoring its behaviour at room temperature and a temperature more reflecting the reality of expression in an intact warm-blooded organism (37^0C).

In addition to gathering data adding to the information about the channels opening, inactivation and desensitisation kinetics (see figures 3.3, 3.5 and 3.6), I have also identified a potentially troublesome aspect of expression and utilisation, of ChR2 in neurones, viz the difference between the initial stimulus and any following stimuli. Desensitisation of ChR2 results in a smaller total current upon successive light flashes, leading to an increased latency to action potential threshold, as the neuronal cell membrane takes longer to charge due to the decrease in summed current through the rhodopsin molecules in the membrane. This potential problem has been addressed by other labs by creating modified versions of ChR2 with more tractable kinetic parameters, such as ChEF and ChIEF (Lin, Lin et al. 2009). These mutations have reduced inactivation achieved through chimeric fusion and site-directed mutagenesis.

I also demonstrated some of the potential for ChR2 (or indeed other light-activated proteins) in neuronal culture, with illumination of ChR2 able to increase activity levels in culture, drive epileptiform activity, even with only small numbers of cells expressing the rhodopsin. This shows that even with a small population of cells (between 2-5%) being activated, large changes to the total network can be achieved.

This fits with some *in vivo* studies, where activation of only a few ChR2-positive neurones can cause changes in an animal's behaviour (Huber, Petreanu et al. 2008). The paradigm of flashing cultured neurones expressing ChR2 has also been used to modulate the structure of the axon initial segment (Grubb and Burrone 2010) in a manner somewhat similar to my enhancement of network activity.

8.2 PKMzeta

PKMzeta is the constitutively active catalytic fragment of PKCzeta, and has been implicated in the maintenance of long term potentiation, by increasing the levels of AMPAR at synapses. During my thesis, I investigated whether levels of synaptic AMPA receptors change in response to incubation with the PKMzeta inhibitor zeta inhibitory peptide (ZIP). Previous work within the Henley lab has shown that incubation with ZIP alters the level of surface expression of GluA1 and GluA2. This was shown using surface biotinylations, and imaging. However, it was not sure in which compartments of the neurones were happening. By blocking neuronal action potentials with the sodium channel blocked TTX, I was able to measure mini-excitatory post-synaptic currents (mEPSCs), which reflect spontaneous fusion of pre-synaptic vesicles of neurotransmitter with the pre-synaptic membrane, and the resultant ionic flows through post-synaptic AMPA receptors.

Unfortunately I saw no difference between either the amplitude of mEPSCs, or the frequency of mEPSCs. This suggests, (but does not prove) that the changes in AMPA receptors are happening at extra-synaptic sites possibly close to the synapse (peri-synaptic) or elsewhere in the neurone (for example onto dendritic shafts, or perhaps the soma).

8.3 Neuronal cultures as an experimental paradigm

Other work in this thesis has explored lines of investigation that utilize neuronal cultures as a central experimental model. This highlights the flexibility of this system. Cultures are a reductionist system, but allow experiments that require levels of access and manipulation that are not feasible in cultured or acute brain slices or in vivo. The ease of access for electrophysiology and imaging, the ability to perfuse on various factors, the co-culture of different cell types, and the possibility of 3-D cell cultures all illustrate the breadth of options arising from neuronal cell cultures. Dissociated cultures allow a large number of experiments and a wide variety of experimental procedures to be performed on sister coverslips isolated form the same original preparation This innate flexibility of neuronal cultures is explored in more detail in Chapters 6 and 7.

References

Ahmed, Z., R. A. Brown, et al. (1999). "Nerve growth factor enhances peripheral nerve regeneration in non-human primates." Scand J Plast Reconstr Surg Hand Surg **33**(4): 393-401.

Banwell, E. F., E. S. Abelardo, et al. (2009). "Rational design and application of responsive alpha-helical peptide hydrogels." Nat Mater **8**(7): 596-600.

Bear, M. F. and R. C. Malenka (1994). "Synaptic plasticity: LTP and LTD." Curr Opin Neurobiol **4**(3): 389-399.

Bhabra, G., A. Sood, et al. (2009). "Nanoparticles can cause DNA damage across a cellular barrier." Nat Nanotechnol **4**(12): 876-883.

Bliss, T. V. and G. L. Collingridge (1993). "A synaptic model of memory: long-term potentiation in the hippocampus." Nature **361**(6407): 31-39.

Bliss, T. V. and T. Lomo (1973). "Long-lasting potentiation of synaptic transmission in the dentate area of the anaesthetized rabbit following stimulation of the perforant path." J Physiol **232**(2): 331-356.

Bosman, S. J., S. P. Nieto, et al. (2005). "Development of mammalian embryos exposed to mixed-size nanoparticles." Clin Exp Obstet Gynecol **32**(4): 222-224.

Cadotte, D. W. and M. G. Fehlings (2011). "Spinal cord injury: a systematic review of current treatment options." Clin Orthop Relat Res **469**(3): 732-741.

Chen G, U. T., Tateishi T (2002). "Scaffold Design for Tissue Engineering." Macromol Biosci **2**(2).

Colley, P. A., F. S. Sheu, et al. (1990). "Inhibition of protein kinase C blocks two components of LTP persistence, leaving initial potentiation intact." J Neurosci **10**(10): 3353-3360.

Derkach, V. A., M. C. Oh, et al. (2007). "Regulatory mechanisms of AMPA receptors in synaptic plasticity." Nat Rev Neurosci **8**(2): 101-113.

Doorn, P. F., P. A. Campbell, et al. (1998). "Metal wear particle characterization from metal on metal total hip replacements: transmission electron microscopy study of periprosthetic tissues and isolated particles." J Biomed Mater Res **42**(1): 103-111.

Dunwoodie, S. L. (2009). "The role of hypoxia in development of the Mammalian embryo." Dev Cell **17**(6): 755-773.

Faraji, A. H. and P. Wipf (2009). "Nanoparticles in cellular drug delivery." Bioorg Med Chem **17**(8): 2950-2962.

Giepmans, B. N., S. R. Adams, et al. (2006). "The fluorescent toolbox for assessing protein location and function." Science **312**(5771): 217-224.

Grubb, M. S. and J. Burrone (2010). "Activity-dependent relocation of the axon initial segment fine-tunes neuronal excitability." Nature **465**(7301): 1070-1074.

Hansbrough, J. F., J. L. Morgan, et al. (1993). "Composite grafts of human keratinocytes grown on a polyglactin mesh-cultured fibroblast dermal substitute function as a bilayer skin replacement in full-thickness wounds on athymic mice." J Burn Care Rehabil **14**(5): 485-494.

Harris, E. W. and C. W. Cotman (1986). "Long-term potentiation of guinea pig mossy fiber responses is not blocked by N-methyl D-aspartate antagonists." Neurosci Lett **70**(1): 132-137.

Hernandez, A. I., N. Blace, et al. (2003). "Protein kinase M zeta synthesis from a brain mRNA encoding an independent protein kinase C zeta catalytic domain. Implications for the molecular mechanism of memory." J Biol Chem **278**(41): 40305-40316.

Hockberger, P. E., H. Y. Tseng, et al. (1989). "Fura-2 measurements of cultured rat Purkinje neurons show dendritic localization of Ca2+ influx." J Neurosci **9**(7): 2272-2284.

Hrabetova, S. and T. C. Sacktor (1996). "Bidirectional regulation of protein kinase M zeta in the maintenance of long-term potentiation and long-term depression." J Neurosci **16**(17): 5324-5333.

Huber, D., L. Petreanu, et al. (2008). "Sparse optical microstimulation in barrel cortex drives learned behaviour in freely moving mice." Nature **451**(7174): 61-64.

Huber, K. M., M. D. Mauk, et al. (1995). "Distinct LTP induction mechanisms: contribution of NMDA receptors and voltage-dependent calcium channels." J Neurophysiol **73**(1): 270-279.

Huber, K. M., M. D. Mauk, et al. (1995). "A critical period of protein kinase activity after tetanic stimulation is required for the induction of long-term potentiation." Learn Mem **2**(2): 81-100.

Jazrawi, L. M., F. J. Kummer, et al. (1998). "Alternative bearing surfaces for total joint arthroplasty." J Am Acad Orthop Surg **6**(4): 198-203.

Kitahara, A. K., Y. Suzuki, et al. (1999). "Facial nerve repair using a collagen conduit in cats." Scand J Plast Reconstr Surg Hand Surg **33**(2): 187-193.

Kohei Yamashita, Y. Y., Kazuma Higashisaka Kazuya Mimura, Yuki Morishita,, T. Y. Masatoshi Nozaki, Toshinobu Ogura, Hiromi Nabeshi, Kazuya Nagano,, et al. (2011). "Silica and titanium dioxide nanoparticles cause

pregnancy complications in mice." Nature Nanotechnology.

Learmonth, I. D. and A. Spirakis (1989). "Current status of total hip replacement. A review of biological and biomechanical factors." S Afr J Surg **27**(3): 84-88.

Lin, J. Y., M. Z. Lin, et al. (2009). "Characterization of engineered channelrhodopsin variants with improved properties and kinetics." Biophys J **96**(5): 1803-1814.

Ling, D. S., L. S. Benardo, et al. (2006). "Protein kinase Mzeta enhances excitatory synaptic transmission by increasing the number of active postsynaptic AMPA receptors." Hippocampus **16**(5): 443-452.

Ling, D. S., L. S. Benardo, et al. (2002). "Protein kinase Mzeta is necessary and sufficient for LTP maintenance." Nat Neurosci **5**(4): 295-296.

Lynch, G. S., T. Dunwiddie, et al. (1977). "Heterosynaptic depression: a postsynaptic correlate of long-term potentiation." Nature **266**(5604): 737-739.

Macchiarini, P., P. Jungebluth, et al. (2008). "Clinical transplantation of a tissue-engineered airway." Lancet **372**(9655): 2023-2030.

Malenka, R. C. and M. F. Bear (2004). "LTP and LTD: an embarrassment of riches." Neuron **44**(1): 5-21.

Malinow, R., D. V. Madison, et al. (1988). "Persistent protein kinase activity underlying long-term potentiation." Nature **335**(6193): 820-824.

McKelvey-Martin, V. J., M. H. Green, et al. (1993). "The single cell gel electrophoresis assay (comet assay): a European review." Mutat Res **288**(1): 47-63.

Mosahebi, A., M. Wiberg, et al. (2003). "Addition of fibronectin to alginate matrix improves peripheral nerve regeneration in tissue-engineered conduits." Tissue Eng **9**(2): 209-218.

Mulkey, R. M., C. E. Herron, et al. (1993). "An essential role for protein phosphatases in hippocampal long-term depression." Science **261**(5124): 1051-1055.

Mulkey, R. M. and R. C. Malenka (1992). "Mechanisms underlying induction of homosynaptic long-term depression in area CA1 of the hippocampus." Neuron **9**(5): 967-975.

Muller, D., P. A. Buchs, et al. (1990). "Protein kinase C activity is not responsible for the expression of long-term potentiation in hippocampus." Proc Natl Acad Sci U S A **87**(11): 4073-4077.

Nagel, G., T. Szellas, et al. (2003). "Channelrhodopsin-2, a directly light-gated cation-selective membrane channel." Proc Natl Acad Sci U S A **100**(24): 13940-13945.

Nel, A., T. Xia, et al. (2006). "Toxic potential of materials at the nanolevel." Science **311**(5761): 622-627.

Nishizuka, Y. (1995). "Protein kinase C and lipid signaling for sustained cellular responses." FASEB J **9**(7): 484-496.

Nishizuka, Y. and S. Nakamura (1995). "Lipid mediators and protein kinase C for intracellular signalling." Clin Exp Pharmacol Physiol Suppl **22**(1): S202-203.

Nohynek, G. J., E. K. Dufour, et al. (2008). "Nanotechnology, cosmetics and the skin: is there a health risk?" Skin Pharmacol Physiol **21**(3): 136-149.

Nohynek, G. J., J. Lademann, et al. (2007). "Grey goo on the skin? Nanotechnology, cosmetic and sunscreen safety." Crit Rev Toxicol **37**(3): 251-277.

Orendi, K., V. Kivity, et al. (2011). "Placental and trophoblastic in vitro models to study preventive and therapeutic agents for preeclampsia." Placenta **32 Suppl**: S49-54.

Osten, P., S. Hrabetova, et al. (1996). "Differential downregulation of protein kinase C isoforms in spreading depression." Neurosci Lett **221**(1): 37-40.

Papageorgiou, I., C. Brown, et al. (2007). "The effect of nano- and micron-sized particles of cobalt-chromium alloy on human fibroblasts in vitro." Biomaterials **28**(19): 2946-2958.

Pastalkova, E., P. Serrano, et al. (2006). "Storage of spatial information by the maintenance mechanism of LTP." Science **313**(5790): 1141-1144.

Sacktor, T. C., P. Osten, et al. (1993). "Persistent activation of the zeta isoform of protein kinase C in the maintenance of long-term potentiation." Proc Natl Acad Sci U S A **90**(18): 8342-8346.

Sajja, H. K., M. P. East, et al. (2009). "Development of multifunctional nanoparticles for targeted drug delivery and noninvasive imaging of therapeutic effect." Curr Drug Discov Technol **6**(1): 43-51.

Santos, S. D., A. L. Carvalho, et al. (2009). "Regulation of AMPA receptors and synaptic plasticity." Neuroscience **158**(1): 105-125.

Schwartz, J. H. (1993). "Cognitive kinases." Proc Natl Acad Sci U S A **90**(18): 8310-8313.

Sharkey, P. F. and J. Parvizi (2006). "Alternative bearing surfaces in total hip arthroplasty." Instr Course Lect **55**: 177-184.

Shema, R., T. C. Sacktor, et al. (2007). "Rapid erasure of long-term memory associations in the cortex by an inhibitor of PKM zeta." Science **317**(5840): 951-953.

Singh, N. P., M. T. McCoy, et al. (1988). "A simple technique for quantitation of low levels of DNA damage in individual cells." Exp Cell Res **175**(1): 184-191.

Sterne, G. D., R. A. Brown, et al. (1997). "Neurotrophin-3 delivered locally via fibronectin mats enhances peripheral nerve regeneration." Eur J Neurosci **9**(7): 1388-1396.

Sterne, G. D., G. R. Coulton, et al. (1997). "Neurotrophin-3-enhanced nerve regeneration selectively improves recovery of muscle fibers expressing myosin heavy chains 2b." J Cell Biol **139**(3): 709-715.

Stone, V., H. Johnston, et al. (2007). "Air pollution, ultrafine and nanoparticle toxicology: cellular and molecular interactions." IEEE Trans Nanobioscience **6**(4): 331-340.

Takai, Y., A. Kishimoto, et al. (1977). "Studies on a cyclic nucleotide-independent protein kinase and its proenzyme in mammalian tissues. I. Purification and characterization of an active enzyme from bovine cerebellum." J Biol Chem **252**(21): 7603-7609.

Tiede, K., A. B. Boxall, et al. (2008). "Detection and characterization of engineered nanoparticles in food and the environment." Food Addit Contam Part A Chem Anal Control Expo Risk Assess **25**(7): 795-821.

Utley, D. S., S. L. Lewin, et al. (1996). "Brain-derived neurotrophic factor and collagen tubulization enhance functional recovery after peripheral nerve transection and repair." Arch Otolaryngol Head Neck Surg **122**(4): 407-413.

Waxham, M. N., R. C. Malenka, et al. (1993). "Calcium/calmodulin-dependent protein kinase II regulates hippocampal synaptic transmission." Brain Res **609**(1-2): 1-8.

Whitworth, I. H., C. J. Dore, et al. (1995). "Increased axonal regeneration over long nerve gaps using autologous nerve-muscle sandwich grafts." Microsurgery **16**(12): 772-778.

Woolfson, D. N. and M. G. Ryadnov (2006). "Peptide-based fibrous biomaterials: Some things old, new and borrowed." Curr Opin Chem Biol **10**(6): 559-567.

Wu, G., Y. Fang, et al. (1998). "Induction of axon-like and dendrite-like processes in neuroblastoma cells." J Neurocytol **27**(1): 1-14.

Yasuda, H., A. L. Barth, et al. (2003). "A developmental switch in the signaling cascades for LTP induction." Nat Neurosci **6**(1): 15-16.

Zhang, S., T. Holmes, et al. (1993). "Spontaneous assembly of a self-complementary oligopeptide to form a stable macroscopic membrane." Proc Natl Acad Sci U S A 90(8): 3334-3338.

Zimmermann, D., U. Terpitz, et al. (2006). "Biophysical characterisation of electrofused giant HEK293-cells as a novel electrophysiological expression system." Biochem Biophys Res Commun 348(2): 673-681.